A critical evaluation of scatterometer-based global ocean surface wind products

L. C. van Cranenburgh

TU Delft

MSc. Thesis

Environmental Engineering

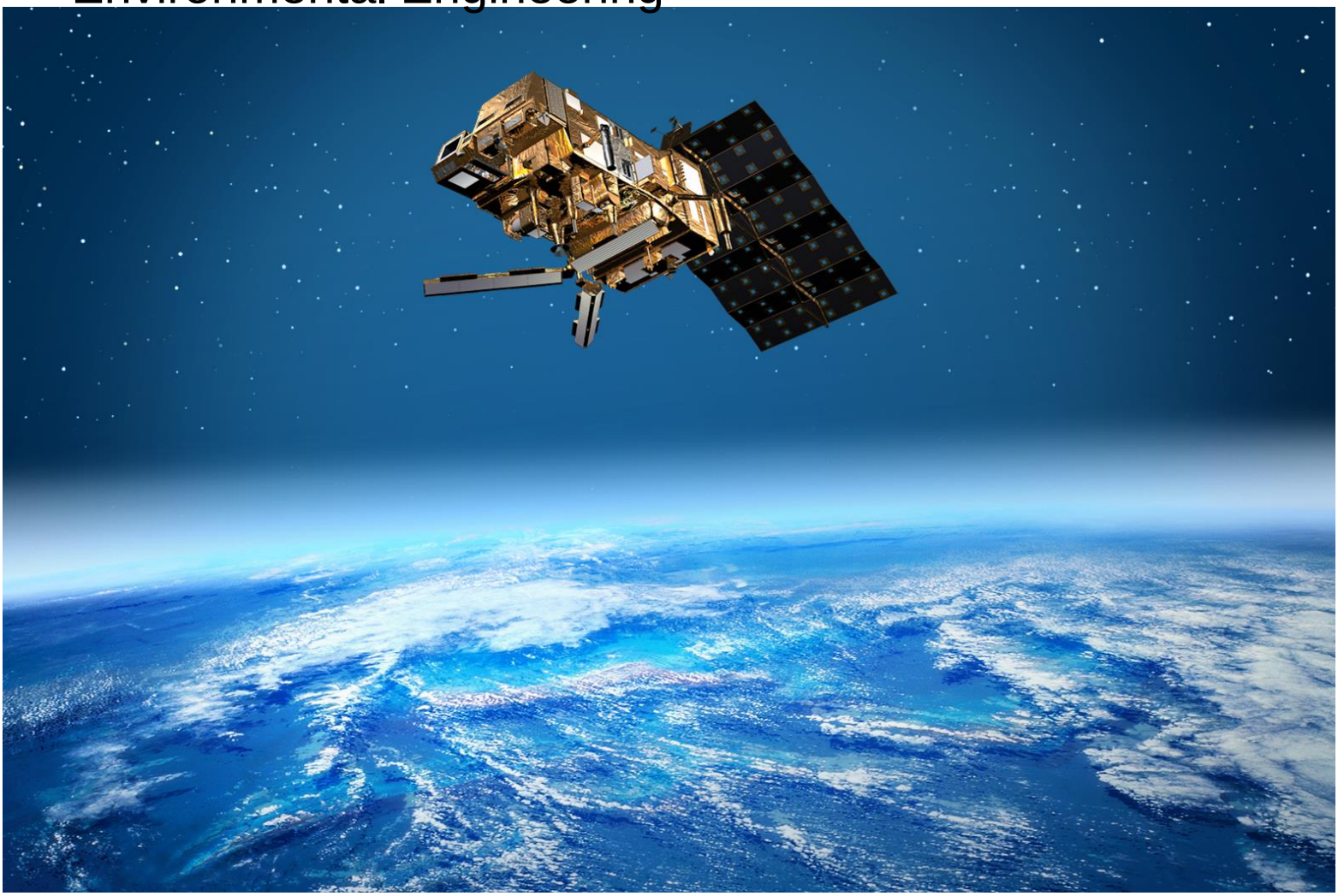

Koninklijk Nederlands
Meteorologisch Instituut
Ministerie van Infrastructuur en Waterstaat

Cover photo: MetOp-A satellite is Europe's first polar orbiting mission. One of the instruments on board MetOp-A is the ASCAT-A scatterometer (ESA, 2006).

A critical evaluation of scatterometer-based global ocean surface wind products

by

L.C. van Cranenburgh

to obtain the degree of Master of Science
at the Delft University of Technology,
to be defended publicly on 16 February 2022.

Student number:	4461312	
Thesis committee:	Prof. dr. A. P. Siebesma,	TU Delft, supervisor
	Dr. A. A. Nuijens,	TU Delft, supervisor
	Dr. ir. C. J. Simão Ferreira,	TU Delft
	Dr. R. H. Giesen,	KNMI, supervisor
	Dr. J. de Kloe,	KNMI, supervisor
	Dr. A. C. M. Stoffelen,	KNMI, supervisor

An electronic version of this thesis is available at http://repository.tudelft.nl/.

TU Delft

Preface

Delft, February 2022

The beginning of my MSc graduation thesis dates back to an email from Ad Stoffelen introducing an internship on satellite-based global ocean surface winds at the Royal Netherlands Meteorological Institute (KNMI). My excitement for this project was triggered by my love for sailing (at sea) and the challenging opportunity to contribute to new knowledge on global ocean winds. I was on board.

This research was carried out in collaboration with the KNMI, specifically with the Research Group of Active Satellite Observations. A guest lecture of Pieternel Levelt inspired me to reach out to the KNMI and it was a privilege to be part of this research group and department for the past 8 months. I consider myself very lucky that I got a glimpse of their impressive knowledge and especially their passion they share for their field of study.

Realising the complexity of wind and satellite instruments before starting, I was prepared for a challenging task. Indeed, this research did not immediately go like the wind. Nevertheless, I have carried out this research with a lot of enthusiasm, tears and laughter and learnt so much throughout, content wise as well as project wise. This project has been accomplished through a lot of hard work from home at first, and, fortunately a significant part of this thesis was also carried out at the headquarters of the KNMI themselves. It goes without saying that I could not have done this alone; therefore I would like to take advantage of this opportunity to express my appreciation to everyone who has been part of the ride.

First of all, I cannot express my gratitude in words to Rianne and Jos for your endless patience, sympathy and help throughout the project. You have stood by my side from day one onwards and I have learnt a lot from you. I also want to thank Ad for his expertise on scatterometers and guidance throughout. Juliette, I am very glad to have met you at the KNMI and thank you so much for all your advice and good talks about all sorts of things such as efficient writing and time management. Finally, I want to express my appreciation to Louise and Pier. It was an honour to be supported by you and I very much enjoyed working together with you.

Besides my graduation committee, the moral support I received from my family and friends helped me get through a sometimes tough time. Thanks to my family for always being there to listen, give advice and remind me that it is also okay to chill. After an energizing day in the Bilt, it was the best to get a warm welcome at home by my roommates who would even listen to my Python struggles, thank you! And of course thanks to all my friends for making my thesis period more fun, including all the days at the TU Delft!

Now, it is time to wind up, celebrate the end of my student time in Delft and more importantly to look forward to what the future has to offer! I am excited to continue to develop myself and embrace new challenges what- and where-ever they may be!

Enjoy reading!

Liselotte

Abstract

By combining satellite observations and model reanalysis winds, a global data set with higher temporal and spatial resolution ocean surface wind fields can be generated. These superior surface wind fields can have various applications, such as wind forcing of ocean models. The Royal Netherlands Meteorological Institute (KNMI) is responsible for the delivery of two different global data sets of combined surface winds, referred to as IFREMER and ERA5*. IFREMER's approach focuses on satellite scatterometer observations which are complemented with model reanalysis winds (ERA5). On the other hand, ERA5* is based on ERA5 model reanalysis and corrected with scatterometer observations. The aim of this research is to evaluate global IFREMER and ERA5* surface winds in terms of spatial and temporal characteristics.

In order to validate the surface winds of IFREMER and ERA5*, a reference system of true winds is required. For this, quality-controlled wind observations from an independent Chinese scatterometer Haiyang-2B have been used. This comparison study has been carried out for the year 2019 focusing on zonal wind, meridional wind and wind speed. IFREMER and ERA5* wind fields have been collocated in time and space to HY-2B wind observations using a 6-hour and 1-hour window respectively. This methodology was applied to overcome differences between the data sets in grid definition, wind representation, spatial resolution and temporal resolution.

On a global scale, IFREMER shows larger average and standard deviation of wind differences with respect to HY-2B than ERA5*, specifically in coastal regions and at higher latitudes. The results of this research suggest that the ERA5* wind product generates more accurate surface ocean winds than IFREMER, except for in the tropics, assuming that HY-2B winds represent the true value. Moreover, at higher wind speeds both global wind products underestimate HY-2B wind, whereby IFREMER already deviates at lower winds than ERA5*. The IFREMER winds showed suspicious satellite tracks and temporal wind inaccuracies, most likely as a result of its 6-hourly resolution. It is recommended that a follow-up investigation is carried out with validation of buoy data in the tropics to investigate the underlying causes of the observed local wind bias.

List of Acronyms

ABL Atmospheric Boundary Layer

ASCAT Advanced Scatterometer

CDS Climate Data Store

CMEMS Copernicus Marine Environment Monitoring Service

ECMWF European Centre for Medium-Range Weather Forecasts

ERA5 ECMWF Re-Analysis v5

ESA European Space Agency

EU European Union

EUMETSAT European Organisation for the Exploitation of Meteorological Satellites

GMF Geophysical Model Function

ICM Institut de Ciencias del Mar

IFREMER Institut Francais de Recherche pour l'Exploitation de la mer

ITCZ Inter Tropical Convergence Zone

KNMI Koninklijk Nederlands Meteorologisch Institituut

LTAN Local Time Ascending Node when crossing the equator

LTDN Local Time Descending Node when crossing the equator

MARS Meteorological Archival & Retrieval System

NCAR US National Center for Atmospheric Research

NCEP US National Centers for Environmental Prediction

NSOAS National Satellite Ocean Application Service

NWP Numerical Weather Prediction

OSI SAF Ocean & Sea Ice Satellite Application Facility

RMSD Root Mean Square Difference

SL Surface Layer

TU Delft Delft University of Technology

U10N 10-m Neutral-equivalent winds

U10S 10-m Stress-equivalent winds

Wind TAC Wind Thematic Assembly Centre

Contents

1

Introduction

Surface winds are a key driver for the behaviour of oceans around the world. At the air-sea interface many processes are directly related to the wind, such as the exchange of gases, upper layer ocean mixing and surface waves (figure 1.1). For example, gas transfer is controlled by complex marine boundary interactions which are influenced by the wind (Wanninkhof, 2014). In order to quantify the ocean-atmosphere flux of a gas like carbon dioxide (CO_2), it is necessary to understand the wind speed and direction. This is in turn relevant for climate monitoring because the oceans are a major sink of CO_2, annually absorbing more than 25% of anthropogenic emissions. Furthermore, 70% of the Earth's surface is covered by water and a quarter of the Earth's population lives in coastal areas (Bôas et al., 2019). Therefore, accurate surface wind data is essential for a complete understanding of the processes occurring at the marine boundary layer relevant to the marine environment and human society.

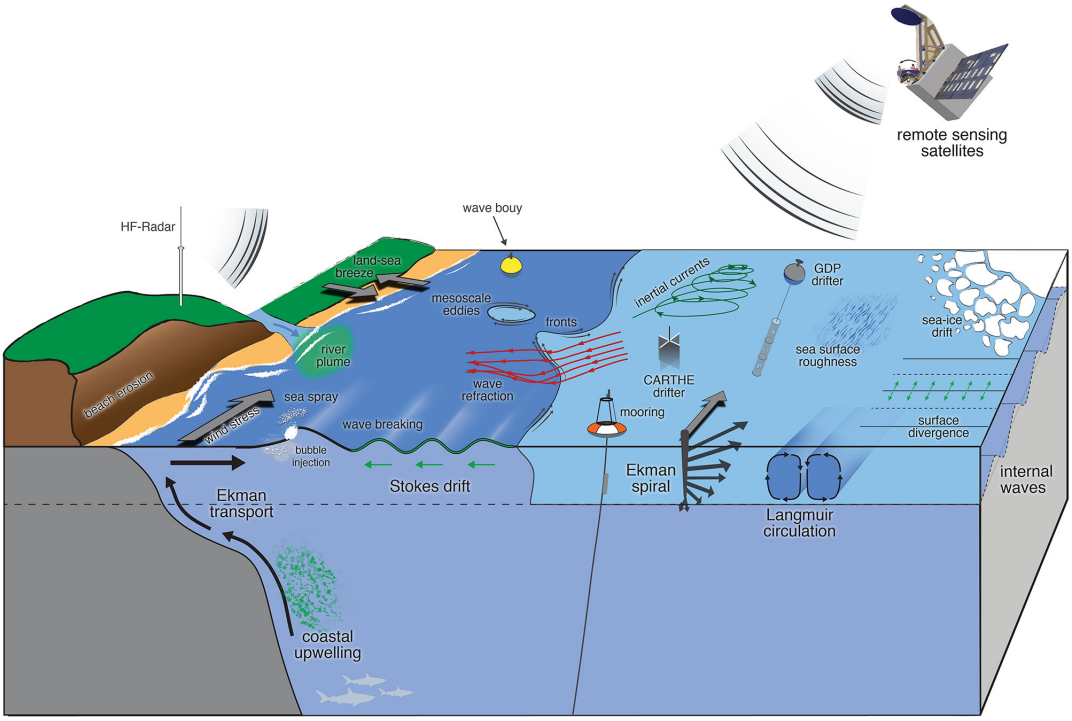

Figure 1.1: Air-sea interactions at the marine boundary layer, closer to the coast and at open ocean (Bôas et al., 2019).

1.1. Research relevance

The importance of correct wind field data can be illustrated by a weather event that affected Venice in November 2019. During this event Venice was victim of extreme high water level, known as ”Acqua Alta”, due to a combination of high spring tide, a higher than average sea level and strong local Sirocco winds pushing seawater into the Venice lagoon (Giesen et al., 2021). Weather forecasts at the time were based on Numerical Weather Prediction (NWP) model winds from the European Centre for Medium-Range Weather Forecasts (ECMWF) which underestimated the strong, local wind gusts. Clearly forecasting in such situations would benefit from higher resolution models together with observations (in situ or remote sensing). Aqua Alta in itself is a natural phenomenon. However, global warming leads to more weather extremes and the increased likelihood of events, such as Aqua Alta, underlining the importance of improved weather forecasting (von Schuckmann et al., 2021).

Besides forecasting weather, NWP models can also be used to recreate data sets of atmospheric parameters like surface winds back in time. An example of such a reanalysis data set is ERA5. Wind fields from these historic data sets are beneficial because they are consistent in space and time. This technique for modelling winds is widely accepted for ocean modelling activities. Alternative methods to obtain surface winds are in situ measurements from buoy networks, ships or remotely sensed wind data from for example scatterometers carried by satellites (Morey et al., 2005). Despite the high accuracy of in situ observations, there are limitations regarding their installations in oceans around the world (Morey et al., 2005). On the other hand, scatterometers, satellite-based active microwave radars, generate highly accurate wind data, but are constrained by their orbital coverage. For example, at a given location on Earth, the current satellites in orbit are unable to provide hourly observations. Therefore, the NWP model winds are often used in ocean models because of their ability to provide global coverage at frequent intervals throughout the day (Morey et al., 2005; Trindade et al., 2014; Li and Bao, 2021). For instance, Jing et al. (2022) recently studied the CO_2 flux in coupled models of the atmosphere and oceans. Jing et al. (2022) showed that improved simulated NWP wind fields brought the simulated flux of CO_2 in ocean models closer to observation-based results.

A recent study conducted by Belmonte Rivas and Stoffelen (2019) demonstrated that NWP surface winds from ERA5, a reanalysis produced by the model of the European Centre for Medium-Range Weather Forecasts (ECMWF), contain systematic errors (Figure 1.2). They compared ERA5 wind data with wind observations measured by Advanced Scatterometer (ASCAT). ASCAT winds are of very high quality (Verhoef et al., 2017) and have a higher spatial resolution of about 25 km than ERA5 which is about 100 km (Vogelzang et al., 2011). ASCAT observations can therefore be considered superior to ERA5. For example, in the tropics ERA5 winds misrepresent the atmospheric flow, particularly the meridional (South to North) wind component (Figure 1.2). Using NWP wind data like ERA5 in ocean models would lead to further errors in their output.

To improve global ocean surface wind fields, modelled winds can be integrated with scatterometer observations. This combination ensures global coverage while maintaining high spatial detail. The Wind Thematic Assembly Centre (Wind TAC), lead by the Koninklijk Nederlands Meteorologisch Instituut (KNMI) as part of the Copernicus Marine Environment Monitoring Service (CMEMS), provides two global wind products for free that combine scatterometer observations with NWP model winds. There are various users that benefit from the global wind products. Until December 2021, the global wind product that was offered in CMEMS was a 6-hourly wind product produced by the Institut Francais de Recherche pour l’Exploitation de la mer (IFREMER). This wind product is referred to as IFREMER in this research. It is mainly based on scatterometer observations and additionally makes use of radiometer and ERA5 winds when scatterometer winds are unavailable. In 2022, CMEMS will add a new wind product to their catalogue, known as ERA* and in this research referred to as ERA5*. ERA5* is developed by the Spanish Institut de Ciencias del Mar (ICM) and based on ERA5 wind fields that are corrected with scatterometer observations.

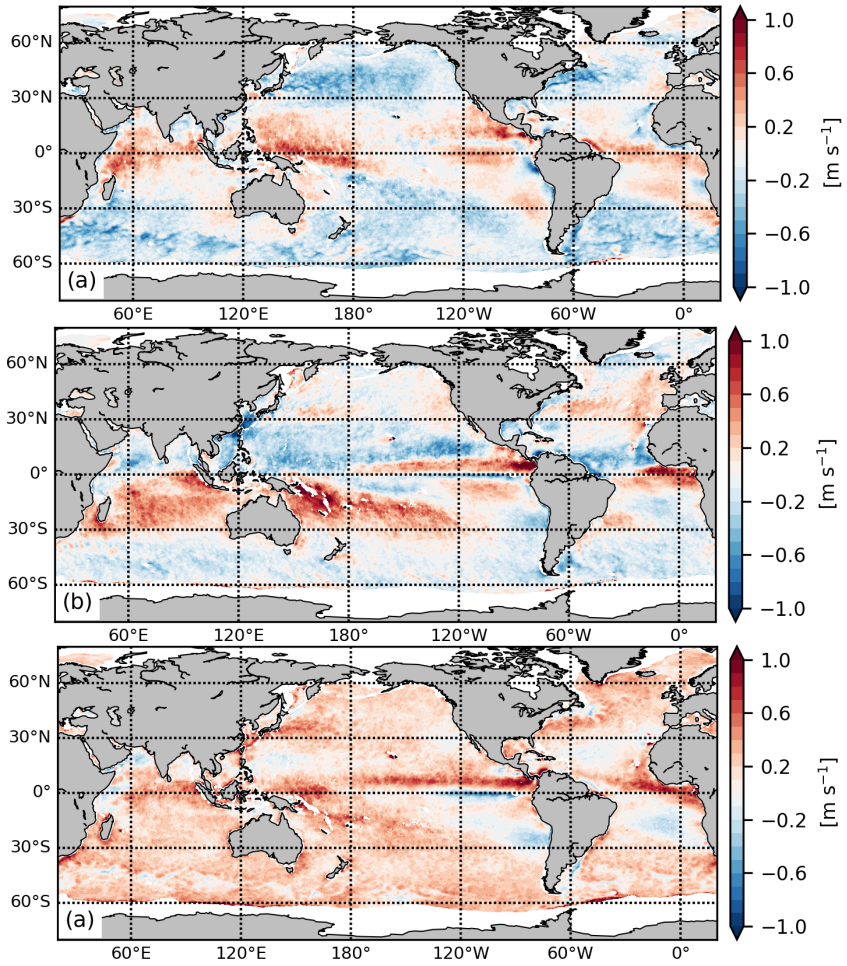

Figure 1.2: Global map of annual mean differences between Advanced Scatterometer (ASCAT) and ECMWF Re-Analysis v5 (ERA5) for zonal wind (a), meridional wind (b) and wind speed (c) over 2019 (produced by R. Giesen after Belmonte Rivas and Stoffelen, 2019).

1.2. Research objectives

The aim of this research is to evaluate these two different global wind products that integrate scatterometer measurements with NWP model winds to create consistent wind fields in time and space. The main question this study aims to answer is:

How well do the CMEMS global wind products - IFREMER and ERA5 - represent the spatial and temporal characteristics of the ocean surface wind fields?*

The sub-questions that follow are:

1. What are the characteristics of the IFREMER and ERA5* products?
2. What are the differences between IFREMER and ERA5* products for various time and space scales?
3. To what extent are wind characteristics accurately represented by each CMEMS wind product?

In order to answer the research question IFREMER and ERA5* winds are compared to ERA5 data and observations from an independent Chinese scatterometer Haiyang-2B. As ERA5 is is available at regular space and time intervals, this data set is, on the one hand used to define a methodology for a fair evaluation of IFREMER and ERA5*, and on the other hand enables direct comparison of wind data in space for short-time scales. Haiyang-2B is chosen as as reference system for true winds as scatterometers are known for their high-quality wind observations (Vogelzang et al., 2011) and because its observations are not used in either IFREMER or ERA5*. A global analysis based on 2019 wind data

is carried out to compare the behaviour of each wind product in time and space.

This research is carried out in collaboration with the KNMI as part of the master's degree in Environmental Engineering at Delft University of Technology (TU Delft). This research originates within the KNMI, specifically the Research & Development group called Active Satellite Observations. This research group is responsible for the continuous processing of wind data at sea measured by scatterometers on board satellites. Various data processing methods are in place to ensure 24/7 weather forecasts, and KNMI seeks to improve these methods at an international scale to enhance other applications such as hurricane forecasts, high waves, storm surges and coupling between the atmosphere and oceans. This research aims to contribute to improving the wind forcing product as input for ocean models for example.

1.3. Report outline

This thesis first sets up a theoretical background in chapter 2 to better understand the global winds at the ocean surface and how wind observations are obtained by scatterometers. Chapter 3 explains the data and methodology used for a fair comparison between the IFREMER and ERA5* winds, including the required data processing of each. Then chapter 4 shares the results of the comparison at different time and spatial scales. This is followed by the associated discussion (chapter 5) and conclusions and recommendations (chapter 6).

2

Global surface winds in observations and in models

This section describes the general global distribution of winds as known from observations and models. Furthermore, NWP model and scatterometer wind data are explained.

There are numerous studies that express the need and emphasise the importance of an accurate representation of global surface winds over sea (Trindade et al., 2014; Desbiolles et al., 2017; Morey et al., 2005; Belmonte Rivas and Stoffelen, 2019; Chelton et al., 2004). Due to the high variability of wind in space and time, an accurate wind product with global surface wind data is still a challenge today. The introduction of satellite-based instruments like the microwave radar scatterometers have significantly improved the spatial representation of global ocean surface wind fields (Vogelzang et al., 2011; Chelton and Xie, 2010). Previously high spatial resolution wind fields could only be achieved by in-situ measurements such as buoys and ships (Chelton and Xie, 2010). However, their sparse distribution restricted wind measurements to small regional scales only. Although satellites have an improved global coverage compared to in-situ measurements, they are still limited to their orbital coverage. There are a wide range of applications like ocean modelling, renewable energy forecasting and climate change modelling that require surface wind data with a global coverage over several decades. Nowadays, these applications mainly make use of simulated winds from NWP models because these winds meet the spatial and temporal requirements of the users. Yet, Belmonte Rivas and Stoffelen (2019) have shown that NWP model winds also have their limitations. Therefore, there is still a demand from the atmosphere and ocean community for an accurate global surface wind product over sea.

2.1. Global wind distribution

Global wind patterns are driven by the unequal distribution of solar radiation at the Earth. Due to the tilt of the Earth's axis, the equator receives more energy per unit area than the poles (Marshall and Alan Plumb, 2008; Landberg, 2015). This discrepancy creates net surplus energy in the tropics (between -30°and 30°latitudes) and an energy deficit at the poles. To ensure that the Earth is in equilibrium, energy is transported from low to high latitudes. Each hemisphere contains three major circulation cells that are responsible for the South-North transportation of air masses between the equator and the poles (Figure 2.1). At the equator, warm air rises and moves either North- or Southward to cooler regions where it sinks back to the surface around 30°N and 30°S of the equator. This circulation is known as the Hadley cell. Between 30°-60°and 60°-90°, the Ferrel and Polar cells drive transportation respectively(NOAA, 2020). Out of the three cells, the Hadley cell yields the strongest circulation flows.

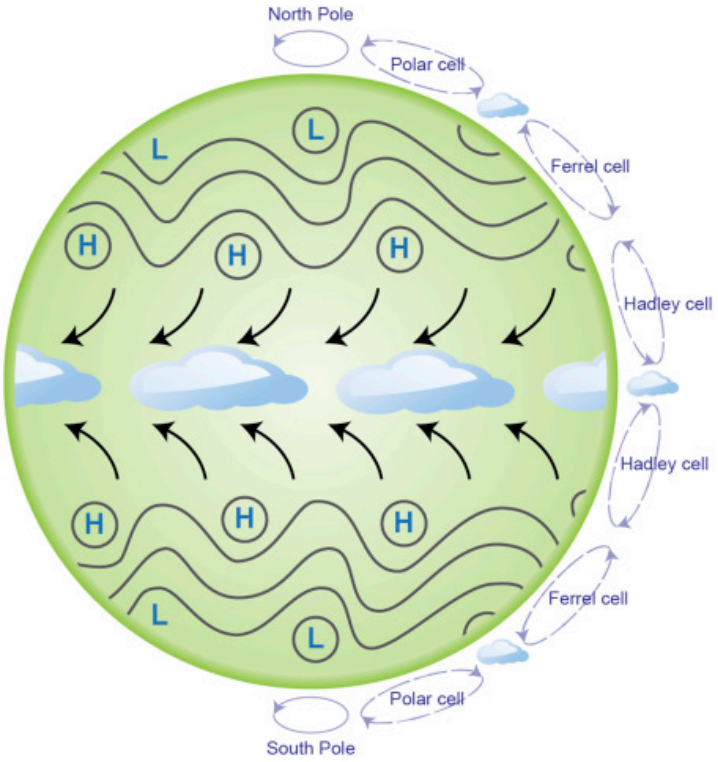

Figure 2.1: General circulation of the atmosphere with a Hadley, Ferrel and Polar cell in both the Northern and Southern hemisphere. Surface winds at higher latitudes are dominated by high and low pressure systems while at lower latitudes easterly Trade Winds dominate (Haupt et al., 2017).

The large-scale atmospheric circulation cells also influence the movement of air masses at the surface. These surface winds would have only flowed along the Earth's longitude lines (North-South direction) were it not for the Coriolis force. The Coriolis force, a direct consequence of the rotation of the Earth, deflects winds in the Northern hemisphere to the right (measured with one's back to where the wind is blowing from), and in the Southern hemisphere to the left (Landberg, 2015). In addition to a meridional (North-South direction) component, surface winds also consist of a zonal component (East-West). Figure 2.2 illustrates that on average the zonal wind component is larger than the meridional wind component. The Coriolis force also varies across latitudes. At the equator, the Coriolis force is zero and it increases towards the poles.

Table 2.1: Weather systems occur at a range of scales in space and time (Coleman, 2015)

Weather motion	Time scale (order of magnitude)	Length scale (m)	Examples of weather phenomenon
Large (synoptic)	days	10^6	mid-latitude cyclones
Meso	hours	10^3 - 10^5	thunderstorms
Micro	minutes-hours	$<10^3$	convective up- and downdrafts

The Coriolis force plays an important role in (surface) winds which are part of atmospheric motion. Atmospheric motion consists of processes occurring at different scales. Low and high pressure systems of the mid-latitudes are examples of large (synoptic) scale weather motion because they stretch over 10 000 km and exist for multiple days. On the other hand, tropical convective up- and downdrafts are an example of micro scale weather phenomenon because of their short duration and local occurrence (Coleman, 2015). Other systems develop at mesoscales (see table 2.1 for a full overview). The large-scale distribution of winds is determined by large-scale synoptic events, but mesoscale systems and convection can change winds on shorter temporal and smaller spatial scales. Regions with similar

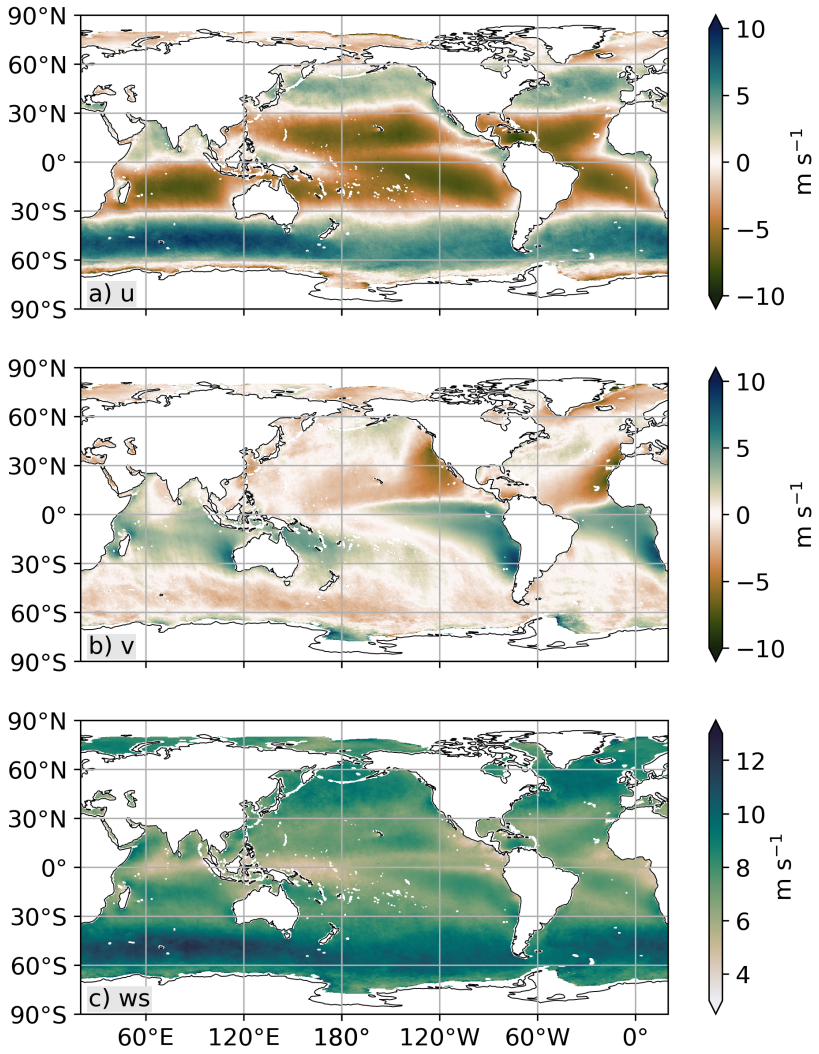

Figure 2.2: Global mean zonal (a), meridional (b) wind components and wind speed (c) plotted on a 0.25°x 0.25°grid based on ERA5 wind data for 2019. Note the different scales of the color bars.

weather systems are referred to as climate zones. Two climate zones of interest in this research are the tropics and the middle latitudes.

In the tropics, surface winds have low wind speeds and predominantly blow from the North East to the South West. These winds are also referred to as the easterly Trade Winds because of their dominant zonal component directed eastwards, highlighted in Figure 2.2c. Near the equator, the easterly Trade Winds from the Northern and Southern hemisphere converge. This is a low pressure area with mean rising motion known as the Inter-Tropical Convergence Zone (ITCZ). It is characterized by low winds (Doldrums) and thunder storms with short and intense rainfall. This weather is typical for the tropics and highly variable in space and time.

Large-scale tropical circulations in the tropics differentiate from the mid-latitude systems due to smallness of the Coriolis parameter and the different nature of energy sources. First of all, a weak Coriolis force in the tropics allows pressure differences diminish quickly before frontal systems can develop. This results in a horizontally uniform pressure (and hence temperature) field in the tropics (Sobel, 2012). Secondly, because the sun shines more directly on the tropics than at higher latitudes, it receives greater solar radiation. Due to the combination of warmer surface temperatures and the presence of abundant ocean water, the atmosphere in the tropics is prone to convection and the formation of (deep)

convective clouds. The formation of convective clouds occurs very spontaneously and is highly fluctuating in time and space (Sobel, 2012). The converging easterly winds in the tropics are therefore prone to strong fluctuations produced by convective storms, such as through their rainfall and thunderstorm outflow and associated gustiness.

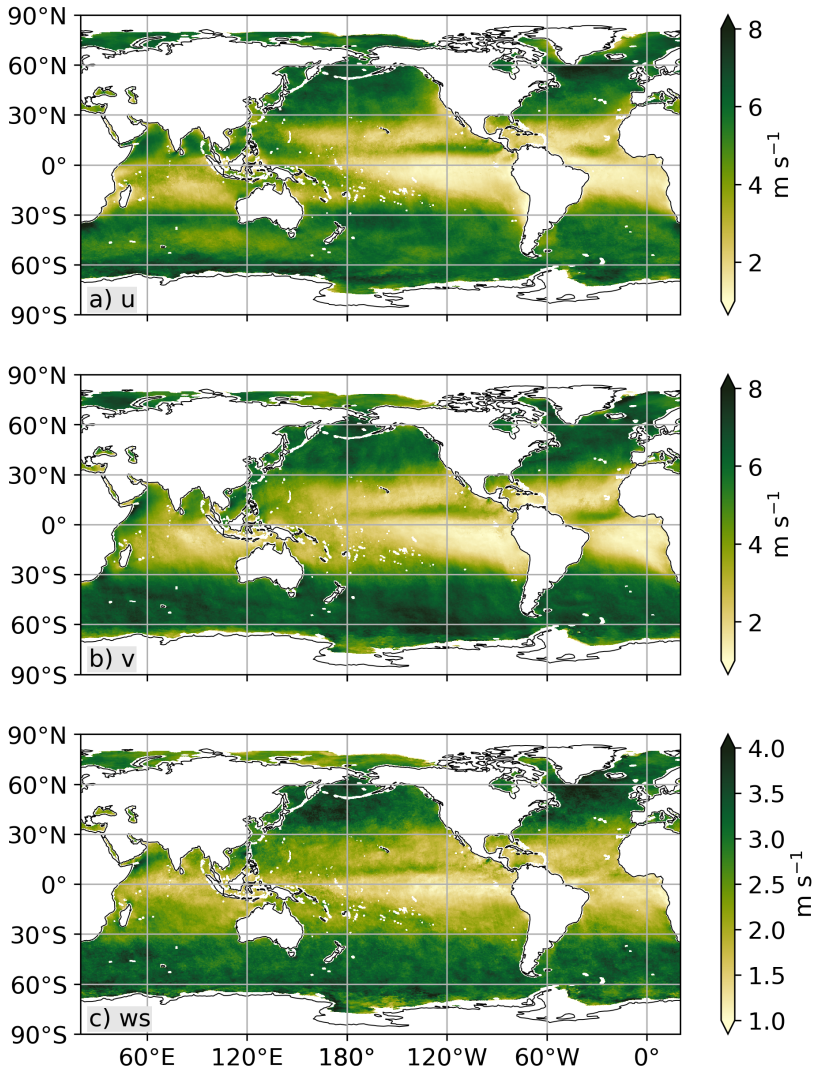

Figure 2.3: Global standard deviation of zonal (a), meridional (b) wind components and wind speed (c) plotted on a 0.25°x 0.25°grid based on ERA5 wind data for 2019. Note the different scales of the color bars.

In the middle-latitudes between 30°-60°, winds are predominantly westerly (Figure 2.2) and show larger variation than in the tropics (Figure 2.3). In the mid-latitudes the Coriolis parameter is considerably greater. Baroclinic eddies in the form of synoptic scale cyclonic low pressure systems and anticyclonic high pressure systems develop. A low pressure systems can be associated with strong winds, clouds and rain last for about 2-5 days (Landberg, 2015). Contrasting a low pressure systems, a high pressure system is associated with calm and cloud-free weather (Marshall and Alan Plumb, 2008).

2.2. Numerical Weather Prediction model winds

The foundations of a Numerical Weather Prediction (NWP) model are the laws of conservation of mass, momentum, heat and moisture. In a NWP model these atmospheric equations are discretized onto a grid. To solve this system of equations, initial conditions of the atmosphere are required. The state of

the atmosphere is initialized using data assimilation. Defined by Talagrand (1997), data assimilation is the ”process in which observations distributed in time are merged together with a dynamical numerical model of the flow in order to determine as accurately as possible the state of the atmosphere”. All available observations from various sources (e.g. buoys, ships, satellites) within a given assimilation window are used as input in a NWP model to generate an analysis for a given time (Haupt et al., 2017). The ECMWF model uses four-dimensional variation data assimilation (4D-Var), so that one can choose the temporal frequency at which the model fits are obtained as analyses (Klinker et al., 1999).
Subsequently to an analysis, the model propagates the information forward in time to generate a forecast (Figure 2.4). The difference between an analysis and a forecast at a certain time step is that an analysis combines the model with observations whereas a forecast only relies on the model. Thus while an analysis is a representation of the true state of the atmosphere at a given time using observations, a forecast approximates the state of the atmosphere by solving the system of equations (Haupt et al., 2017). The addition of observations to an analysis may cause very small-scale, detailed structures to be added to the model field. To ensure that the subsequent forecast remains stable, these small scale structures are damped resulting in a smoother wind field.

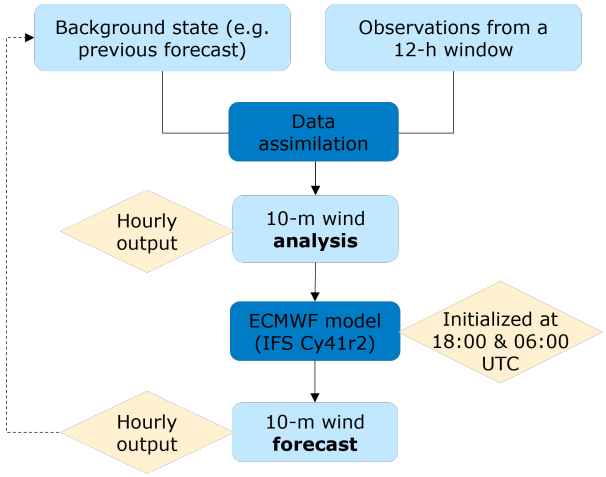

Figure 2.4: NWP modelling cycle of input data sources and output hourly 10-m analysis and forecast winds.

NWP models are not only used for generating forecasts, they are also used to obtain a historical global data set for several decades in the past. Such a data set is known as a reanalysis. A reanalysis is built up on many consecutive analyses that are reinitialized each time using data assimilation (ECMWF, 2020). In this research, the atmospheric reanalysis data set ERA5 is used. ERA5 is the fifth version of reanalysis and is produced by the ECMWF in 2018. ERA5 was run with the Integrated Forecast System (IFS) Cy41r2 which was used operationally by the ECMWF for medium-range forecasting (up to 10 days) from March to November 2016 (Hersbach et al., 2020). ERA5 covers the period 1978-present and has a horizontal resolution of 31 km and 137 vertical layers (Dee, 2022).

Since the ECMWF model uses 4D-var assimilation, a new analysis can be produced at every hour. ERA5 thus includes wind data at 10-m reference height as hourly analyses and forecasts (Figure 2.4). A 12-hour assimilation window is used. The analysis consists of the forecast from 12 hours earlier and all observations between 09:00 and 21:00 or between 21:00 and 09:00, if starting at 18:00 or 06:00 respectively. The analysis provides the initial conditions from which more than one forecast can be generated. Valid forecasts are issued after 3 and up to 12 hours after initialization. This is because during the first 3 hours, the model has to incorporate and smooth the disturbances introduced by observations.

A major advantage of ERA5 surface wind fields is its global coverage and high temporal and improved spatial resolution, especially in relation to its preceding reanalysis versions. Yet, ERA5 also has limitations because it is produced by a NWP model. Despite the continuous improvement of NWP modeling, NWP model winds are generally less accurate in the tropics than at higher latitudes (Dias et al., 2018). This is a direct consequence of NWP models only being able to solve structures as small as 100 km.

As a result, NWP small scale winds are inferior to scatterometers while for large spatial scales NWP and scatterometer winds lie close together (Vogelzang et al., 2011).

2.3. Scatterometer winds

A scatterometer is an active microwave radar located on satellites in space. Based on the roughness of the sea surface, surface wind observations can be retrieved from the electromagnetic radiation emitted and received by scatterometers. The received backscatter is processed to obtain a measurement for the wind speed and wind direction. There are different types of scatterometers. They may operate at different frequencies, and they may also vary in radar design. This research involves wind observations from two types of scatterometers: a fixed fan-beam operating at C-band frequency and a rotating pencil-beam scatterometer with Ku-band frequency.

2.3.1. Measurement principle

As an active remote sensing instrument, the scatterometer emits a pulse of electromagnetic microwave (EM) radiation and measures the signal of the returning radiation. The signal of the returning EM radiation depends on the roughness of the sea surface. At the sea surface Bragg scattering occurs (Figure 2.5). This is when electromagnetic radiation and water waves of similar wave lengths interact. Because microwave radiation has a wavelength in the order of centimeters, constructive interference can occur causing the waves to remain in phase and reflect off the sea surface in all directions. The direction of reflection is influenced by the sea surface roughness. When the sea is very calm and nearly a flat surface during little wind, the radar beam is mostly reflected forward with very little backscatter back to the instrument. As the wind becomes stronger and waves become larger, Bragg scattering increases and a more intense signal is reflected back to the scatterometer (EUMeTrain, 2017). Because Bragg scattering only occurs with waves of similar wavelength, scatterometers are only sensitive to the wind-driven centimeter-scale capillary waves rather than very large waves (Stoffelen, 1998a).

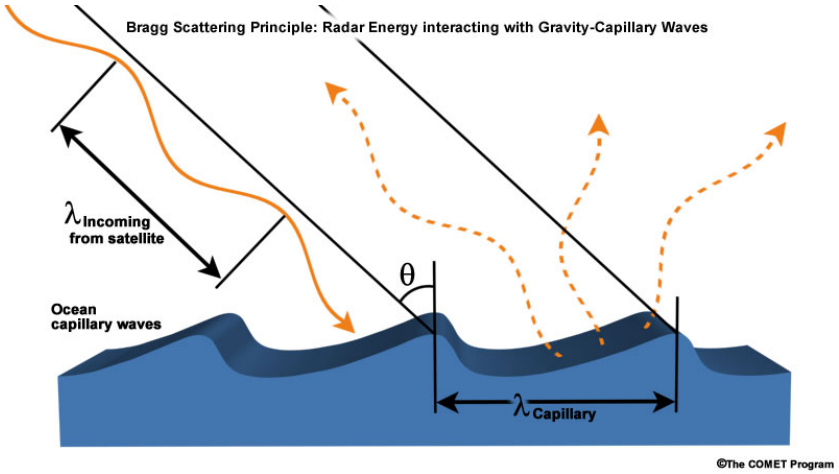

Figure 2.5: At the sea surface, a microwave radar beam emitted by a scatterometer interacts with capillary waves (cm order of magnitude) and is reflected in all directions. This is known as Bragg scattering. The intensity of the backscatter received at the scatterometer is dependent on the roughness of the ocean surface that is driven by the surface wind (Figure obtained from COMET, 2015).

There are many types of scatterometers having different operational frequencies, polarizations, antenna design and antenna look angles. In this research, surface winds observed by the European Advanced Scatterometer (ASCAT), a C-band with fixed fan-beam antenna, and Chinese Haiyang-2B, a Ku-band with rotating beam antenna, are used and described in the next two sections.

C-band with fixed fan-beam antenna

A fan-beam scatterometer, like ASCAT, contains multiple fixed antennas. ASCAT was launched by the European Space Agency (ESA) and operated by European Organisation for the Exploitation of Meteorological Satellites (EUMETSAT). ASCAT consists of a series of 3 scatterometers A, B and C, carried by

three individual satellites (Osi, 2019). ASCAT operates at a frequency of 5.255 GHz (corresponding to a wavelength of 5 cm) (EUMeTrain, 2017). This type of scatterometer is also known as a C-band radar.

ASCAT collects wind data from two sets of three vertically polarized antennas, each with a different azimuth and incidence angle. Observations from different angles are necessary to determine the wind direction. The incidence angles range between 25-65°because at these incidence angles the main backscattering mechanism is Bragg scattering (Figa-Saldaña et al., 2002). No energy is emitted directly below the scatterometer (where incidence angles are <25°) because at this angle only the forward scatter is observed which is less sensitive to wind speed and direction than the backscatter. ASCAT measures backscatter from two 550 km swaths that are separated by a nadir gap of approximately 670 km (COMET, 2015). A swath is divided into Wind Vector Cells (WVCs) of 25 by 25 km which is specific for the ASCAT data in this research. For each WVC, three independent backscatter measurements are obtained with a short time delay.

ASCAT is located on a sun-synchronous polar orbiting satellite. A sun-synchronous polar orbit crosses the polar regions and is synchronised to always be in the same position relative to the Sun (ESA, 2020). This means that the satellite always travels a certain region at the same local time. The Local Time Ascending Node when crossing the equator (LTAN) of ASCAT is 21.30 UTC and 12 hours later and earlier is the descending node. The MetOp satellite has a repeat cycle of 29 days, this is the time between two observations from the exact same location. As the Earth rotates, the satellite covers a different ground track in each subsequent cycle (Figure 2.6).

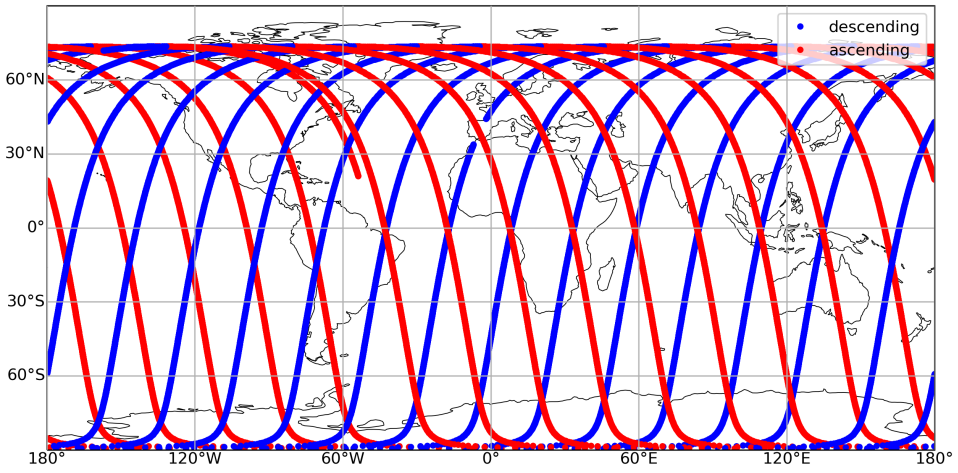

Figure 2.6: 24 hour satellite tracks of ascending and descending orbits of ASCAT-A located on Metop-A. The satellite has a higher coverage at the poles compared to other latitudes.

Ku-band with rotating pencil-beam antenna

A Ku-band scatterometer emits radiation at a frequency of 13.4 GHz (2 cm wavelength). Examples of Ku-band scatterometers are ScatSat-1 (OSCAT) and Haiyang-2B (HY-2B), this research mainly focuses on the latter. HY-2B was launched in 2018 by the Chinese National Satellite Ocean Application Service (NSOAS) and consists of a rotating pencil beam antenna (EUMeTrain, 2017). This allows the radar to cover all azimuth angles within a 1800 km wide swath. HY-2B emits a horizontally and vertically polarized beam at incidence angles of 42°and 48°respectively (SAF, 2021). Due to the rotational scanning, there are 4 measurements collected within each WVC; one while the scatterometer looks forward and one when it looks backward, by both horizontally and vertically polarized beams (SAF, 2021). A WVC is approximately 25 by 35 km. Furthermore the quality of the wind retrieval depends on the positioning of the backscatter in the swath, being poorest in the nadir and outer parts of the swath (Vogelzang and Stoffelen, 2018).

Like ASCAT, HY-2B also has a sun-synchronous polar orbit, but with different equator crossing times. HY-2B has an ascending node and descending node at 18.00 and 06.00 UTC respectively (Zhao et al., 2021).

Comparison of C-band vs Ku-band wind quality
Table 2.2 summarizes the different features that belong to ASCAT-A,B,C and Haiyang-2B, two different types of scatterometers. As a result of their different radar design, the quality of their wind retrievals also varies from one to another. Wind observations by ASCAT show more detail than by Haiyang (Stoffelen, 2019). This is because during the processing of Haiyang-2B backscatter, extra spatial filtering is necessary to determine the wind direction. This results in a smoother wind field. Additionally, C-band radars are less sensitive to rain than Ku-band because they operate at a lower frequency (Portabella et al., 2012; Dawei and Hui, 2015). However, a Ku-band scatterometer can observe higher wind speeds than a C-band scatterometer which is especially useful in regions where cyclones occur frequently. (EUMeTrain, 2017).

Table 2.2: Summary of scatterometer features of ASCAT-A,B,C and Haiyang-2B

	ASCAT-A,B,C	**HY-2B**
Orbit	Sun-synchronous	Sun-synchronous
LTAN	21:30	18:00
Frequency	C-band, 5.255 GHz	Ku-band, 13.4 GHz
Antenna	Fixed fan-beam	Rotating pencil-beam
Polarization	HH	HH + VV
Incidence angles	25-65°	41°+ 49°
Swath width	2x 550 km	1800 km
Spatial resolution	25 km	25 km

2.3.2. Wind data processing
A backscatter measured by the scatterometer is first normalized (σ_0) and then converted into a wind vector at 10 m (10-m winds are widely accepted), u_{10}, using three processing steps shown in Figure 2.7 (Stoffelen, 2019).

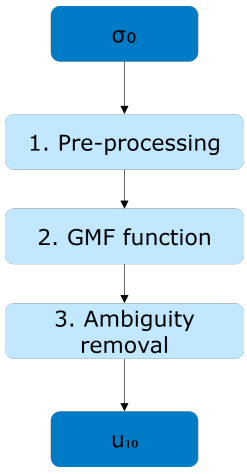

Figure 2.7: The 3 data processing steps that are taken to convert a normalized backscatter signal to a 10-m wind field.

First of all, the quality of the normalized backscatter measurement is checked if it is according to expectations. NWP model winds are used as reference wind in this first pre-processing step. Also, any noise signal is removed.

In the second step, the normalized backscatter signal is converted into a wind speed and set of possible wind directions using an empirical Geophysical Model Function (GMF). This function relates the normalized radar backscatter cross section to a 10-m (equivalent neutral) wind vector, u_{10N}, and is defined as follows (EUMeTrain, 2017):

$$\sigma_0 = GMF(u_{10N}, \theta, \phi, \rho, \lambda) \tag{2.1}$$

σ_0 is the backscatter cross section, θ represents the incidence angle, ϕ is the relative azimuth angle to determine wind direction, λ is the radar wavelength and ρ the radar polarization.

Besides the variables that are accounted for in the GMF function (equation 2.1), the intensity of the backscattered signal is also influenced by other factors. These factors include rain, salinity and sea surface temperature (SST) (Portabella et al., 2012; Wang et al., 2017). As the effects of these parameters are supposed to be small, they are not considered by the GMF. As a result, the function has the advantage of being independent of any NWP model (De Kloe et al., 2017). However, a disadvantage is that an average global wind profile for the atmosphere is used even though the profile shape varies according to the conditions (stable vs neutral vs unstable) of the atmospheric boundary layer ABL (De Kloe et al., 2017).

Finally, the inversion of the GMF function generates multiple wind vector solutions, usually two (for fixed fan-beam antennas) or more (for rotating pencil-beam scatterometers) (Vogelzang and Stoffelen, 2018; Stoffelen, 2019). This means that the latter requires additional spatial filtering to obtain a unique wind vector cell in this step. In order to remove the wind direction ambiguity and select the most accurate wind solution, the wind vector is compared to a background wind field. For example in ASCAT processing, operational ECMWF wind forecasts are used as reference wind. Explained in simple terms, the wind vector with the smallest error is chosen (Vogelzang and Stoffelen, 2018). As this step involves NWP model winds, there is a model influence in scatterometer wind measurements.

Level-4 winds

To obtain a global wind product, also referred to as a level-4 (L4) product, the wind speed and wind direction at the location of measurement are subjected to further data processing. The measured wind fields are interpolated to a regular grid in a level 3 product. So a level 3 product contains validated data mapped on a uniform space-time grid. When the gaps in a L3 product are filled with data from other instruments and models, a L4 product is produced (Figure 2.8). Thus a L4 product contains winds that are consistent in time and space.

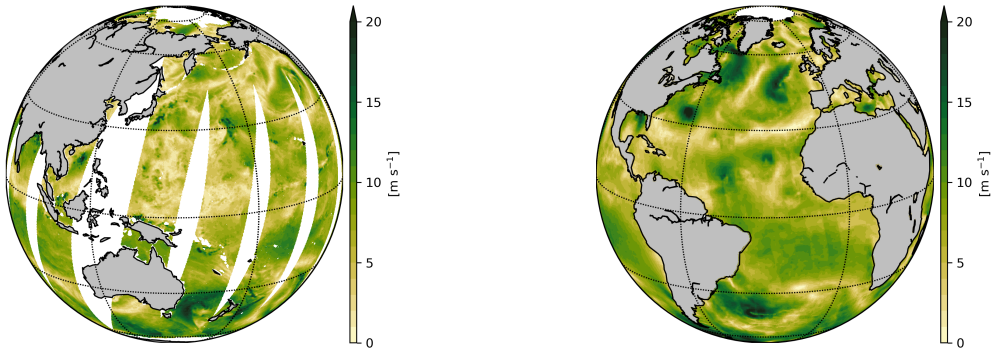

Figure 2.8: Difference between scatterometer data processed to a level-3 (left) and to a level-4 (right) product (produced by R. Giesen).

In this research, only L3 (HY-2B) and L4 (ERA5, IFREMER, ERA5*) data is worked with. This means that all data sources are provided on the same fixed regular grid. However, there may be differences in resolution and grid definition between the various sources.

Neutral- and stress-equivalent winds

For practical purposes, wind measurements are standardized by the World Meteorological Organisation at a height of 10-m, u_{10}. For example, NWP models produce such 10-m winds and measurements from moored buoys at a different altitude are rescaled to estimate a 10-m wind. A scatterometer measures the ocean surface roughness which is directly related to the stress exercised by the wind at the

ocean surface. This roughness is converted to a valid wind measurement at 10 m above the surface by inversion of the GMF function. The GMF function is traditionally derived using global statistics by comparing radar backscatter and NWP model 10-m winds (De Kloe et al., 2017). This means that the GMF is based on an average atmospheric wind profile, which tends to resemble neutral stability conditions, to translate the ocean surface roughness to a wind measurement at 10 m. Hence a 10-m scatterometer wind represents a neutral-equivalent wind. On the contrary, a NWP model provides the 10-m wind as the real local wind. As a result, during stable conditions, a NWP model wind will be too high at 10-m compared to the scatterometer 10-m result for a similar surface wind (see the red line in Figure 2.9a). For unstable conditions there is more mixing of momentum in the boundary layer and the vertical gradient in wind speed is more gradual. In this case the NWP model 10-m wind is too low compared to a neutral-equivalent 10-m scatterometer wind (see the blue line in Figure 2.9a). Therefore, during stable conditions the NWP model wind is adjusted to a lower wind speed and vice versa during unstable conditions.

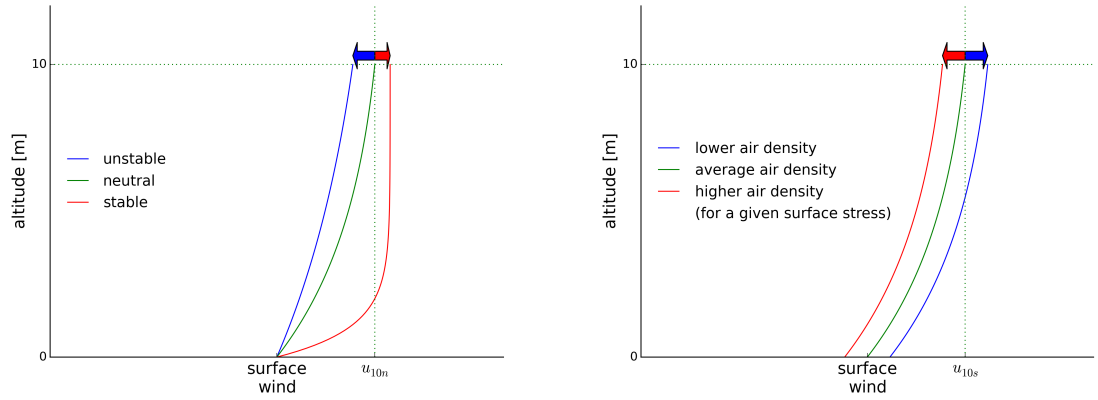

(a) Surface layer profile for different atmospheric stabilities

(b) Surface layer profile for different air mass densities

Figure 2.9: Schematic view showing the effect of the atmospheric stability (a) and air mass density (b) on the profile of the surface layer and how this leads to differences between 10-m winds (De Kloe et al., 2017).

The ”neutral wind conversion” applied to NWP model winds corrects for the stability of the surface atmospheric layer and consists of two steps. First, the NWP model 10-m winds are translated to near surface winds using a realistic profile of the atmosphere. The main information needed to estimate the atmospheric profile is the temperature difference between the ocean surface and the atmosphere just above the surface, i.e. if the water is warm and the air is cold, the air gets heated by the water, and it tends to rise upwards, leading to unstable conditions (De Kloe et al., 2017). On the other hand, if the ocean surface is cold and the air is warmer, the air cools down, and has no tendency to rise. These are stable conditions. Secondly, the near surface winds are relocated to 10 m using an average neutral wind profile. By converting NWP model winds to neutral-equivalent winds, a more fair comparison with scatterometer 10-m wind measurements is achieved.

In addition to a neutral wind conversion, De Kloe et al. (2017) presents another wind conversion of model winds to stress-equivalent winds (u_{10s}). The reason to prefer stress-equivalent winds over neutral-equivalent winds is the inclusion of air density that makes the comparison between satellite winds to buoys or NWP data physically more consistent than neutral-equivalent winds. This is because the scatterometer wind measurement is derived from an ocean stress observation that is directly related to the wind just above the ocean surface. The ocean stress is for the most part affected by the near surface wind and for a very small part by the air mass density through the coupling of the air and the ocean. The coupling between the air and ocean surface is affected by the mass density of the air, i.e. air with smaller mass density can transfer less momentum to the ocean surface than air with higher mass density, at the same surface wind. Thus a given surface wind will result in a higher ocean surface stress for higher air density and vice versa for lower air density. Since the GMF is derived using global statistics, an average air mass density is used in the fit between NWP model winds and radar backscat-

ter observations. As a consequence, for higher than average air density, a scatterometer surface wind that is scaled to 10 m height using an average air density profile will, produce a too low 10-m wind estimate in comparison to the 10-m NWP model wind (see red line in Figure 2.9b). This is because the scatterometer measurement is related to the real ocean surface wind stress that is present. For lower than average air density, the situation is opposite. A given NWP model neutral-equivalent 10-m wind will produce less ocean surface stress than is actually present. Instead of adjusting the GMF function, De Kloe et al. (2017) proposes an extra conversion to rescale model neutral equivalent winds to stress-equivalent winds based on the following relation:

$$u_{10s} = u_{10n}\sqrt{\frac{\rho_{air}}{\langle\rho_{air}\rangle}} \tag{2.2}$$

where $\langle\rho_{air}\rangle$ is a global average air density above the ocean ($1.225\,\mathrm{kg/m^3}$). The effect of stress-equivalent wind adjustments is smaller than a neutral-equivalent wind conversion. At higher latitudes above 60°where the atmosphere has lower temperatures and therefore higher mass density, the correction becomes more relevant than at lower latitudes. For example, in February the air in the Northern polar region is very cold resulting in a larger difference (>0.5 m/s) between neutral- and stress-equivalent winds compared to the rest of the world (<0.2 m/s) Figure 2.10.

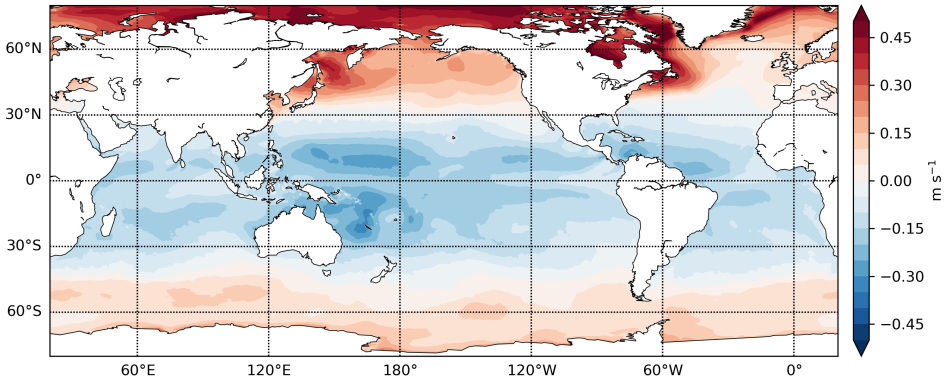

Figure 2.10: Average difference between u_{10s} and u_{10n} ERA5 winds between 1-28 February 2019 (produced by R. Giesen, after De Kloe et al. (2017).

3

Data & Methods

Global wind fields from four different data sources, i.e., IFREMER, ERA5*, ERA5 and Haiyang-2B, are used in this study for the year 2019. These data sets are freely available online for any user. To compare and evaluate IFREMER and ERA5* winds in terms of spatial (how well are small spatial scales resolved) and temporal resolution (how accurate are the winds in time), they are collocated with Haiyang-2B winds. This chapter describes each data source and the methodology that is applied in this study.

3.1. Data sources

Each data source is provided as NetCDF-4 format. The variables that are of interest in this study are the zonal (u) and meridional (v) wind components from which a third variable, wind speed (ws), is computed:

$$ws = \sqrt{u^2 + v^2} \tag{3.1}$$

Other variables that are imported from each data source are: the measurement time (from seconds since a reference date to the corresponding date and time) and quality flags (such as land-sea flag). Table 3.2 gives an overview of the technical characteristics of each data source.

3.1.1. L4 wind products

The two main data sources of interest in this study are IFREMER and ERA5. Both are level-4 (L4) wind products constructed from a combination of wind observations by satellite-based instruments and model reanalysis (Table 3.1).

IFREMER

In this study IFREMER winds refer to the IFREMER CERSAT Global Blended Mean Wind Fields, produced by Institut Francais de Recherche pour l'Exploitation de la mer (IFREMER) for the past 20 years. The IFREMER wind product for 2019 was downloaded from the Surface Wind Wind Thematic Assembly Centre (Wind TAC) under the 'Global Ocean Wind L4 Reprocessed 6-hourly Observations', within Copernicus Marine Environment Monitoring Service (CMEMS). The 6-hourly IFREMER wind product is available at a regular longitude and latitude grid of 0.25° resolution, within latitude range -80°-80°. Although Bentamy and Fillon (2012) suggest that the IFREMER winds represent a 6-hourly average, it is suspected that this is not the case.

At every synoptic IFREMER time (00h:00, 06h:00, 12h:00, 18h:00 UTC), a wind field is computed based on all observations from scatterometers (ASCAT-A,B,C and ScatSat-1) and radiometers (SSMIS F17, F18 and WindSat). L4 winds are calculated by applying the objective method, based on the kriging technique with external drift, on these observations and ERA5 wind analyses to fill missing gridcells (Bentamy et al., 2020). In simple terms this means that for a specific location firstly all scatterometer observations within a 6-hour interval are considered (for a visualisation of 6-hourly observations see Figure A.3 in appendix A.2). The scatterometer inputs that are used are ASCAT-A, ASCAT-B and

ScatSat-1. If this leads to a poor spatial coverage, additional radiometer observations from the same 6-hour interval are used. The radiometer data is provided by the Special Sensor Microwave Image Sounder (SSMIS) on F17 and F18 and by WindSat (see Table 3.1). To fill any gaps, remote sensing observations from a 12-hour window are interpolated using the kriging technique with ERA5 neutral-equivalent winds. The method was originally developed for the calculation of daily averaged winds from scatterometers only (Bentamy and Fillon, 2012). A more detailed visualisation of the IFREMER method is given in A.1.

ERA5*
The ERA5* level-4 winds for 2019 were retrieved from the website of the World Ocean Circulation project (www.worldoceancirculation.org/). It is the only data set covering a year of data generated with the scatterometer correction applied to ERA5, as described in (Trindade et al., 2014). The ERA5 hourly wind fields represent stress-equivalent 10-m winds produced from short-term forecasts. A scatterometer correction, defined as a running mean computed from all ASCAT-A,B,C and ScatSat-1 OSCAT observations within a 3-day window, is applied to every hourly ERA5 wind to obtain an hourly ERA5* wind field. ERA5* winds are provided at a regular level 4 grid and at a 0.125° spatial resolution.

ERA5* is based on ERA5 with a scatterometer-based correction to improve the surface wind fields in ERA5. The aim on a longer term is to provide an improved ocean forcing product for the ocean modeling community (Trindade et al., 2014). The methodology of ERA5* can be summarized in three main steps:

1. 10-m stress-equivalent (U10S) meridional and zonal wind components from scatterometer sensors are spatially interpolated to a regular 12.5 by 12.5 km level 3 (L3) grid.
2. ERA5 winds are converted from 10-m neutral-equivalent (U10N) to U10S for consistency with the scatterometer defined winds. They are also interpolated to the L3 grid.
3. At every grid point and time sample, a scatterometer based correction is applied. In case there is poor scatterometer sampling and some scatterometer based corrections have a gap, these gaps are filled with KNMI U10S ERA5 winds only.

The scatterometer correction that is applied to ERA5 is based on a 3-day averaged difference between collocated scatterometer observations and ERA5 winds at a specific location (x,y) and time (t_f) (for a detailed example see Figure A.5 in appendix A.3). The scatterometer observations used for the correction are retrieved from different scatterometers, k (summarized in Table 3.1). By combining measurements from the different scatterometers, more wind observations can be used to enhance the L4 ERA5* wind product (Trindade et al., 2014). The SC procedure is generalized in equations 3.2 and 3.3, where M represents the total collocated scatterometer observations within a 3-day interval ($t_f \pm$ 1.5 day).

$$SC(x, y, t_f) = \frac{1}{M} \sum_{t=1}^{M} (u_{10S}^{SCAT_k}(x, y, t) - u_{10S}^{ERA5}(x, y, t) \tag{3.2}$$

$$u_{10S}^{ERA5*}(x, y, t_f) = u_{10S}^{ERA5}(x, y, t_f) + SC(x, y, t_f) \tag{3.3}$$

Comparison of IFREMER and ERA5* characteristics
IFREMER and ERA5* wind products consist of the same scatterometer observations. Additionally, IFREMER uses radiometer observations. Both L4 wind products involve ERA5 data, whereby IFREMER applies analyses and neutral-equivalent winds and ERA5* is based on ERA5 stress-equivalent forecasts (Table 3.1).

In order to illustrate the different features of the two different L4 wind products, the wind fields of each wind product were considered separately using a case of a frontal weather system that occurred off the East coast of Japan on 1 February 2019 at 12:00 UTC (Figure 3.1). The ERA5 neutral-equivalent analysis was also plotted as reference comparison.

Table 3.1: Comparison of data sources that are used in the IFREMER and ERA5* wind products

Input data	Frequency (GHz)	Swat width (km)	Repeat cycle (days)	LTDN, LTAN	IFREMER	ERA5*
Scatterometer						
ASCAT-A	C-band	2 x 550	29	9:30, 21:30	yes	yes
ASCAT-B	C-band	2 x 550	29	9:30, 21:30	yes	yes
ASCAT-C	C-band	2 x 550	29	9:30, 21:30	yes	yes
ScatSat-1	Ku-band	1800	2	8:45, 20:45	yes	yes
Radiometer						
SSMIS F17	19.35-85.5	-	-	18:37	yes	no
SSMIS F18	19.35-85.5	-	-	16:32	yes	no
WindSat	6.8-37	-	-	18:00	yes	no
Model						
ERA5	n.a.	n.a.	n.a.	n.a.	Analyses, neutral wind	Forecasts, stress-equivalent wind

ERA5* winds show the most spatial variability compared to IFREMER and ERA5 (Figure 3.1). In fact, the front that is visible in Figure 3.1b is less well resolved by IFREMER in Figure 3.1a. This difference is probably a consequence of ERA5* being an hourly product while IFREMER is a 6-hourly product. A 6-hourly product can never capture the spatial detail of a hourly product. Although frontal systems usually exist for several days, there will be variation in the front over a 6-hour interval. It seems like IFREMER depicts this variation less well than ERA5*. Besides that the front is less well defined for IFREMER, it also contains block-like structures that may result from the spatial interpolation, which are not seen in ERA5* and ERA5. Overall, all 3 figures show a similar spatial distribution of high and low zonal wind speeds, whereby IFREMER shows higher wind speeds (>18 m/s) in regions where ERA5* and ERA5 reach up to 16 m/s.

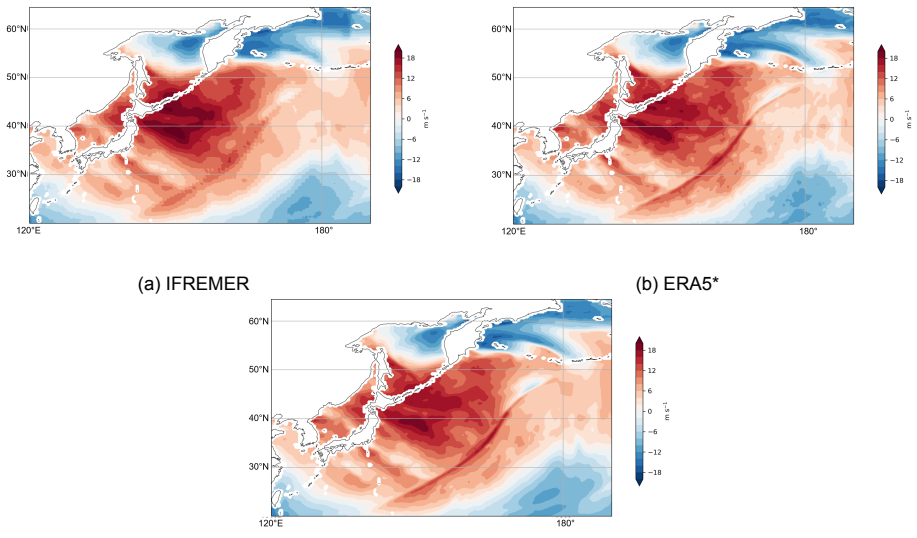

(a) IFREMER (b) ERA5*

(c) ERA5

Figure 3.1: A case of a frontal weather system that occurred off the East coast of Japan on 1 February 2019 at 12:00 UTC. Zonal wind speed for IFREMER (a), ERA5* (b) and ERA5 (c). Colors indicate the wind speed in m/s.

.

3.1.2. ERA5

ERA5 stress-equivalent (analysis and forecast) winds are obtained from the Meteorological Archival & Retrieval System (MARS) at a 0.25°grid spatial resolution and hourly time resolution. ERA5 hourly forecasts are constructed from two analysis fields at 09h:00 and 21h:00 UTC. All observations within the 12-hourly window between these two analysis times are assimilated (Hersbach et al., 2020). The starting point for an analysis fields is initiated 9 hours before, at 18h:00 and 06h:00 respectively. ERA5 winds are generated with the Integrated Forecasting System (IFS) Cy41r2 which was operational in 2016 by ECMWF.

3.1.3. HY-2B scatterometer

HY-2B data is not included in either the IFREMER or ERA5* product and was therefore chosen as independent scatterometer for validation purposes. An alternative independent scatterometer to HY-2B that was also considered due to its availability for 2019 data was HY-2A. However, HY-2B was preferred because of its improved quality of wind measurements compared to HY-2A (Yang and Zhang, 2018).

The HY-2B data was provided as level-3 product on a regular 0.25°x 0.25°grid, separated in ascending and descending orbital track files to avoid data loss, by the Koninklijk Nederlands Meteorologisch Instituut (KNMI). One complete (ascending and descending) orbit lasts for approximately 104 minutes, thus one orbit file covers half of this time (approximately 50 minutes). During one day there are around 27 orbit files available. However, in reality the number of orbit files varies from day to day. This is because on some days, certain orbits may be missing because of varying reasons, such as technical deficiencies of the spectrometer instrument. For IFREMER, ERA5* and ERA5, there are 4, 24 and 24 data files available per day respectively.

All scatterometers in this research are situated on satellites in sun-synchronous orbit. They travel over the polar regions several times a day and always observe a point on Earth at the equator at the same local time of the day. For example, the equator crossing Local Time of the Ascending Node (LTAN) of HY-2B is 18:00 UTC and 21:30 UTC of ASCAT-A,B and C. The Local Time of the Descending Node (LTDN) is 12 hours earlier/later. Furthermore, HY-2B is a rotating pencil-beam scatterometer that operates at Ku-band frequency and is known to be more sensitive to rain (Dawei and Hui, 2015) and sea surface temperature (SST) effects than C-band scatterometers (Wang et al., 2016, 2017). ASCAT-A,B,C all operate at C-band frequency (fan-beam scatterometers) and are therefore less sensitive to rain (Portabella et al., 2012).

Table 3.2 presents an overview of the different data sources that are used in this research.

Table 3.2: Overview of technical characteristics of IFREMER, ERA5*, HY-2B and ERA5 data sources

Data source	**IFREMER**	**ERA5***	**ERA5**	**HY-2B**
Time period	2019, 6-hourly	2019, hourly	2019, hourly	2019, orbital
Resolution	0.25	0.125	0.25	0.25
Stress- vs neutral	Neutral	Stress-equivalent	Stress-equivalent	Stress-equivalent
Model data	Analysis	Forecast	Forecast	Forecast
Representation	Average	Instantaneous	Instantaneous	Instantaneous
Latitude range	[-80, 80]	[-89.9375, 89.9375]	[-89.8750, 89.8750]	[-89.8750, 89.8750]
Longitude range	[-180, 179.75]	[-179.9375, 179.9375]	[0.125, 359.8750]	[0.125, 359.8750]
Institutional source	IFREMER	ICM	MARS	KNMI

3.2. Data Processing

For verification with HY2B winds, the IFREMER, ERA5* and ERA5 winds are collocated to HY2B winds in space and time. ERA5 winds are already defined at the same grid points as HY2B winds. However, before collocation, IFREMER and ERA5* are first processed to the same coordinate grid points as HY2B (see table 3.2 for defined latitude and longitude coordinates). Secondly, all data points that are covered by land or partly covered by land are removed by applying the land-sea flag that is included in each IFREMER and ERA5* product. These two steps are crucial to ensure a fair comparison and consider only data of interest, i.e. ocean surface wind data.

3.2.1. Grid and resolution

The IFREMER and ERA5* L4 products were processed to the same latitude and longitude grid. First, all data sets are shifted and/or flipped to the same range and order of coordinates. The range of latitude coordinates includes [80, -80] as beyond this range no data is available for the IFREMER product. The longitude coordinates range from [0, 360] and cover the entire globe.

While the IFREMER and ERA5 winds are available at a resolution of 0.25°, ERA5* winds are defined on a finer grid of 0.125°. The HY-2B L3 data is available at a 0.25°grid. When defining the methodology for a fair comparison, a choice had to be made to use ERA5* at 0.12°resolution or reduce its resolution to 0.25°to match the other data sets. Because the goal of this study is to evaluate ERA5* winds, it was preferred to use ERA5* at its original resolution of 0.125°.

3.2.2. Land-sea-ice mask

The focus of this research is wind observations from only the oceans because there are no scatterometer observations available over land. Filtering out data points over land can be achieved by means of a land-sea mask. The IFREMER and ERA5* L4 wind products each provide their own land-sea-ice mask which differs from each other. To ensure that both data sets only consider the same grid cells with valid ocean winds, it is important that a consistent land-sea-ice mask is applied. In order to achieve this, the ERA5 land-sea mask was applied to both IFREMER and ERA5* in the wind difference fields with ERA5. In the HY-2B wind collocations, ERA5* and IFREMER each applied their own land-sea ice mask. These data points are flagged. A conservative approach was chosen. This means that when reading the collocated wind fields all data points flagged by either IFREMER or ERA5* were removed to ensure consistency between the compared winds. For a full description of application of the the land-sea-ice mask, please refer to appendix B.

3.3. Collocation of data sources

In dual collocation, two independent data sets are brought together. Collocation involves the selection of data points from both data sets that overlap in time and space, possibly making use of interpolation. By collocating each data source (IFREMER, ERA5* and ERA5) with independent HY-2B winds the different wind fields can be compared. If HY-2B winds are assumed to be perfect (which they are not), then the wind differences with either IFREMER, ERA5* and ERA5 can be considered as errors. However, it should be noted that there are also other factors that can cause these differences such as differences in temporal and spatial representation (Vogelzang and Stoffelen, 2012).

HY-2B was chosen as independent scatterometer because its data is not used in either IFREMER and ERA5*. That is also the reason that ECMWF NWP reanalysis data was not an option as ERA5* is a corrected version of ERA5. Also, in-situ measurements such as buoy data were not chosen due to their lack of spatial coverage. However, buoy data could be an interesting additional data set in triple collocation analysis. As moored buoys are predominantly located in the tropics and coastal regions, this analysis would be restricted to these locations.

By means of collocation, an estimate of the average and variance of differences for IFREMER and ERA5* could be obtained for the year 2019. Each data source (IFREMER, ERA5* and ERA5) is brought together in time and space to HY-2B winds before they can be fairly compared to one another. The collocation procedure consists of three steps which are described below.

3.3.1. Step 1: Collocating data files in time

A HY-2B orbit file is taken as starting point for the collocation. Alternatively, another data source file such as ERA5* could have been chosen. As IFREMER and ERA5* both require validation via HY-2B, it was most logical to search for IFREMER and ERA5* data files that overlap with one HY-2B file in time rather than vice versa. Another reason why HY-2B was preferred as lead off is that it contains the least number of data points in space and time. If a L4-product was chosen instead, then there would always be a greater number of data points without a matching HY-2B field. Moreover, the coordinates of a L4-product are constant in time and space, therefore one can precisely know where to search to couple a HY-2B wind to a corresponding L4 data point.

Only one output collocation file was created, in which every data source is collocated to HY-2B. The main reason for combining the collocated wind fields of different sources in one output file is because combinations of only data points available across all data sources can easily be selected. In addition, the creation of one output file requires less computational power than if a separate collocation file were to be produced for each data source (IFREMER, ERA5* and ERA5) separately. A visual representation of collocating the 4 four different data files in time is shown in Figure 3.2. It should be noted that multiple, usually no more than two, ERA5*, ERA5 and IFREMER can overlap with one HY-2B file.

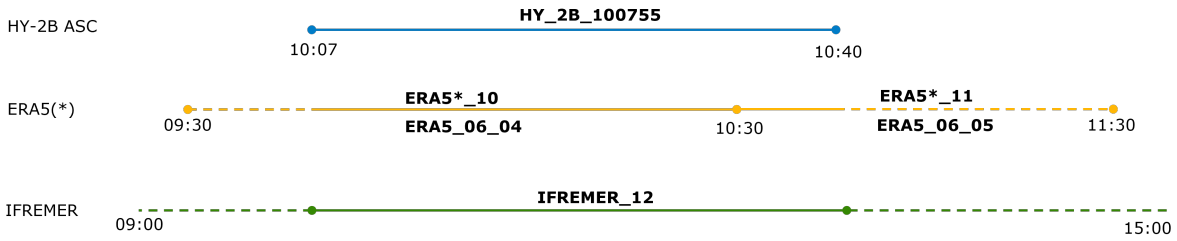

Figure 3.2: Example of collocating IFREMER, ERA5* and ERA5 files in time to one HY-2B file.

3.3.2. Step 2: Applying quality control flags

In the second collocation step, the variables of interest of each data set are read and checked on their quality. During quality control, all data points that could possibly have a reduced quality due to the presence of rain, ice, land or other reasons causing wind retrieval to work less well are removed. From each data set, the latitude and longitude coordinates, zonal wind (u) and meridional wind (v) and quality control flags are read. On top of that the wind vector cell index of the scatterometer data is also imported.
The quality flags of IFREMER, ERA5*, ERA5 and HY-2B are different. Especially for the latter, the quality control flags are crucial to select only wind observations that are valid and remove all other contaminated ones. Before the flags are applied, all missing data values are first removed. The quality flags from HY-2B that are applied in this research are:

- KNMI flag: KNMI quality control (including rain) rejection (#131072)
- Ice flag: some portion of the wind vector cell is over ice (#16384)
- Land flag: some portion of the wind vector cell is over land (#32768)
- KP flag: any beam noise content above threshold (#1048576)
- Invert flag: not enough good σ_0 available for wind retrieval (#8192)
- Rain flag: rain flag algorithm detects rain (#512)

redAnother form of scatterometer quality control, is to distinguish between wind retrieval from the outer/sweet/inner swath. This could be a suggestion of future.
Both IFREMER and ERA5* contain only a land-sea flag that discards all data points above land or (sea) ice. Next to the importance of selecting valid data points only, the IFREMER and ERA5* data sets are shifted 180°to match the longitude range of HY-2B (see 3.2 for detailed longitude coordinates).

3.3.3. Step 3: Collocating wind fields in time and space

Once all variables of interest of the different data sources have been quality checked and shifted to the same order of longitude coordinates as HY-2B, it is time for the collocation of wind fields in time and space. For each HY-2B observation, the ERA5*, IFREMER and ERA5 file that overlaps in time is selected (only applicable when multiple data files match with the period covered by the Hy-2B orbit file).
As ERA5 is already interpolated to the exact same grid as HY-2B, the corresponding ERA5 wind field at the same latitude and longitude coordinates as the HY-2B observation is found. For IFREMER and ERA5*, an extra interpolation step is required. For every HY-2B observation, the four closest IFREMER and ERA5* wind fields are selected and averaged with equal weights to obtain an estimate of the wind field at the same coordinates as HY-2B (see Figure 3.3).

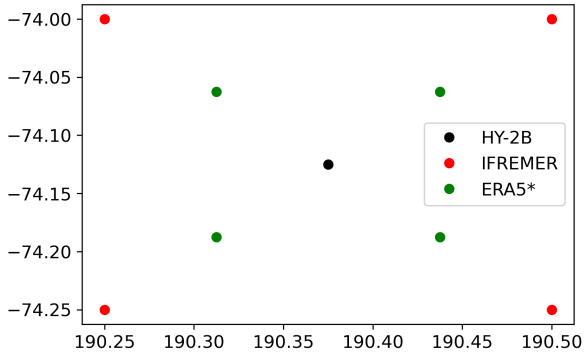

Figure 3.3: Example of IFREMER and ERA5* wind fields that are interpolated to the same grid point as HY-2B wind field. The interpolation is carried out by averaging with equal weights.

Before assigning the collocated wind fields to a new text file, one final check is carried out to preserve the accuracy of the data. Only if all four IFREMER or ERA5* wind fields are valid (i.e. not one of the wind fields is masked due to land or ice contamination), is the new averaged wind fields considered valid. Otherwise, the averaged wind field is assigned a NaN value together with an extra flag value of 1 to indicate that it is not included due to land/ice contamination.

3.4. Statistical parameters

The ASC and DES collocated data files are analysed separately because ascending orbits occur under different conditions to descending orbits. Ascending HY-2B orbits cross the equator at local time 18:00 whereas the local time of the descending node (LTDN) is 06:00. Thus ascending observations give an indications of wind conditions at the end of the day and descending observations give an indication of wind conditions at the end of the night/early morning. The distinction between day and nighttime observations is advantageous to distinguish certain weather phenomena such as tropical thunderstorms that occur mostly during the day.

For a fair analysis, only HY-2B collocated winds that are available across all data sets (IFREMER, ERA5* and ERA5) are considered. For example, this means that only wind data within -80°to 80°latitude are considered as no IFREMER data is available outside this range. Furthermore, the quality control flags by HY-2B are applied.

To give insights in the product characterisation of ERA5* and IFREMER and quantify the found differences with HY-2B, several statistical parameters are computed. The statistics are applied to both zonal (u) and meridional (v) wind components and wind speed (ws). As the same methodology is used for all three wind variables, only the zonal component equations are shown in this section.

Mean

The mean represents the average wind deviation of data set B (eg. IFREMER or ERA5*) to data set A, where A represents the 'true' wind observed by HY-2B. The mean of the differences between two data sets gives an indication of the bias and accuracy of IFREMER or ERA5* wind. Firstly, the difference

between two wind fields (Δu) at a specific grid point (x,y) is computed in equation 3.4, followed by the mean ($\overline{\Delta u}$) of the differences at this grid point over a certain period in time (T) in equation 3.5.

$$\Delta u_{AB}(x,y,t) = u_A(x,y,t) - u_B(x,y,t) \tag{3.4}$$

$$\overline{\Delta u}_{x,y,T} = \frac{1}{T}\sum_{t=1}^{T} \Delta u_{x,y,t} \tag{3.5}$$

To compare the mean of the differences across multiple climate zones, the mean is computed by latitude bin (either per 5°or 1°). The computation of this mean ($\overline{\Delta u}_{XYT}$) is shown in equation 3.6.

$$\overline{\Delta u}_{XYT} = \frac{1}{T}\frac{1}{Y}\frac{1}{X}\sum_{t=1}^{T}\sum_{y=1}^{Y}\sum_{x=1}^{X} \Delta u_{x,y,t} \tag{3.6}$$

A weighted mean is used when the input is binned data (n) via 2D histograms, taking into account the frequency of occurrence of a data point as weight (w_i). The weighted mean (Δu) over a number of data points N is calculated as:

$$\overline{\Delta u}_{NT} = \frac{1}{N}\frac{1}{T}\sum_{n=1}^{N}\sum_{t=1}^{T} \Delta u_{n,t} * w_i \tag{3.7}$$

Standard deviation

Whereas the mean quantifies the bias of a data set (when compared to a 'true' reference system), the standard deviation (σ) gives insights into the dispersion of these differences, i.e. the amount of variation between the differences in comparison to the mean difference. σ is independent of the bias and therefore a valuable statistical parameter used to comment on the precision of a data set.

A low standard deviation indicates that many differences lie close to the mean difference, while a high standard deviation indicates that the differences are spread out over a wider range. In this analysis, the standard deviation of the wind fields of one data set as well as the standard deviation of the wind differences between two different data products is computed, the latter is shown in equation 3.8.

$$\sigma\Delta u_{x,y,T} = \sqrt{\frac{1}{T}\sum_{t=1}^{T}(\Delta u_{x,y,t} - \overline{\Delta u}_{x,y,T})^2} \tag{3.8}$$

where Δu represents the difference of zonal wind (eq. 3.4), $\overline{\Delta u}$ is the mean difference at grid point (x,y) and N is the number of HY-2B collocations at grid point (x,y) in time sample T. Thus x refers to the longitude coordinate and y to the latitude coordinate.

To compare the standard deviation of the differences across multiple climate zones, the standard deviation is averaged over latitudes (either per 5°or 1°latitude bin). The computation of this standard deviation (σ_{XYT}) is shown in equation 3.9.

$$\sigma\Delta u_{XYT} = \sqrt{\frac{1}{T}\frac{1}{Y}\frac{1}{X}\sum_{t=1}^{N}\sum_{y=1}^{Y}\sum_{x=1}^{X}(\Delta u_{x,y,t} - \overline{\Delta u}_{XYT})^2} \tag{3.9}$$

where t is the total number of differences in a given time interval T (eg. 2019), Y is the total number of differences in a given latitude bin (e.g. between 0°- 5°) across all longitudes (X).

Root Mean Square Difference (RMSD)
To quantify the correlation in the scatter plots, the root-mean square difference (RMSD) is included. RMSD measures the dispersion of ERA5* or IFREMER around HY-2B, considered to be the true wind, and therefore is a measure of accuracy. A smaller RMSD indicates better correspondence between two data sets. It should be noted that RMSD does not exclude any bias effects between 2 data sets.

$$\mathrm{RMSD}_{HY2B,ERA5*} = \sqrt{\frac{1}{N}\sum_{i=1}^{N}((u_{HY2B,i} - u_{ERA5*,i})^2} \tag{3.10}$$

where N is the total number of collocations in a given sample and i is a collocated wind value.

Pearson's correlation coefficient (r)
A common method to express the correlation between two data sets is via Pearson's correlation coefficient (Wikipedia, 2022). This is a normalized measure of statistical dependency of one data set on the other. A value close to 1 represents a perfect correlation. Because Pearson's correlation coefficient is computed by using two histograms as input, Pearson's computation includes the weight of a data point based on its frequency of occurrence.

4

Results

In this chapter the results of the IFREMER and ERA5* wind product comparisons with firstly ERA5, and secondly HY-2B are presented and analysed. The results are quantified using statistical parameters. This chapter presents the results of this validation through a yearly and seasonal analysis in terms of mean and standard deviation of the differences on a global scale.

4.1. Product characteristics

4.1.1. Short timescales

By comparing the IFREMER and ERA5* wind products to ERA5, an improved understanding of the temporal and spatial characteristics of each L4 product over short-time scales (less than a month) is obtained. As all three data sets are available on a regular level 4 grid, the IFREMER, ERA5* and ERA5 wind data can be directly compared to one another in space. To ensure that only winds occurring at the same location are compared, ERA5* is first reduced to a 0.25°grid by averaging with equal weight to match ERA5 resolution winds. Furthermore, in this comparison it should be noted that 6-hourly IFREMER wind fields are used versus hourly IFREMER and ERA5* wind fields. It was not decided to look at 6-hourly averaged ERA5 or ERA5* because the focus of this comparison is to gain insights of the spatial behaviour of each L4 product in comparison to ERA5.

IFREMER and ERA5* differences with ERA5 were computed and averaged for different timescales. A difference wind field was obtained by subtracting ERA5 neutral-equivalent winds and ERA5 stress-equivalent winds from IFREMER and ERA5* respectively. These differences for all three wind variables were averaged for a day, week and month in 2019. Here, the meridional wind component (v) is included because it shows the ERA5 systematic bias of Figure 1.2 most clearly (see appendix C for zonal wind and wind speed).

The largest (>1 m/s) differences between ERA5 and ERA5* that are still visible in weekly and monthly averages occur in the tropics (Figure 4.1). These differences in the tropics represent the scatterometer correction that is applied in ERA5* and are in line with the bias of Figure 1.2. In some regions, such as West of Africa, the differences found in these results tend to be larger (>1 m/s) than the systematic bias (<1 m/s) found by Belmonte Rivas and Stoffelen (2019). This is most likely because their study was based on a yearly average compared to a monthly average used in this study.

For ERA5 differences with IFREMER, the largest daily averaged differences occur at higher latitudes. However, these differences at higher latitudes diminish when averaging for a week and month. In fact, the differences between IFREMER and ERA5 become smaller when averaging over a longer period of time. The close resemblance of IFREMER to ERA5 is surprising because, based on their methodology description, one would expect IFREMER to mainly use scatterometer observations and only little ERA5 data (Desbiolles et al., 2017). If IFREMER would rely more on scatterometer observations than ERA5, then larger differences with ERA5 than ERA5*, which relies heavily on ERA5, would be anticipated. Yet, an opposite trend is visible suggesting that IFREMER includes more ERA5 data than their

methodology suggests.

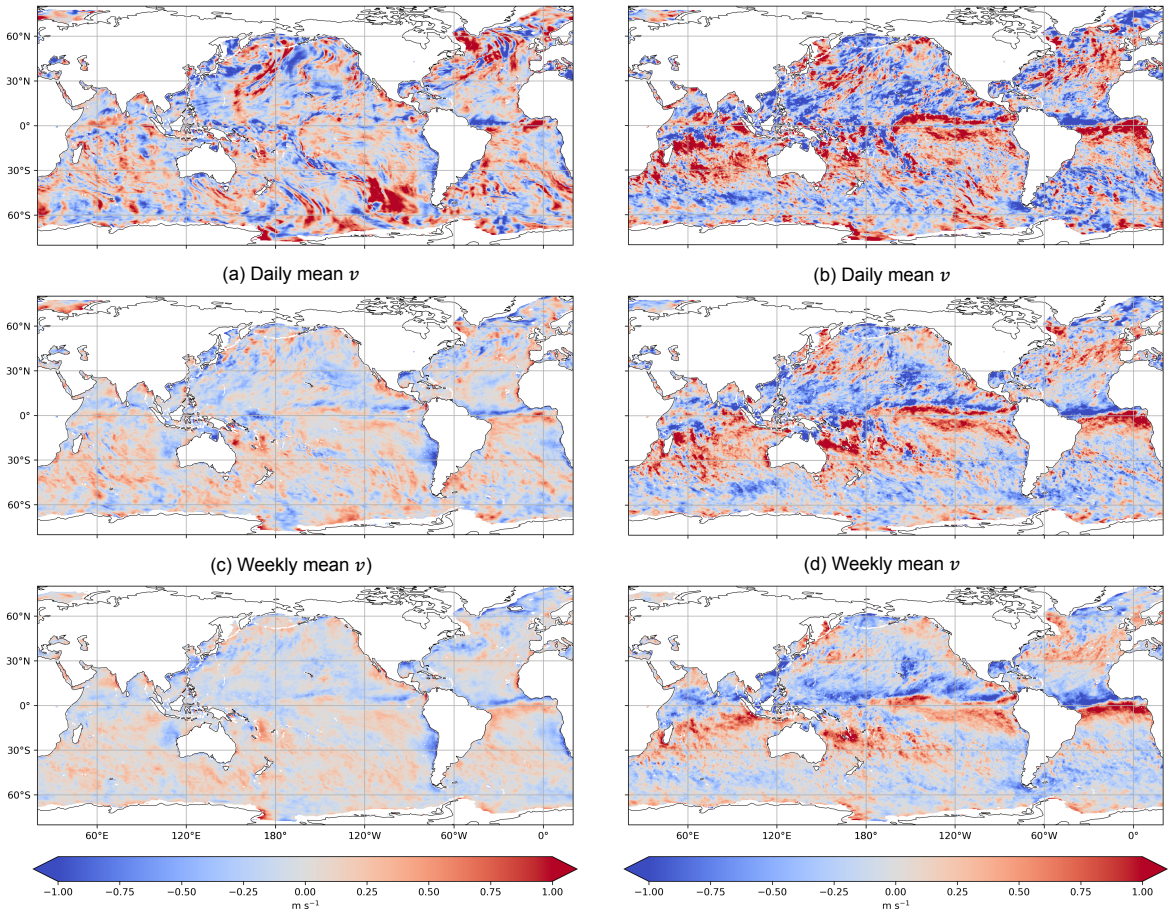

(a) Daily mean v

(b) Daily mean v

(c) Weekly mean v)

(d) Weekly mean v

(e) Monthly mean v

(f) Monthly mean v

Figure 4.1: Mean meridional wind (v) differences between IFREMER and ERA5 (a, c, e) and ERA5* and ERA5 (b, d, f) averaged over a day (2 February 2019), a week (2-9 February 2019), and a month (February 2019) plotted on a 0.25°grid. Positive differences in red indicate that ERA5 is larger than either IFREMER or ERA5*.

4.1.2. Individual wind data points

To examine the accuracy of the ERA5* and IFREMER wind fields, their wind fields were compared to wind observations from an independent scatterometer Haiyang-2B (HY-2B), whereby HY-2B served as a proxy for true wind. ERA5*, IFREMER and ERA5 (included for comparison) were collocated to HY-2B winds in time and space for the year 2019. Considering the 12 hour difference between HY-2B wind observations during an ascending and descending orbit, and hence change in weather, the orbital data are analysed separately. As the correlation results between ASC and DES rarely differed, this validation section only uses ASC figures (DES figures can be found in appendix D.

The correlation of IFREMER and ERA5* with HY-2B for the meridional and zonal wind components differ from one another in a number of respects. The scatter cloud for the zonal wind (u) of IFREMER is wider than of ERA5* (Figure 4.2). The RMSD in u for IFREMER is also higher than for ERA5*, 1.35 versus 1.17 m/s respectively. Likewise, IFREMER has a larger RMSD in v than ERA5*. The RMSD in v for IFREMER is 1.41 m/s which means that the spread between IFREMER and HY-2B has increased in comparison to u. By eye, the scatter cloud in v is also wider than in u. The RMSD in v for ERA5* is 1.13 m/s. This suggests that ERA5* meridional winds are more closely correlated to HY-2B than its zonal winds whereas an opposite trend is visible for IFREMER.

In comparison to the individual wind components, the IFREMER and ERA5* wind speeds are better

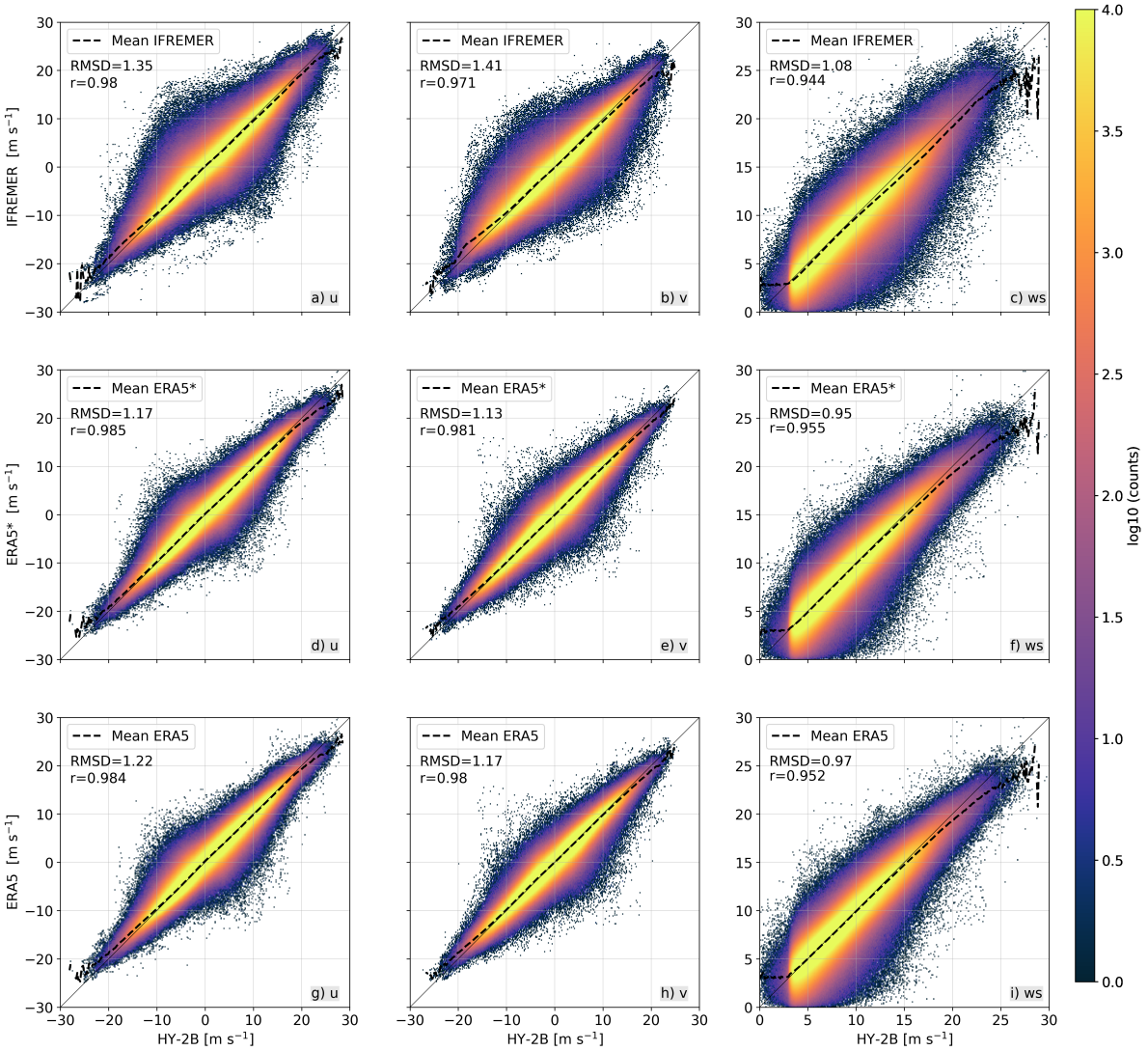

Figure 4.2: HY-2B global ascending quality-controlled winds for 2019 plotted against collocated IFREMER winds (a,b,c), ERA5* winds (d,e,f) and ERA5 winds (g,h,i) for variables u, v and ws..

correlated to HY-2B. This is illustrated by a higher Pearson correlation coefficient (r) and lower RMSD of 1.08 and 0.95 m/s for IFREMER and ERA5* respectively. A remarkable observation to point out is the cutoff of HY-2B winds at approximately 3 m/s (Figure 4.2). Also, the individual meridional and especially the zonal wind components show a slight twist around roughly 3 m/s. Even if the twist is only noticeable to some degree, it seems that there are significantly fewer observations of HY-2B winds below 3 m/s. Since the cutoff is present in the wind speed correlations of all three IFREMER, ERA5* and ERA5 sources, it is most likely that the significant reduction of HY-2B wind speeds <3 m/s is a result of the HY-2B scatterometer quality control.

On average, it can be concluded that for u and v scatter plots, the IFREMER and ERA5* averaged winds between -10 and 10 m/s approach the 1:1 line well (Figure 4.2). The good correlation is also denoted by a Pearson correlation coefficient close to 1 (between 0.94 - 0.99). ERA5* has a higher r than IFREMER for all three variables. This is also seen by eye by the closer correspondence of the ERA5* mean values to the 1:1 line. At higher wind speeds above 10 m/s, on average ERA5* and IFREMER tend to underestimate HY-2B winds. For example, the ERA5* and IFREMER mean wind speed starts to deviate from the HY-2B wind speed at values above 13 and 9 m/s respectively.

Moreover, it is interesting to compare the correlation with HY-2B of IFREMER and ERA5* to the cor-

relation of ERA5 to comment on the results of the L4 products with reference to NWP reanalysis data. Out of all three data sources,ERA5* correlates best with HY-2B for all three wind variables, followed by ERA5, and lastly by IFREMER. The improved correlation between ERA5 and ERA5* is marginal. For example, the RMSD of ERA5* for wind speed is 0.95 compared to 0.97 m/s of ERA5. Strikingly, IFREMER has a worse correlation with HY-2B than ERA5. If considering HY-2B as a proxy for true winds, then these results suggest that ERA5* performs slightly better than ERA5 and IFREMER performs worse than ERA5.

Distribution of wind bias

Both IFREMER and ERA5* underestimate higher wind speeds in comparison to HY-2B which is also depicted in the distribution of wind speed differences for all three wind variables (Figure 4.3). This distribution was computed by counting the differences per 1 m/s bin in u, v andws, whereby a perfect correlation has an average of 0. Neither IFREMER or ERA5* have a perfect correlation with HY-2B. In fact, both IFREMER and ERA5* have an average larger than 0 which confirms that they underestimate HY-2B wind speeds. While the average differences of ERA5* centres at 0.1 m/s for wind speed, this is 0.25 m/s for IFREMER wind speed. This confirms the assumption that IFREMER underestimates winds more than ERA5*.

Besides the bias distribution of wind speed, it is also worthy to remark a similar shift to the right in the distribution of the zonal and meridional wind differences. However, there is one exception which is that the average distribution of ERA5* u differences is -0.01 m/s, indicating a shift to the left.

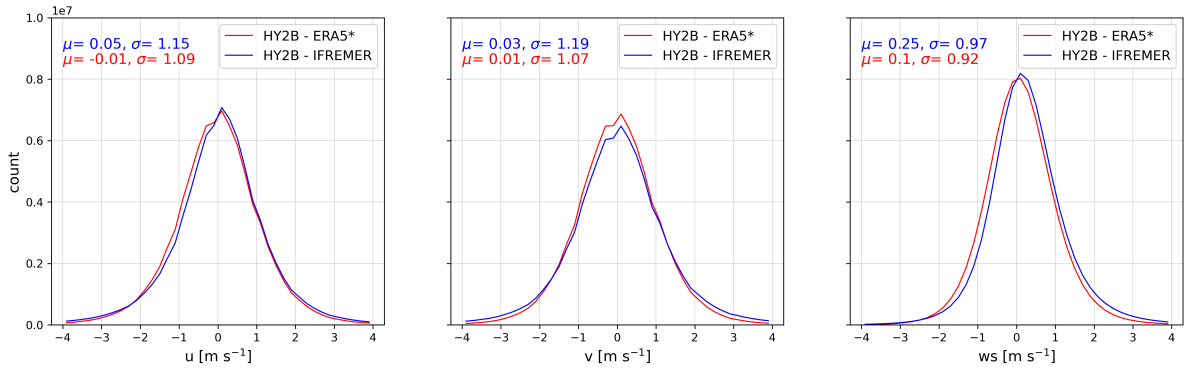

Figure 4.3: Frequency of occurrence of differences binned by 1 m/s between HY-2B and IFREMER (blue) and HY-2B and ERA5* (red) for u, v and ws.

Wind bias as function of wind magnitude

The mean wind differences become larger as function of the wind speed, whereby IFREMER differences start increasing at around 9 m/s compared to 13 m/s for ERA5*. The mean IFREMER bias increases more between wind speeds of 10 – 20 m/s than between 20-25 m/s. On the other hand for ERA5*, the mean bias shows the largest increase between 20 – 25 m/s wind speeds. This is consistent with the scatter plots in Figure 4.2.

The general scatter plots and histograms above, suggest that overall ERA5* correlates better with HY-2B than IFREMER across zonal wind, meridional wind and wind speed variables, as indicated by a higher Pearson correlation coefficient and lower RMSD. High wind speeds (>10 m/s) are underestimated by the L4 products compared to HY-2B winds. The wind differences increase with wind speed, whereby IFREMER already shows larger differences at lower wind speeds than ERA5*.

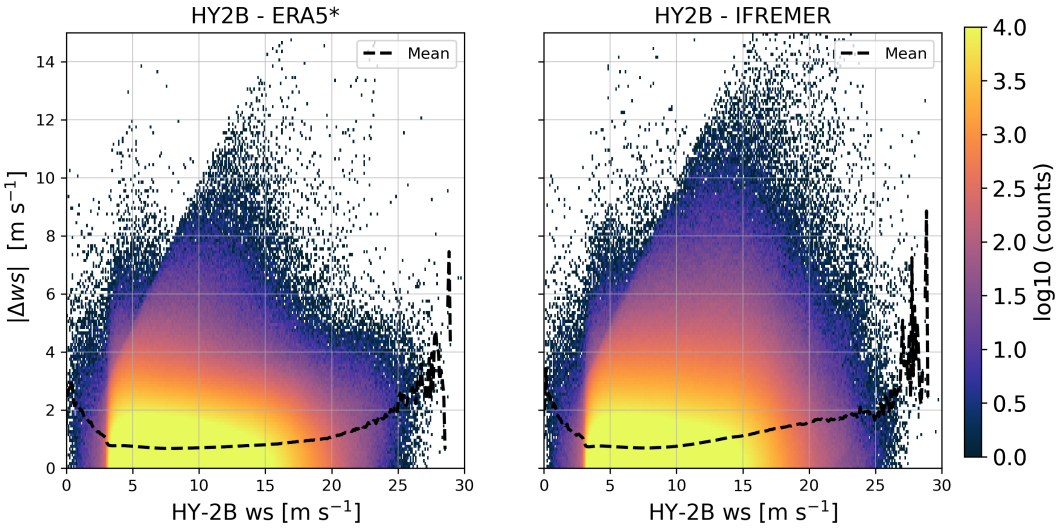

Figure 4.4: Absolute wind speed differences between HY-2B and IFREMER (left) and HY-2B and ERA5* (right) as function of HY-2B wind speed magnitude.

4.1.3. Seasonal averages across latitudes

In order to investigate the role of seasons on the differences between the ascending HY-2B and L4 products collocated winds, the mean and standard deviation of the wind differences are computed as function of latitude (binned by 5°latitude) for each season (e.g. MAM stands for March, April, May).

Mean wind differences

The mean differences between HY-2B and IFREMER tend to be larger in the tropics than at higher latitudes (Figure 4.5). Mean differences in u behave differently in the Northern and Southern hemisphere. In the Northern hemisphere, the largest mean differences occur in DJF and the lowest in JJA. In the Southern hemisphere, the mean differences are very similar in all four seasons. They decrease polewards, whereby around 60°S, the mean differences rapidly shift from 0.1 to -0.25 m/s, likely representing the change in westerlies to easterlies. In contrast to u, mean differences in v are highest in the tropics in both hemispheres during DJF. This is peculiar because one would expect greater mean wind differences in the respective winter seasons of each hemisphere, which would be JJA in the Southern hemisphere. Perhaps positive and negative differences compensate each other because in the standard deviation (Figure 4.6), the seasonal cycle can be recognized in v.

The mean differences in wind speed are highest in the Southern hemisphere reaching a maximum of 0.5 m/s at 40°S in all seasons except JJA. However, for JJA and SON, the mean differences continue rising further South of 40°. In the Northern hemisphere, mean differences in JJA and SON also continue rising further North beyond 40°while DJF and MAM decrease. This is peculiar, because according to the seasonal variation in wind speed, one would expect greater mean differences in DJF and MAM at these latitudes. Whereas there are inter-seasonal variation increases beyond 40°, between 20-40°in both hemispheres there is little seasonal variability.

The mean differences of wind speed for ERA5* behave similar to IFREMER in the Northern hemisphere, but show a different pattern in the Southern hemisphere, whereby mean differences South of 40°decrease in JJA and SON. The mean differences in DJF and MAM seasons tend to be lower at higher latitudes in both hemispheres in comparison to other seasons. In fact, DJF and MAM have highest mean differences of around 0.25 m/s in the tropics while

Unlike IFREMER, the ERA5* wind differences in u and v show little variation across latitude. The mean differences in u show a small dip at the equator, especially in MAM. MAM and DJF vary the most across latitudes, while the mean differences in u in JJA and SON in the Northern hemisphere stay quite constant around 0 m/s. On the contrary in the Southern hemisphere, the mean differences in u in JJA and SON increase polewards until around 50°beyond which they decrease. A similar pattern is also

observed in the mean differences in v and occurs in all 4 seasons. In fact, the mean differences of v show very little seasonal variability. DJF varies the most from JJA between 0 and 30°S.

On average ERA5* differences are lower than IFREMER across all latitudes and in all seasons for the three wind variables, except in the region around the equator (Figure 4.5). At the equator, the mean differences of ERA5* in wind speed during the DJF months seem to be of a similar order of magnitude as IFREMER (0.3 m/s). This mean difference in wind speed of 0.3 m/s is relatively low for IFREMER compared to higher latitudes, but a maximum for ERA5* (Figure 4.5).

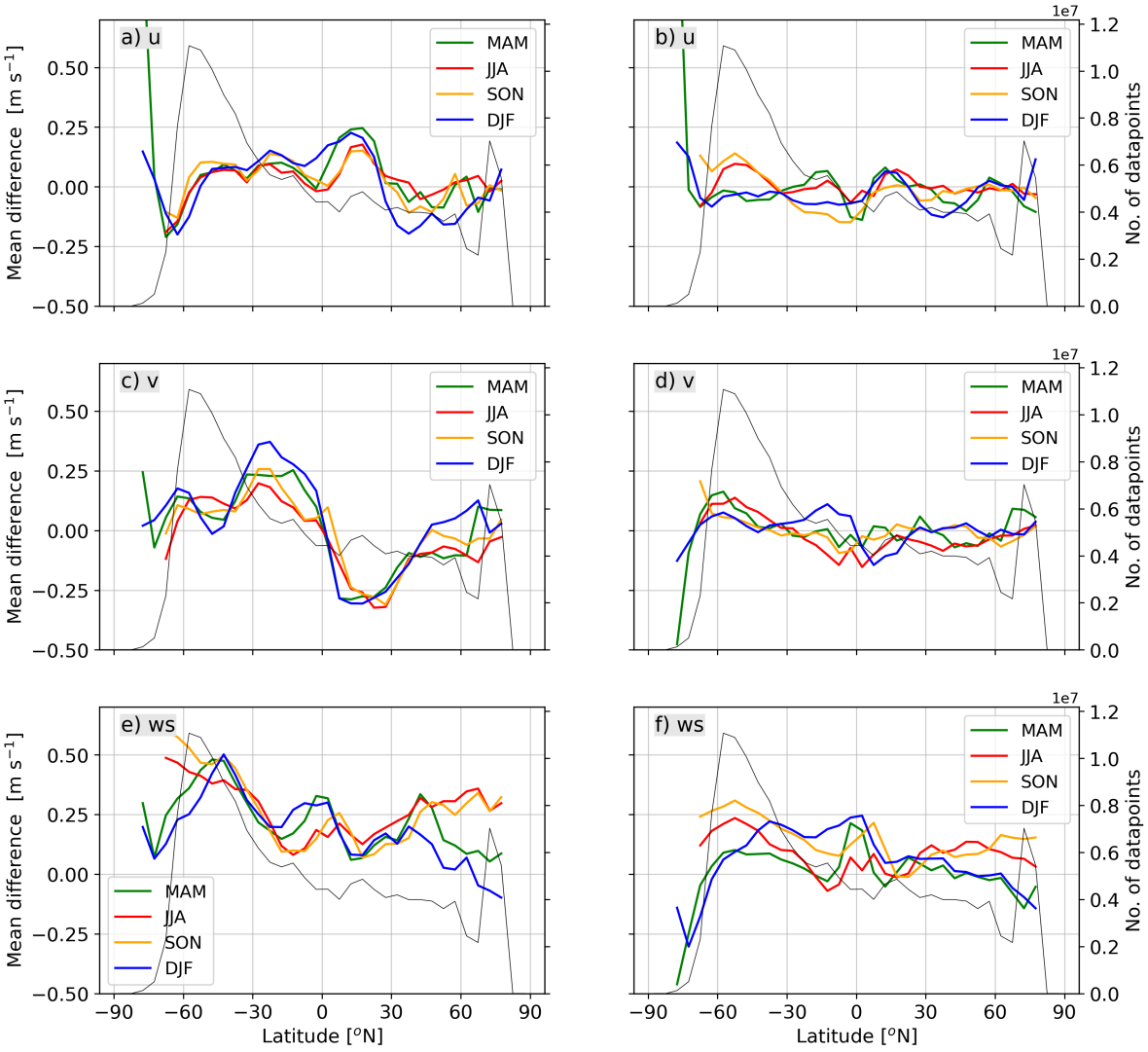

Figure 4.5: Seasonally-averaged differences of zonal, meridional wind and wind speed between HY-2B and IFREMER (a,c,e) and HY-2B and ERA5* (b,d,f) averaged per latitude bin of 5°.

Standard deviation of wind differences

The standard deviation (σ) of the differences for all three wind variables is very similar for both IFREMER and ERA5* across the latitude range (Figure 4.6). For IFREMER, σ is higher at high latitudes (>50°) than in the tropics. σ decreases towards the equator, reaching a minimum between 20°-10°beyond which it increases to a maximum around the equator. Like IFREMER, ERA5* shows a similar trend across latitudes in the tropics, whereby the σ around the equator reaches a significantly higher maximum in ERA5*. At the equator, σ of ERA5* wind speed differences is 0.25 m/s larger than IFREMER (Figure 4.7). On the other hand, ERA5* shows less latitudinal variation in σ than IFREMER. Moreover, outside the tropics ERA5* has significantly lower σ than IFREMER (Figure 4.7).

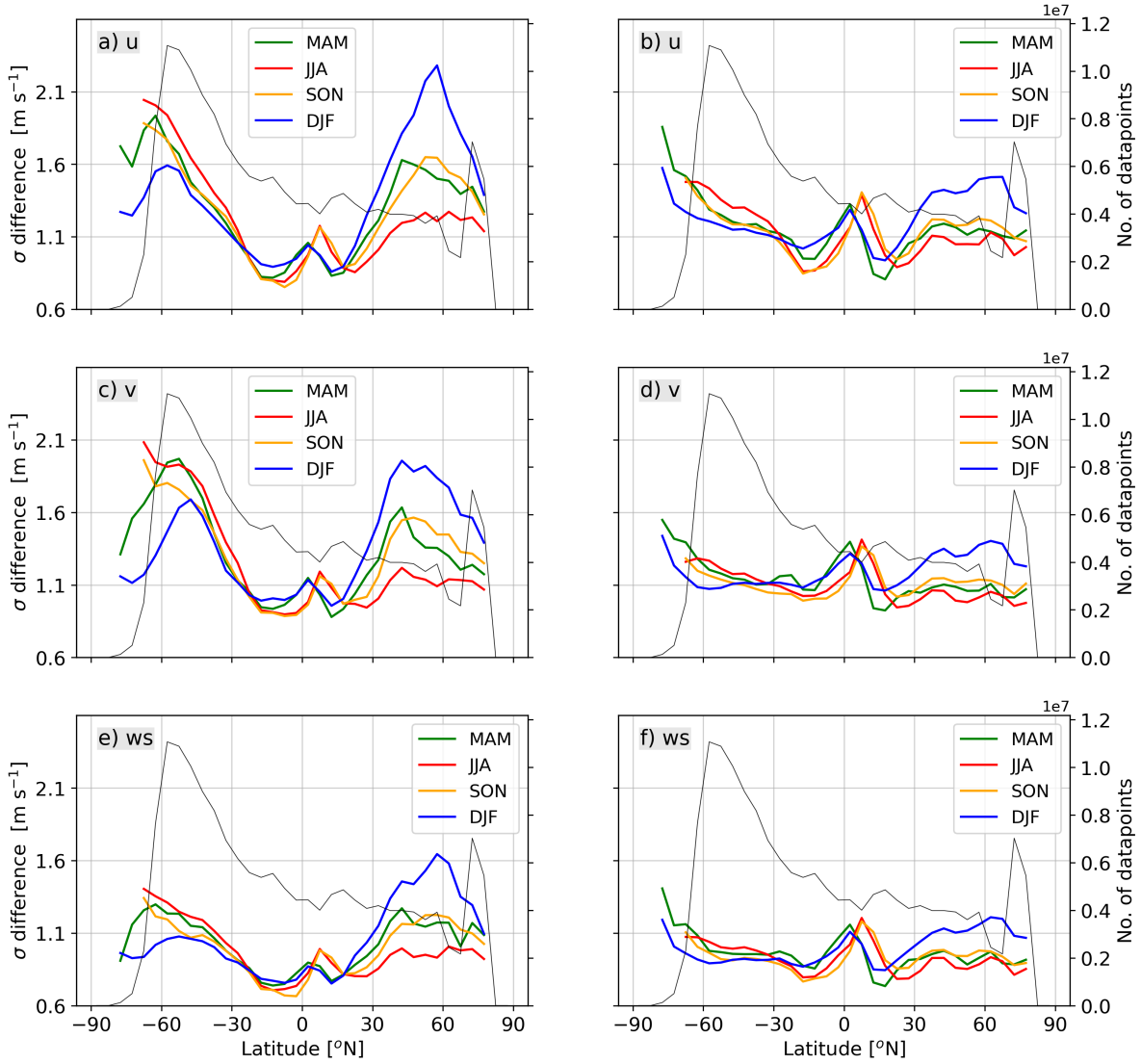

Figure 4.6: Seasonally-averaged standard deviation of zonal, meridional wind and wind speed differences between ascending HY-2B and IFREMER (a,c,e) and HY-2B and ERA5* (b,d,f) averaged per latitude bin of 5°.

Besides latitudinal variation, the standard deviation of the u, v and wind speed differences for each L4 product also show seasonal fluctuations (Figure 4.6). The seasonal variation seems to depend on the wind speed. With larger wind speeds, it is expected that the differences between HY-2B and, for example, IFREMER are larger and thus also the σ of the differences. Larger wind speeds are associated with winter seasons while summer seasons have lower wind speeds. These seasonal variations are also reflected in the standard deviation of the differences across all wind variables (Figure 4.6). For instance, both IFREMER and ERA5* have largest σ in the Northern hemisphere during DJF and in the Southern hemisphere during JJA. Furthermore, the σ in the Northern hemisphere of both IFREMER and ERA5* has more inter-seasonal variation than the Southern hemisphere, whereby DJF and JJA differ the most from each other. In the Northern hemisphere, the inter-seasonal variation is most pronounced in the mid-latitudes and also significantly larger for IFREMER than for ERA5*.

IFREMER has a remarkable outlier in σ (>2.1 m/s) of zonal wind differences at 60°N during DJF (Figure 4.6). This is, on the one hand, not surprising as 60°N corresponds to a region of extremely high wind speeds at eg. South of Greenland. In addition, there are significantly fewer data points at these latitudes due to large land masses which means that only few large deviations are needed to generate

such a large σ. On the other hand, the σ of u differences of ERA5* are not as extreme as IFREMER at 60°.

Furthermpre, the Northward movement of the maximum σ in the tropics for JJA and SON is noteworthy because it can be directly linked to the movement of the ITCZ. The ITCZ moves towards the summer side of the equator which is Northwards in the Northern hemisphere during JJA and SON. The maximum σ directly reflects the ITCZ as the ITCZ is known for its tropical thunderstorms associated with highly variable winds. As a result, it is difficult to obtain accurate wind fields in this region which is also depicted by a peak in standard deviation (Figure 4.6).

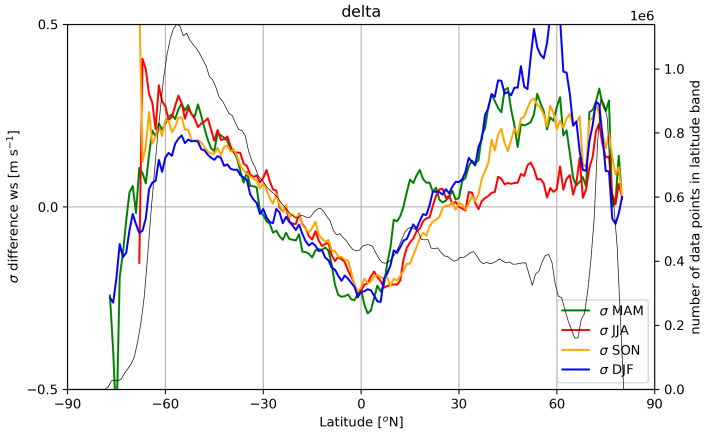

Figure 4.7: Delta plot created by subtracting the σ of wind speed differences of ERA5* from IFREMER. Latitude bin width is 1 °. Negative values mean that ERA5* has a larger standard deviation than IFREMER and vice versa.

4.2. Spatial wind fields

This section evaluates the spatial wind fields of IFREMER and ERA5*. The mean and standard deviation of differences of zonal, meridional wind components and wind speed are analysed on a global scale, at higher latitudes and in the tropics.

4.2.1. Global scale

Mean differences of wind speed

The mean differences in wind speed between HY-2B and IFREMER are larger than ERA5* (Figure 4.8). There are only a few areas where IFREMER mean winds correspond well with HY-2B. Areas where mean differences between IFREMER and ascending HY-2B winds are smaller than 0.1 m/s are more abundant equatorward of 30°than at higher latitudes. For example, they occur in the Indian ocean between 0°and 30°S and in the East of the North Atlantic ocean. Only the former region is also an area of agreement of mean differences with ascending HY-2B (Figure 4.8). In the subtropics (10°- 25°) there are four distinct regions North and South of the Equator in the Pacific Ocean and in the Atlantic Ocean where IFREMER mean winds are very similar to HY-2B. Especially in the descending orbit data these differences are almost 0 m/s, while the ascending differences increase slightly to -0.2 m/s (indicating that IFREMER overestimates winds here).

While areas of good correlating IFREMER and HY-2B winds are scarce, there are many regions across the globe where IFREMER differs from HY-2B (Figure 4.8). Large wind differences (approximately 1 m/s order of magnitude) are mainly found along the western coasts of South and Central America, Africa, Madagascar and north of Australia. The latter two are only clearly visible for descending orbits. Differences are also considerable (>1 m/s) off the East coast of Indonesia and in the Pacific Warm Pool region. Furthermore, between 30°S - 60°S, there is a rather uniform band of mean wind speed differences of around 0.5 m/s across all longitudes. Slightly higher values are found south of Madagascar, Australia and Latin America (more clearly visible in descending than ascending). Another interesting feature to note is the visibility of satellite tracks, in the Pacific and Atlantic Ocean, which follow either

ascending or descending orbits. This pattern is not visible for ERA5* differences and therefore is a problem associated with IFREMER data only.

The visibility of the satellite tracks in the IFREMER difference plots can possibly be caused by the use of ScatSat-1 in IFREMER. As these tracks are visible in annual average differences (Figure 4.8), it implies that they always occur at the same location. Since orbits from remote sensing instruments also repeat themselves (eg. ASCAT orbits have a repeat cycle of 29 days), orbital tracks can still be visible in annual average differences over. A similar orbital pattern is observed in monthly differences between ScatSat-1 and ECMWF model winds (see appendix F). The quality of wind observations by ScatSat-1 vary across the swath because of they are measured by a rotating pencil-beam antenna. When the repeat cycle is long these differences are averaged out, but ScatSat-1 has a short repeat cycle of 2 days, making these patterns persistent. Since ERA5* also includes ScatSat-1 observations, one may expect similar orbital differences as for IFREMER to be visible (Figure 4.8). Yet, these are not as clearly visible because of two possible reasons. Firstly, in ERA5* the scatterometer observations are averaged over multiple days, as a result of which the effects of the orbits partly disappear. They will not disappear entirely because of the 2-day repeat cycle, the orbits will still be visible in an annual average. Secondly, the ICM processes the data of ScatSat-1 using a new version of the processor, which causes the orbital effects to partly disappear. Thus it seems like observations from ScatSat-1 in combination with the way in which the data is processed leads to artificial structures in the IFREMER product. This is undesirable for the users of the IFREMER wind product because it causes abrupt wind deviations at such artificial fronts.

The bias of IFREMER in coastal regions can have several causes such as the effect of the diurnal cycle and poor scatterometer observations in coastal areas. The Indian Pacific Warm Pool is known to be a region with highly variable weather due to moist convection where it is difficult to retrieve accurate wind measurements from scatterometers as well as from NWP models. The middle latitudes, particularly in the Southern hemisphere, are also known as the storm tracks associated with fast varying, large weather systems and high winds. There may be several reasons as to why IFREMER shows larger differences with HY-2B. One of the reasons could be that IFREMER's 6-hourly winds cannot account for the rapidly changing weather systems in time.

In comparison to IFREMER, ERA5* mean differences are significantly smaller in Figure 4.8. In fact, the mean ERA5* differences are very close to zero across most oceans and visible as small scattered dot-like structures. Like IFREMER, ERA5* also shows good agreement with HY-2B in the subtropics and. unlike IFREMER, in the middle latitudes. While in the subtropics these differences are slightly negative (-0.1 m/s), they become slightly positive between 30°and 60°and negative again below 60°S. Negative differences correspond to regions of overestimation by ERA5* and vice versa. The differences become are a darker red between 30°-60°for ascending tracks.

An obvious region that stands out is the Indian Pacific Warm Pool where there is a clear patch of dark red, indicating wind differences of >1 m/s. Another dark red stripe occurs exactly on the equator West of America. On the West coast of America, there are also some dark red spots at 10°N. The descending collocated winds furthermore show some darker red areas West of Africa and in the Indian Ocean. A final difference to observe is the darker blue area North of Antarctica around 180°longitude.

ERA5* winds show good agreement with HY-2B global ocean winds and shows significant improvement to IFREMER winds on a global level. Only in the tropics, particularly along the equator, are the differences between HY-2B and ERA5* significantly large (1 m/s). As already mentioned in the differences with IFREMER, the Indian Pacific Warm Pool is known for its difficult weather. In this region moist convection and its associated small-scale structures are likely to play a role in causing wind differences.

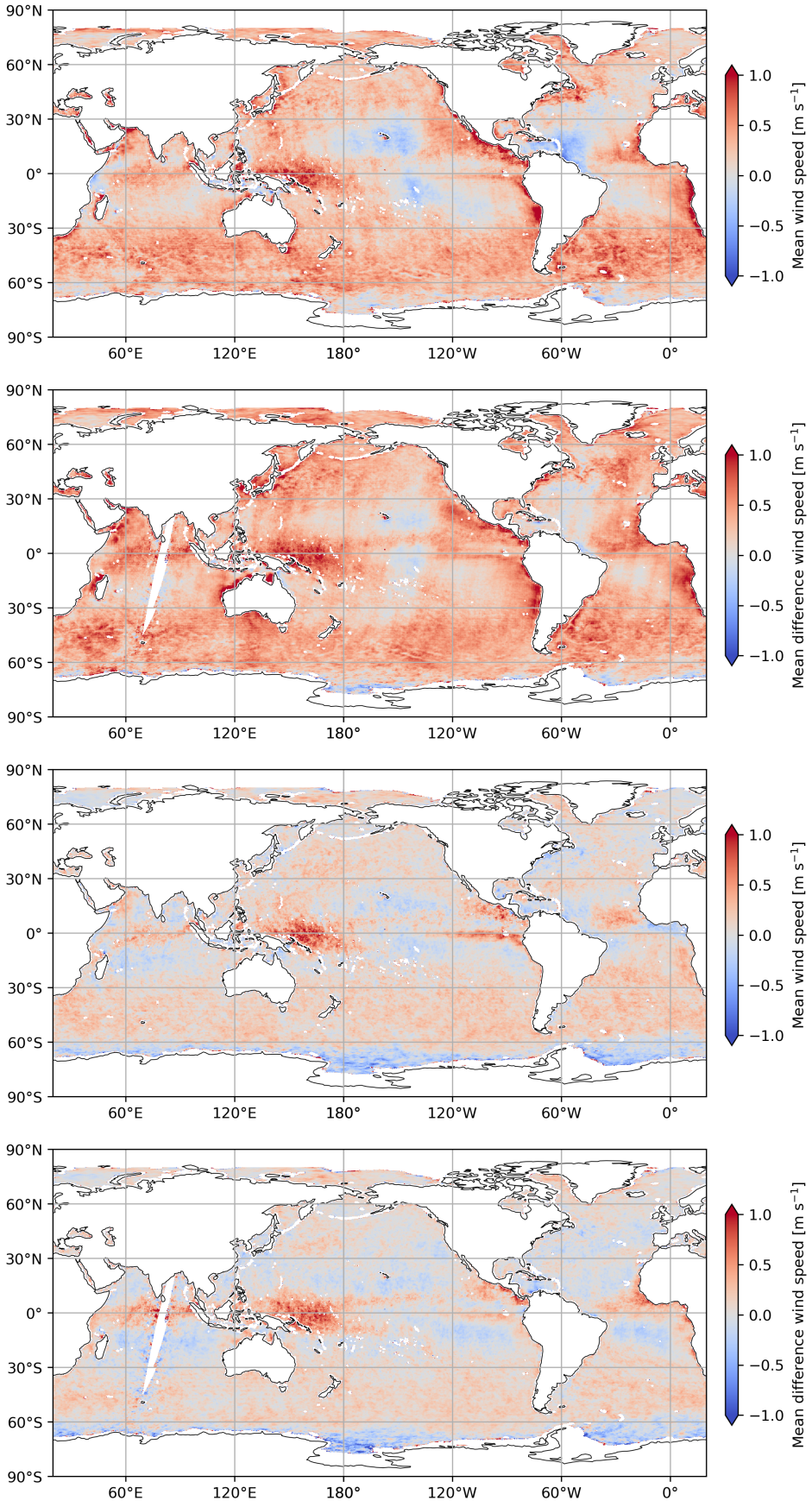

Figure 4.8: Average differences for wind speed between HY-2B and IFREMER (top figures) and HY-2B and ERA5* (bottom figures) on a 0.25 °grid cell for 2019. The second figure from the top and bottom figure are computed using HY-2B descending orbits (LTDN 06:00), while the other two figures are based on HY-2B ascending orbits (LTAN 18:00).

Mean differences for wind components

Apart from a wind speed analysis, the individual zonal and meridional IFREMER and ERA5* wind differences with HY-2B were also analysed (Figure 4.9). For IFREMER, v differs more from HY-2B than u, especially in the Pacific ocean. IFREMER underestimates the meridional wind by roughly 0.3 m/s in both the Northern and Southern hemisphere (Figure 4.9). Locally mean u and v differences can exceed 0.5 m/s. This occurs at for instance the West coast of Madagascar, South America and Southern Africa. The visibility of satellite tracks appear in u differences in the North Pacific ocean. Furthermore, u shows very localized differences specifically in the West coast of North America, India and Africa.

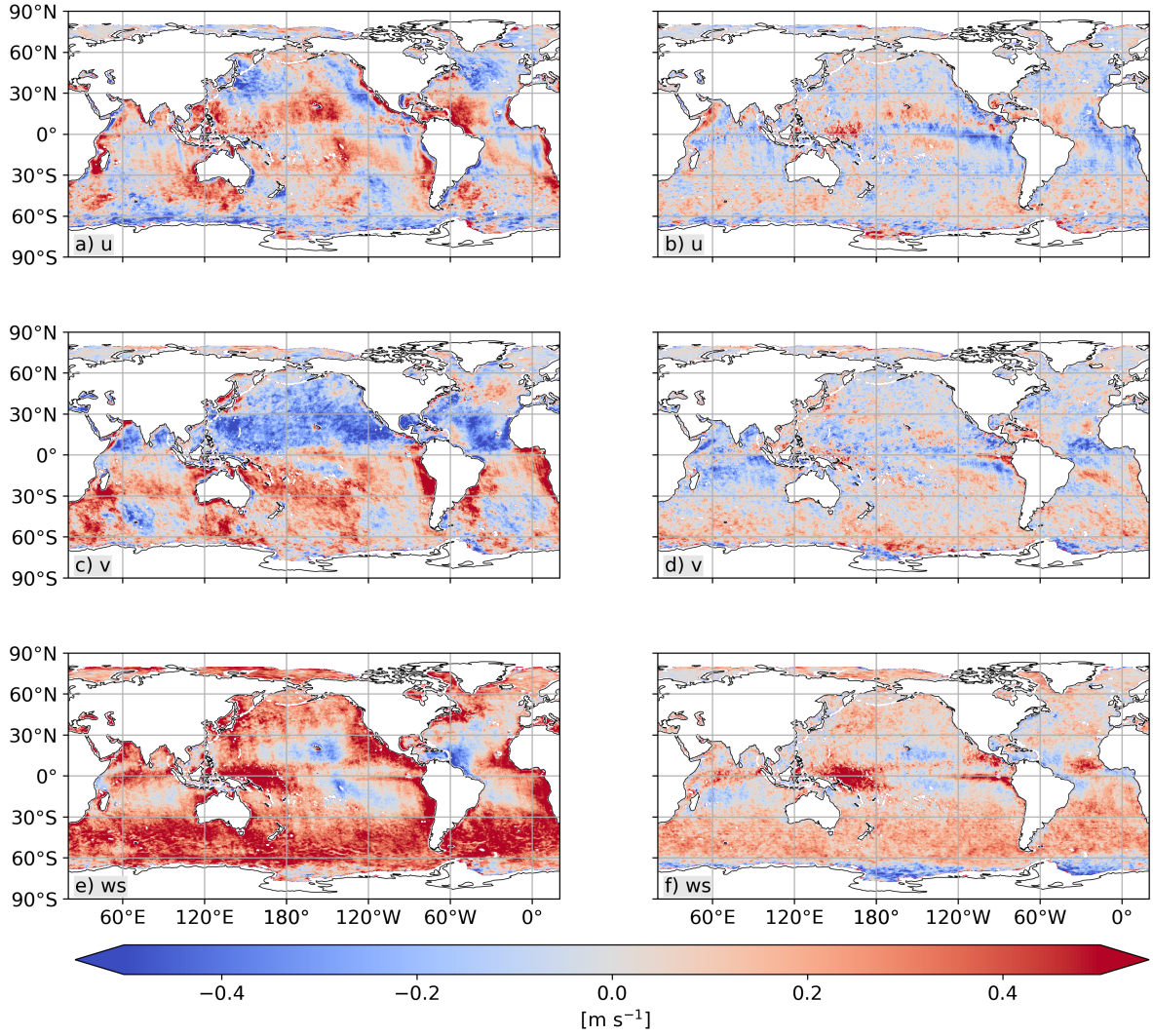

Figure 4.9: Mean differences for wind variables u, v, ws between ascending HY-2B and IFREMER (a,c,e) and HY-2B and ERA5* (b, d, f) for 2019 plotted on a 0.25°grid. Positive differences in red indicate that HY-2B winds are larger than either IFREMER or ERA5*.

Contrasting to IFREMER, ERA5* mean differences for u and v are significantly smaller in size. Especially outside the tropics, the differences for both u and v are scattered in small dot-like structures and are less than 0.3 m/s. Unlike IFREMER, ERA5* u and v correlate very well with HY-2B in coastal regions. The biggest mean differences of 0.5 m/s or larger only occur occasionally and are mostly concentrated between 30°S and 30°N of the equator. In the zonal wind component, the largest differences are particularly found in the Western Pacific Warm Pool and in the ITCZ.

Standard deviation of wind differences

Besides the mean differences of 2019, the spatial standard deviation of the differences for each wind component and wind speed were also analysed for 2019 (Figure 4.10).

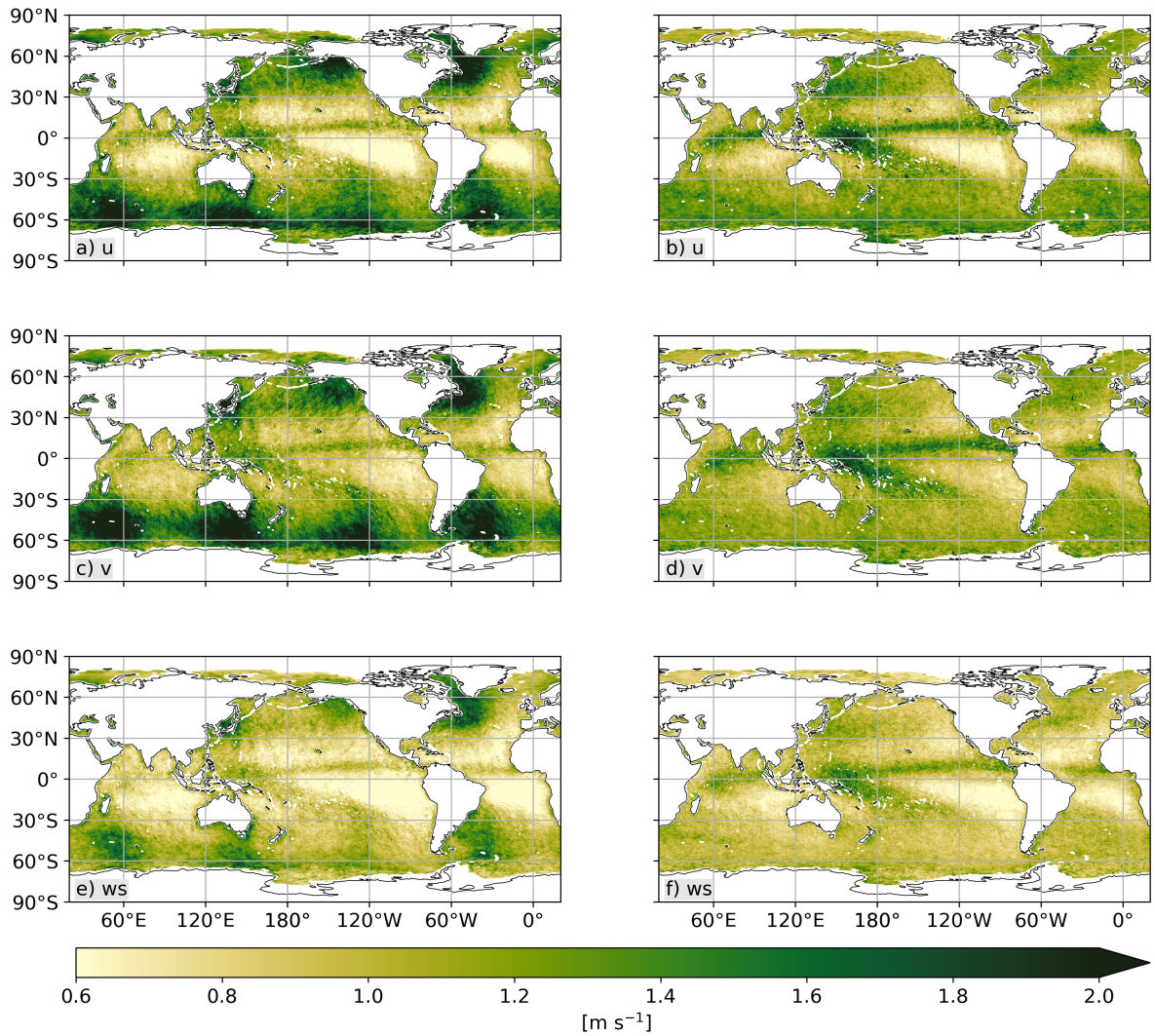

Figure 4.10: Standard deviation of differences for wind variables u, v, ws between ascending HY-2B and IFREMER (a,c,e) and HY-2B and ERA5* (b, d, f) for 2019 plotted on a 0.25°grid. Positive differences in red indicate that HY-2B winds are larger than either IFREMER or ERA5*.

Interestingly, IFREMER has distinct areas with high (>2 m/s) and low (<0.6 m/s) standard deviation of differences (Figure 4.10). Regions with low standard deviation occur between -30°and 30°latitude, with lower σ for u than v. These regions correspond to low wind speeds and persistent easterlies, which are probably the cause for the low σ especially in u. On the other hand, at higher latitudes, IFREMER has remarkably high standard deviation. Most striking are the four patches of >2 m/s in the Southern hemisphere, around the roaring Forties (around 40°S), and two in the Northern hemisphere. The patches in both the N. and S. hemisphere occur around the same longitude coordinates, 50°and 130°W, whereby the N. hemisphere misses two at 50°and 130°E probably because of land coverage. The repetitive pattern, almost like a sinus wave, of these outliers suggests that time differences between IFREMER winds and HY-2B observations play a role. Similar spatial observations of standard deviation of the differences are also found for wind speed, but smaller in size (Figure 4.10).

IFREMER's outliers in standard deviation are not present for ERA5*. ERA5* does have the same regions of low σ as IFREMER (Figure 4.10). Also like IFREMER, although more pronounced for

ERA5*, is the band of high σ of 1.8 m/s for ERA5* just N. of the equator. This band seems to follow the location of the ITCZ. Especially for wind speed Figure 4.10, this band has the highest σ for ERA5* compared to the rest of the world.

4.2.2. High latitudes

This section explores potential causes for the mean and standard deviation of the u, v and wind speed differences at high latitudes. Three possible effects are investigated.

Effect of 6-hour averaging

The effect of 6-hourly averaging was investigated by degrading hourly ERA5* wind fields to 6-hourly ERA5* wind fields at the same synoptic times as IFREMER. For example a 6-hourly average ERA5* wind field at 12:00 UTC, included the wind fields between 9:00 and 15:00 UTC, whereby the outer most wind fields are only included by half the weight to ensure 6-hour instead of a 7-hour average.Figures 4.11a and 4.11b show that differences introduced by averaging over 6-hours tend to be higher in the mid-latitudes than in the tropics. This is likely to be a direct consequence of the higher wind speeds at higher latitudes. The results for the ascending and descending data differ in a number of respects.

There are some ascending differences introduced by 6-hourly averaging (Figure 4.11) that overlap with mean differences of HY-2B and IFREMER (Figure 4.8). Examples where overlap occurs are in the northern Pacific Ocean, Southeast of South America, North of Central America. The descending differences introduced by 6-hourly averaging overlap in similar regions as the ascending differences. Additionally, the mean descending differences between hourly and 6-hourly ERA5* are larger in size in the Southern mid-latitudes than of ascending differences.

Furthermore, it seems that large differences of 0.4 m/s are followed by areas of smaller differences of 0.2 m/s in a sinus pattern (Figure 4.11b). This means that there is a high chance that the large differences found between HY-2B and IFREMER in the Southern latitudes can be related to the fact that IFREMER is a 6-hourly product that does not capture the weather systems of the Southern mid-latitudes well.

However, the differences observed in coastal regions for IFREMER do not seem to be directly linked to 6-hourly averaging (Figure 4.11). Although larger differences are generated as a result of 6-hourly averaging of descending data in the Northwest coast of Madagascar and Australia corresponding to larger IFREMER descending differences, other coastal regions, such as West of South America and Africa do not show overlap. Thus it seems like other factors, for instance the diurnal cycle, play a more significant role in coastal regions. See appendix E

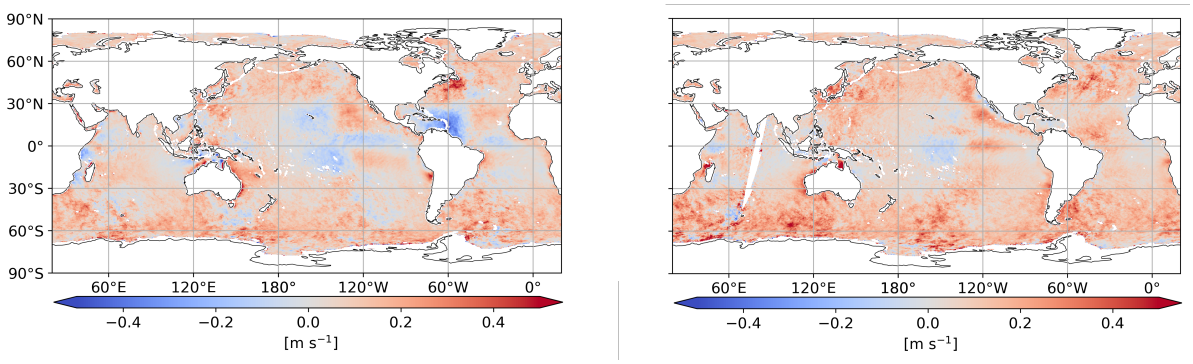

(a) ASC (b) DES

Figure 4.11: Global maps on 0.25°x 0.25°cells of average wind speed difference between hourly ERA5* and 6-hourly ERA5* collocated winds with ascending (a) and descending (b) HY-2B observations.

Effect of daily variation of winds

To check whether there is a relation between the differences with HY-2B and the daily variation of the wind, the daily standard deviation ($\sigma_{x,y,day}$) of ERA5* wind speed was computed for a winter (DJF) and

summer (JJA) season in 2019 (equations 4.1 and 4.2).

$$\overline{ws}_{x,y,day} = \frac{1}{T}\sum_{t=1}^{T=24} ws_{(x,y,t)} \tag{4.1}$$

$$\sigma_{x,y,day} = \frac{1}{N}\sum_{n=1}^{N=season} \sqrt{\frac{\sum_{t=1}^{T=24}(ws_{x,y,t} - \overline{ws}_{x,y,day})^2}{T}} \tag{4.2}$$

where $\overline{ws}$ equals the mean daily wind speed based on the total number of hours in a day (T),ERA5* wind fields at grid cell (x,y) available for every hour(t). The daily standard deviation is averaged over the length of DJF and JJA season (N).

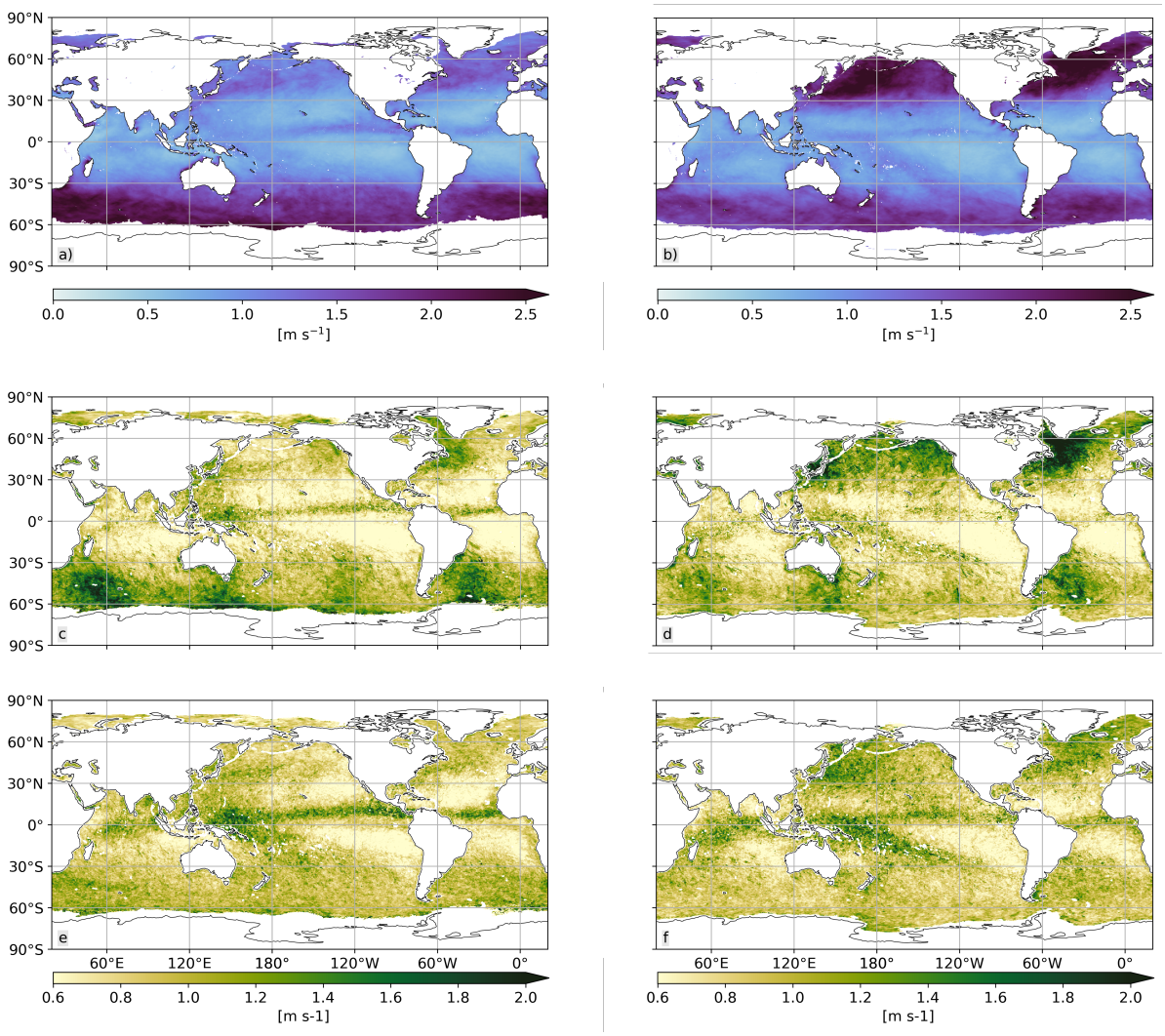

Figure 4.12: Global maps on 0.25°x 0.25°cells of the daily variation (equation 4.2) of wind speed JJA (a) and DJF computed using ERA5*. The 3-monthly averaged standard deviation of the differences (equation 3.8) for ws between HY-2B and IFREMER for JJA (c) and DJF (d) are also shown. Likewise, (e,f) are the same results for HY-2B and ERA5*.

During DJF, the daily variation of surface winds is highest in the mid-latitudes (between 30°-60°), whereby it is larger in the Northern (>2.5 m/s) than in the Southern hemisphere (around 1.5 m/s) (Figure 4.12). Across longitudes, the daily variation is quite constant. Small variations occur West of North America, where winds vary relatively less throughout the day, and Southeast of South America, where slightly higher variations are seen (Figure 4.12). In JJA, daily winds vary significantly more

in the Southern mid-latitudes compared to the Northern mid-latitudes(Figure 4.12). The largest daily variations occur in the Southern Indian Ocean and Southern Atlantic ocean. The tropics have very small daily variation (around 0.5 m/s), presumably due to its lower wind speeds resulting in smaller variations than at higher latitudes.

Areas with higher σ of differences for ws for IFREMER correspond to areas with higher daily variation. This positive correlation is observed in both DJF and JJA. For example, high σ (>2 m/s) in the North Atlantic ocean, specifically South of Greenland is directly related to high daily variation. Furthermore, σ in the Northern Pacific ocean is significantly higher in DJF than in JJA and a similar pattern is seen for the daily variation between these two seasons. This suggests that there is a positive correlation between σ in the mid-latitudes and daily wind variation. The Southern mid-latitudes, seems to have four regions of extremely high σ (>2.5 m/s) of differences for ws for IFREMER, which are more apparent in JJA than in DJF. However, the daily variation in JJA seems quite constant across longitude. This suggests that there is another factor that has a larger influence on the standard deviation of the differences for IFREMER.

Large standard deviation of differences for ERA5* wind speed also coincide with regions of high daily variation. Although the maximum standard deviation is smaller in size for ERA5* than for IFREMER, higher σ still stands out from surrounding, lower σ areas. For example, in DJF, the highest σ (around 1.3 m/s) is found Northwest of the Pacific ocean and Northwest of the Atlantic ocean (Figure 4.12). This is also where the highest daily variation occurs.

Overall, standard deviation of differences for ERA5* is significantly lower at high latitudes than for IFREMER. This is most likely as ERA5* is mainly based on ERA5 NWP model data, which is known to capture large-scale wind systems well and therefore performs well in the mid-latitudes. IFREMER, on the other hand, performs consistently worse in the mid-latitudes. There seems to be a positive correlation between high σ of differences and daily variation of wind at high latitudes.

Effect of time difference with HY-2B

The four extremes of σ of differences for IFREMER for all three wind variables are suspected to result from time differences. There are two possibilities that can lead to these time differences. First of all, the IFREMER product uses scatterometer observations from ASCAT and ScatSat-1 that have a local equatorial overpass time of 21.30 (ASC) and 9.30 (DES). This means that there is a certain time difference, depending on the longitudinal coordinates, between the available scatterometer observations and the synoptic IFREMER time (06, 12, 18, 00). Secondly, there is also a time difference between the Haiyang-2B observations (06:00 LTDN and 18:00 LTAN) and the synoptic IFREMER time. The effects of both circumstances were investigated by computing the time difference between the local time of a HY-2B observation transformed into a UTC time and the closest IFREMER time. The time difference was computed as function of longitude. This time difference was compared with the standard deviation of the HY-2B and IFREMER differences for the meridional wind component because this wind variable had the most distinct pattern of four extremes. A positive correlation between the time difference between the local time of HY-2B observations and IFREMER as function of longitude was found (Figure 4.13).

Figure 4.13 shows that when the time difference between an IFREMER wind and HY-2B observation is at its maximum of 3 hours, then the standard deviation of the difference between IFREMER and HY-2B is also greatest. This suggests that IFREMER winds in the mid-latitudes in the Northern and Southern hemisphere become less accurate as the time lag with HY-2B observations grows. Remarkably, the extremes only occur in the mid-latitudes and not in the tropics. This may be related to the variability of the weather, which is significantly higher in the extratropics compared to the tropics (Figure 4.12). This suggests that the scatterometer observations at a specific time are affected by the daily variability of the wind, reflected by larger standard deviation of the differences for IFREMER when larger time differences occur. The fact that these extremely high standard deviations are not present for the differences of ERA5* suggests that they are related to IFREMER being a 6-hourly product.

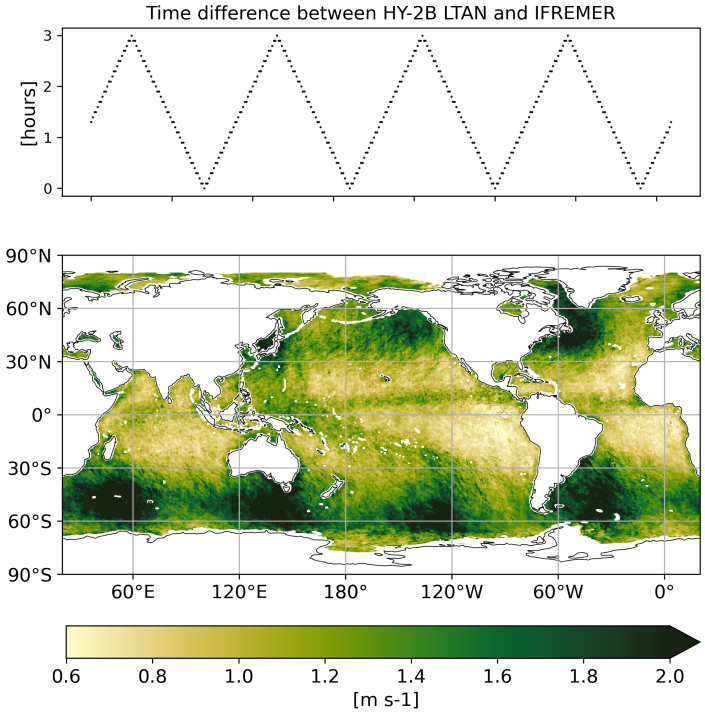

Figure 4.13: Standard deviation of differences between HY-2B and IFREMER for the meridional wind component over 2019. Overlay is the time difference in hours between the equatorial overpass time of HY-2B and IFREMER wind.

4.2.3. Tropics

Between 20°S-20°N, defined as the tropics in this section, the standard deviation of differences between Haiyang-2B and ERA5* are larger than for IFREMER for wind speed (Figure 4.7) and also for the individual wind components. Also, ERA5* showed relatively large mean differences in the Western Pacific Warm Pool and along the equator in comparison to the rest of the world (Figure 4.9). Moreover the tropics are a region where the dynamics of the weather are not completely understood today. Therefore, the tropics formed an interesting region for further investigation of the IFREMER and ERA5* wind fields.

Whereas global ERA5* winds correlated better with HY-2B than IFREMER, the opposite is true for winds in the tropics (20°S-20°N). Remarkably, ERA5* has a higher RMSD than IFREMER for all three wind variables which is in line with the higher σ for ERA5* (Figure 4.7). The RMSD for u and v for ERA5* are 1.06 and 1.14 m/s respectively compared to 0.92 and 1.01 m/s for IFREMER. The Pearson correlation coefficient of ERA5* is smaller than of IFREMER, with little variation between u, v and ws. This implies that ERA5* winds correlate less well than IFREMER with HY-2B winds between 20°S - 20°N.

In comparison to ERA5, IFREMER winds still correlate better with HY-2B observations for u, v and ws. When comparing the HY-2B correlation of ERA5* with ERA5, it is only slightly better. For example, ERA5* has a RMSD of 1.06 and 1.14 m/s for u and v respectively. The RMSD ERA5 scores lie closer to ERA5* for u than v shown by 1.08 and 1.21 m/s.

Similarly, to the correlation for wind speed at a global scale, the scatter cloud for the tropics for wind speed shows significantly fewer HY-2B wind speeds lower than 3 m/s. The removal of these low winds is more clearly visible in the zonal than meridional wind component for both IFREMER and ERA5* (Figure 4.14).

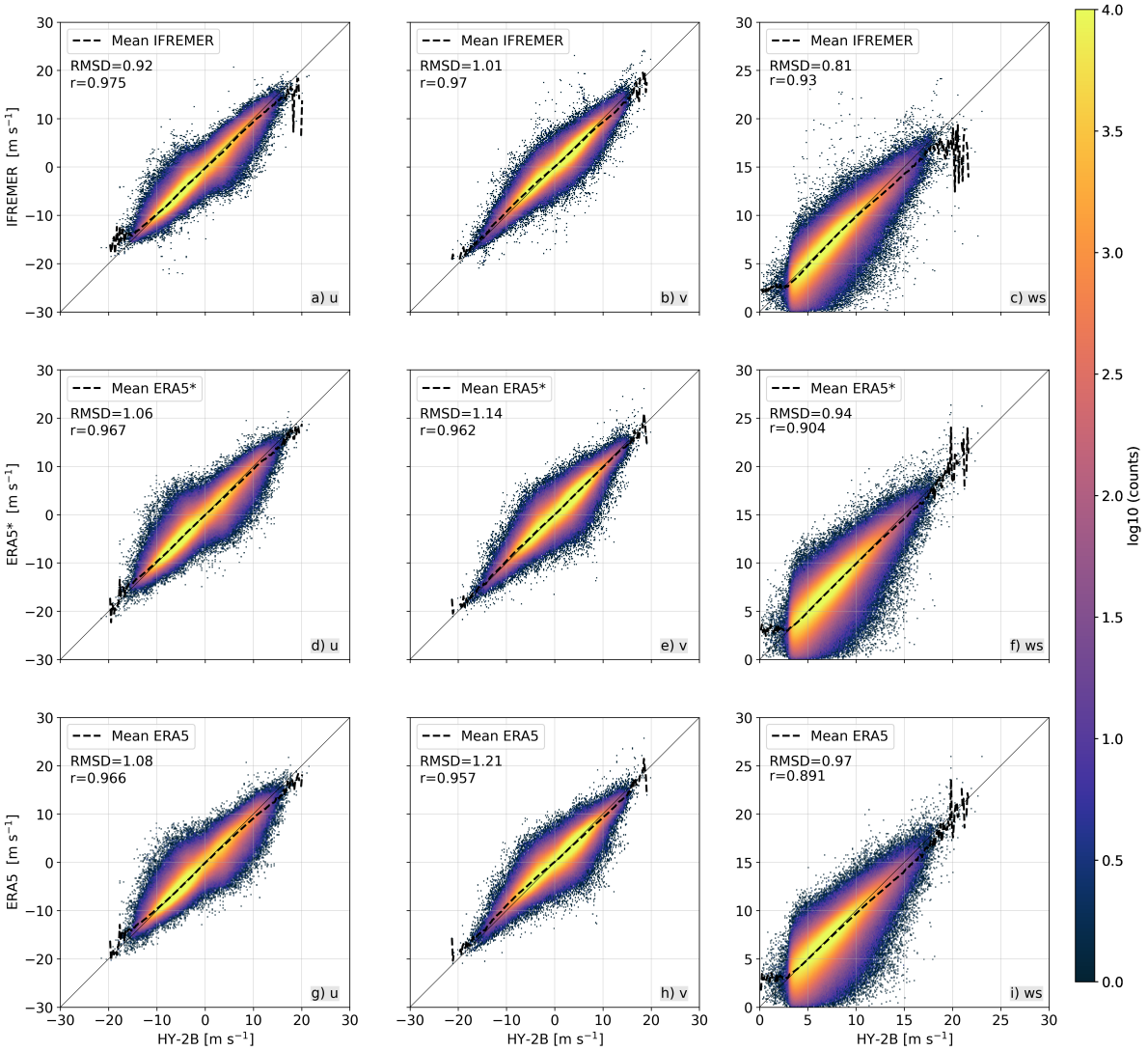

Figure 4.14: HY-2B ascending winds for 2019 between -20°- 20°latitudes only, after quality control, plotted against collocated IFREMER winds (upper row), ERA5* winds (middle row) and ERA5 winds (lower row) for variables u (left), v (middle) and wind speed (right).

There are several reasons that can cause IFREMER to resemble HY-2B winds more than ERA5* in the tropics. First of all, due to the way in which HY-2B backscatter measurements are processed, it only resolves spatial structures as small as 75 km. This is quite a coarse resolution for a scatterometer. For example, ASCAT can resolve structures of up to 25 km due to different processing. Like HY-2B, IFREMER does not contain these small-sized structures as a result of the Kriging technique applied in the creation of 6-hourly winds. As the tropics are characteristic to low wind speeds and small-scaled spatial wind structures, which are not captured by both IFREMER and HY-2B, this leads to IFREMER resembling HY-2B winds more.

Thirdly, the wind differences with HY-2B in the tropics may be generated due to conditional sampling. Figure 4.14 shows that HY-2B winds below 3 m/s are rejected as a result of quality control. Yet, the average wind speed in this region is extremely low (<5 m/s, see Figure 2.2). During HY-2B quality control, IFREMER and ERA5* winds below 3 m/s are not rejected. Thus there are probably some wind field collocations with IFREMER and/or ERA5* winds lower than 3 m/s and HY-2B winds higher than 3 m/s. These wind field collocations will generate larger differences than if the winds had been collocated with HY-2B before quality control (and removal of winds <3 m/s). This means that the wind sample on which this analysis is based is not an accurate representation of the true wind sample. This phenomenon is known as conditional sampling (Stoffelen, 1998b). Figure 4.15 show what happens

when also all IFREMER and ERA5* winds below <3 m/s are removed. Between the top and bottom rows of Figure 4.15, the differences are reduced in size, especially for ERA5* and in the areas where the differences were initially larger. Also, by removing winds <3 m/s, ERA5* looks more like HY-2B than IFREMER does. This proves that some of the errors along the equator are introduced by conditional sampling.

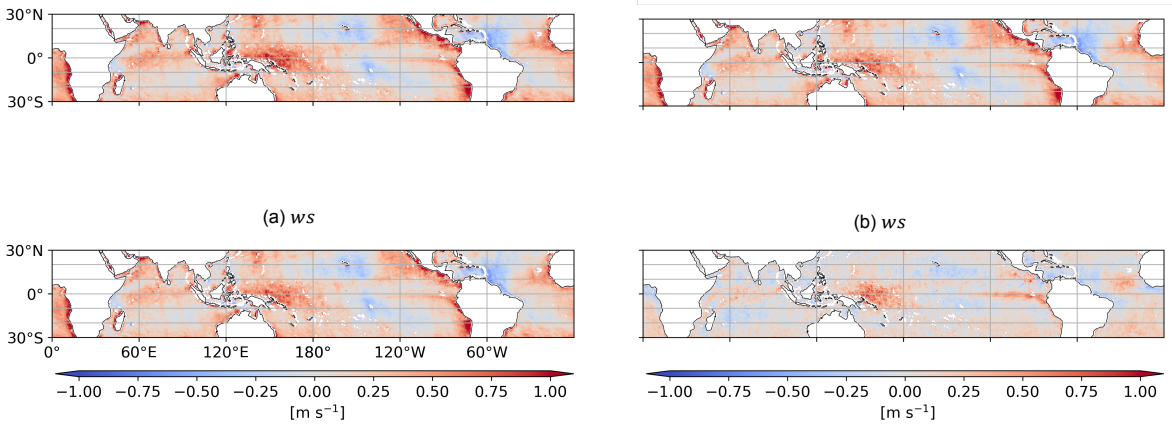

(c) After removal of < 3 m/s

(d) After removal of < 3 m/s

Figure 4.15: Mean differences between HY2B-IFREMER (a,c) and HY2B-ERA5* (b,d) for wind speed for 2019 on a 0.25°x 0.25°grid. The difference between the top and bottom row shows how conditional sampling of collocated HY-2B winds causes larger differences shown in darker red in (a,b) than in (c,d).

5

Discussion

This study evaluated global ocean surface winds from two level-4 (L4) wind products, IFREMER and ERA5*. Wind fields from the two L4 products were evaluated with wind observations from an independent scatterometer Haiyang-2B (HY-2B). This chapter places the results into a broader perspective and discusses the limitations associated with the analyses performed in this research.

5.1. Broader implications

The results showed that on a global scale ERA5* correlates best with HY-2B winds, followed closely by ERA5, while correlation coefficients are slightly lower for IFREMER. Particularly the RMSD with HY-2B winds is considerably larger for IFREMER than for ERA5* and ERA5. These results are promising for ERA5* because it confirms that the scatterometer-based correction leads to improved wind fields compared to ERA5, assuming HY-2B to represent the true wind. On the other hand, the worse correlation of IFREMER in relation to ERA5 is reason for concern because IFREMER's goal is to produce improved ocean winds compared to model reanalysis. In the tropics, the mean ($\overline{\Delta ws}_{x,y,T}$)and standard deviation ($\sigma\Delta ws_{x,y,T}$) of the differences between ERA5* and HY-2B are larger than outside the tropics while this is the opposite for IFREMER. In the tropics, IFREMER correlates best with HY-2B, followed by ERA5* and lastly by ERA5. The tropics are a region where the relatively large $\overline{\Delta ws}_{x,y,T}$ and $\sigma\Delta ws_{x,y,T}$ should be further investigated. At higher latitudes, the differences with HY-2B for IFREMER are larger than for ERA5*. These results suggested that large $\sigma\Delta ws_{x,y,T}$ are caused by time differences of maximum 3 hours with HY-2B observations. This is a direct consequence of IFREMER's 6-hourly resolution. In addition, the differences for IFREMER were relatively large compared to ERA5* in certain coastal regions and satellite tracks were visible.

ERA5*

This study has demonstrated the added value of ERA5* relative to ERA5. The scatterometer based correction in ERA5* that accounts for small-scaled (<100 km) structured winds seems to be realistic. This is denoted by a lower RMSD for ERA5* than ERA5, whereby the best improvement is achieved in the meridional wind component in the tropics. A recent study that also validated ERA5* winds against HY-2B observations showed similar results across latitudes (Portabella, M., personal communication 2022). In the tropics, the $\overline{\Delta ws}_{x,y,T}$ and $\sigma\Delta ws_{x,y,T}$ between ERA5* and HY-2B are larger than outside the tropics. When analysing these results for the tropics, one should keep in mind that increased wind variability due to convection and rain in this region are likely to play a role in high wind differences. Because the study by Portabella is only based on one month of data (February 2019) and our results are based on a smaller sized sample because many HY-2B observations are rejected because of the rain quality control flag (Figure G.1), the tropics are a region that should be further investigated to validate these results. ERA5* showed good correspondence with HY-2B in coastal regions. This is also in line with a similar validation study for the new product manual of ERA5* (Portabella et al., 2021).

IFREMER
Contrasting to our results, an earlier study by Desbiolles et al. (2017) concluded that the IFREMER product showed improved results in comparison to model reanalysis. In their study they compared IFREMER winds for 1992-1999 to non-independent scatterometer observations, buoy data and model reanalysis. For the latter, they used ERA-Interim which is the predecessor of ERA5. Their IFREMER wind product was constructed from observations from other scatterometers and radiometers than used in the IFREMER product in our study. However, it is still intriguing that in comparison to ERA5, IFREMER is not per definition a better wind product, except for perhaps in the tropics. It is known that ERA5 has shown an overall imrpovement of 20% (Belmonte Rivas and Stoffelen, 2019) compared to ERA-Interim which may partly clarify the results in Desbiolles et al. (2017). Additionally, a more recent study by (Bentamy et al., 2021) assessed 6-hourly IFREMER winds computed from scatterometer observations and also Synthetic Aperture Radars (SAR), which are known for their on a 0.125°grid. They compared the IFREMER winds and three wind reanalyses (including ERA5) with non-independent scatterometer winds for three specific coastal upwelling regions up until the year 2018. In their analysis IFREMER winds showed the lowest RMSD and they concluded that IFREMER's deviation from pure scatterometer observations is not a function of time. There are many possible causes that can explain why this conclusion deviates from what we find here, such as differences between the study year, location and input data are likely to play a role.

5.2. Limitations

5.2.1. Validation with HY-2B

HY-2B scatterometer observations were chosen as reference data for the true wind because of three main reasons. First of all, HY-2B is considered an independent scatterometer in comparison to ERA5* and IFREMER wind because HY-2B observations are not used as an input data source for the two L4 wind products. Secondly, Haiyang-2B crosses the equator at a different local time (18:00, 06:00) than the scatterometer observations used in IFREMER and ERA5* (21:30, 09:30). This means that by comparison with HY-2B, the representativity of the IFREMER and ERA5* winds can be assessed at another time than at which the scatterometer observations are available. The time difference between HY-2B and the scatterometer observations in IFREMER and ERA5* is interesting because wind speed and wind direction can vary throughout the day as a result of the diurnal cycle of the movement of weather systems. Thirdly, a scatterometer has a higher global coverage than in-situ measurements enabling analysis of wind fields at a global scale. Even though Haiyang-2B was chosen as reference data for true wind, it has a few limitations which are discussed below.

HY-2B independence
HY-2B is not fully independent because it relies on the ECMWF operational model for (a) wind ambiguity removal and (b) calibration of the instrument. The former takes place during scatterometer processing when the most probable wind direction from several back scatter retrievals is determined. Secondly, for calibration of the scatterometer measuring instrument the operational ECMWF NWP model is also used. Although the operational weather model of the ECMWF is a different, improved version of the one used for the creation of ERA5, they are almost the same. This means that HY-2B, although only very small, has two dependencies with both ERA5* and IFREMER and cannot entirely be considered as a true independent data source. It is difficult to quantify the effect of these small dependencies on our results. If HY-2B would be fully independent, then the differences with IFREMER and ERA5* could increase slightly in size.

HY-2B as proxy for true wind
Like any instrument, wind observations taken by the Haiyang-2B scatterometer contain potential measurement errors. Although the application of quality control flags ensures that suspicious wind measurements are removed, the risk of unknown instrumental deficiencies and processing limitations remain. These instrumental are expected to be very minor. However, great care should be taken when referring to HY-2B winds as true winds, because the scatterometer is not a perfect instrument.

Quality control flags
Several flags are applied to HY-2B scatterometer winds for quality control purposes to ensure that only valid HY-2B winds are considered in the analysis. A disadvantage of quality control is that it changes

the sample of the wind data. After applying the KNMI, ice, land, KP and invert flags, 69.1% of the HY-2B observations remained. For example, by applying the KNMI and/or rain flag, all wind observations that are taken during rainy conditions are removed (equal to 13.3% of observations). This means that the statistics in this study are only based on roughly two thirds of all HY-2B observations and only representative of dry weather conditions. In order to discard fewer HY-2B observations, a less conservative rain flag could be applied. A recent study by Xie et al. (2020) investigated a new rain flag that can lead to a higher wind retrieval accuracy and removal of fewer observations in rainy conditions.

Furthermore, by applying quality control, all HY-2B winds below 3 m/s are removed. This may be a consequence of the KP quality control flag. Because IFREMER and ERA5* winds smaller than 3 m/s are not removed, the comparison with HY-2B produces larger differences than if only IFREMER and ERA5* winds above 3 m/s were considered. This is a consequence of conditional sampling. It is a problem that occurs often as a result of quality control and leads to misrepresentation of reality of the data. It is suggested that the quality control flags should be adjusted in future processing of HY-2B scatterometer data.

5.2.2. Collocation method

The goal of collocating IFREMER and ERA5* with HY-2B winds was to obtain an indication of the performance of each L4 product.

Temporal and spatial resolution differences

HY-2B, IFREMER and ERA5* differ in spatial and temporal sampling. For the collocation in time, IFREMER has larger time differences with a HY-2B observation than ERA5*. This is because the IFREMER wind fields have a 6-hourly temporal resolution. Collocating IFREMER winds to an individual HY-2B wind observation can lead to a maximum time difference of 3 hours. ERA5* is produced hourly and therefore has a maximum time difference of 30 minutes with HY-2B.

Moreover, the distance between the grid cells for HY-2B, IFREMER and ERA5* is not only dependent on the spatial resolution, but also on the grid definition. Despite the different resolutions of all three data sets, they are also defined on different coordinates. This means that the winds had to be brought together in space. Due to the coordinate definition of ERA5* winds and its 0.125° resolution, they lie closer to HY-2B winds in space than IFREMER. In order to collocate the wind fields from all three data sets in space, the four nearest surrounding data points of IFREMER or ERA5* were averaged with equal weights to obtain a representative wind field at the same grid point as the HY-2B observation. An average is likely to have a lower wind speed than the individual wind data points. This may clarify why, at higher wind speeds, IFREMER and ERA5* winds were weaker in comparison to HY-2B. An alternative method would be to interpolate the IFREMER and ERA5* winds to the grid point of the HY-2B wind observation. However, this method will also result in lowering of the highest wind speeds. Another option that would preserve the highest wind speeds, would be to choose the data point of IFREMER and ERA5* that lies closest to a HY-2B observation. This is likely to lead to smaller underestimation of IFREMER and ERA5* at higher HY-2B wind speeds, though spatial discrepancy is neglected.

Stress- vs neutral-equivalent winds

Another difference between the data sets is the geophysical representation of the winds. HY-2B and ERA5* both represent stress-equivalent winds, whereas IFREMER is a measure of neutral winds. The difference between neutral and stress-equivalent winds becomes more significant (>0.4 m/s) above 60°, near polar regions, than in the tropics (<0.2 m/s). The order of magnitude of the $\overline{\Delta ws}_{x,y,T}$ and $\sigma\Delta ws_{x,y,T}$ between HY-2B and IFREMER are 0.5 and up to 2 m/s respectively. This suggests that the difference between neutral and stress-equivalent winds can partly clarify the relatively high $\overline{\Delta ws}_{x,y,T}$ and $\sigma\Delta ws_{x,y,T}$. However, since there is no clear increase in differences for IFREMER towards the poles around 60°, it is unlikely that the role of neutral winds has a large effect on the results as other factors are likely to play a bigger role.

ERA5 forecasts vs analyses

Furthermore ERA5* is based on ERA5 forecasts while IFREMER includes ERA5 analyses. Since IFREMER is supposed to be heavily based on scatterometer observations, it is unlikely that the ERA5

analyses have a large effect on the results. The use of ERA5 analyses in IFREMER would lead to less smooth wind fields than ERA5*. However, the results did not indicate such a difference. Therefore, it is unlikely that the difference between analyses and forecasts have affected the results.

6

Conclusions & Recommendations

The main objective of this research was to evaluate the ocean surface wind fields of two global scatterometer-based wind products, IFREMER and ERA5*, in time and space. This section presents the main conclusions drawn from the results and gives recommendations for future research.

6.1. Conclusions

This study presents both IFREMER and ERA5* wind fields as valuable global ocean surface wind products, and points out that ERA5* performs better at higher latitudes than IFREMER while the opposite seems to be true in the tropics. This conclusion was reached by comparing IFREMER and ERA5* to ECMWF Re-Analysis v5 (ERA5) and an independent scatterometer Haiyang-2B (HY-2B) using 2019 data. ERA5 was used to evaluate IFREMER and ERA5* wind fields behaviour over short time scales and to help define a fair methodology to compare the different data sets. Scatterometer HY-2B winds are considered a proxy for true winds and enables ”an independent” assessment of the behaviour of IFREMER and ERA5* winds. The general characteristics of each global wind product were quantified using various statistical parameters including Pearson’s correlation coefficient (r), Root Mean Square Difference (RMSD), mean and standard deviation. The former RMSD and r also highlight aspects of the behaviour of the individual IFREMER and ERA5* wind fields.

The results show that ERA5* correlates slightly better with HY-2B winds than IFREMER on a global scale for 2019, demonstrated with an r of 0.955 vs 0.944 for the wind speed variable. Although r is smaller than 1 (a perfect correlation), the high correlation coefficients indicate that the winds from both L4 products are valid and reliable. ERA5* also has a smaller RMSD than IFREMER (0.95 vs 1.08 m/s). This suggests that ERA5* seems more accurate than IFREMER, assuming HY-2B to be a representative of true surface winds.

Both IFREMER and ERA5* underestimate the HY-2B winds at higher wind speeds above 9 and 13 m/s, respectively. As wind speed continues to increase, IFREMER and ERA5* also show larger deviations with HY-2B. Three possible factors that may contribute to the underestimation of the two L4 wind products are discussed below. First of all, as a result of the coarse resolution of NWP models compared to the scale of wind fluctuations, ERA5 is less likely to resolve very high wind speeds. This is because high wind speeds tend to occur very locally and at a smaller spatial scale than the finest spatial resolution of a NWP model. Both ERA5* and IFREMER include ERA5 data in their products. In fact, results suggest that IFREMER relies more on ERA5 data (Figure 4.1) than was initially clear from IFREMER’s methodology. Secondly, both IFREMER and ERA5* apply averaging to their scatterometer observations. In IFREMER, gradients in the wind fields are smoothed out (Figure 3.1) and this diminishes extremes. The scatterometer correction in ERA5* is based on a 3-day average which leads to a reduction of the highest wind speeds. These two factors could clarify why the L4 wind products underestimate high wind speeds of HY-2B. Thirdly, ERA5* and IFREMER wind fields are collocated in space with HY-2B wind fields by averaging the four nearest wind fields to a HY-2B observation with equal weights. This will flatten extremes and lead to an overall lower wind speed.

On a global scale, the mean ($\overline{\Delta ws}_{x,y,T}$) and standard deviation ($\sigma Deltaws_{x,y,T}$) of differences for wind speed between ERA5* and HY-2B are scattered in dot-like structures across the oceans while for IFREMER, they appear in patches with visible satellite tracks. Also, ERA5* tends to have lower $\overline{\Delta ws}_{x,y,T}$ (<0.5 m/s) than IFREMER (>0.5 m/s). The satellite tracks are a problem introduced by IFREMER as these artificial structures do not seem to be present in ERA5* differences. It seems like the satellite orbits are a result of the use of ScatSat-1 data. Even though ERA5* also includes ScatSat-1, a newer processor and averaging of the observations may explain why the orbits do not seem a problem in ERA5*. The satellite tracks in IFREMER are undesirable for wind users because it introduces abrupt wind changes that are not originally present.

IFREMER $\overline{\Delta ws}_{x,y,T}$ in coastal regions are significant in size (>1 m/s) and can, amongst other reasons, be possibly attributed to the diurnal cycle. As a result of the diurnal cycle, winds vary a lot throughout the day which a 6-hourly wind product can capture less well than an hourly wind product. As a result, IFREMER seems to have wind bias in coastal areas. On the other hand, the results do not show any bias for ERA5* in coastal regions, suggesting that it performs well near the coast.

When evaluating specific climate zones, both IFREMER and ERA5* wind fields correspond very well with HY-2B winds in the subtropics (between 20°- 30°). This climate zone is known for its persistent trade winds which are well captured by both L4 products. In the middle latitudes, IFREMER has significantly larger standard deviation of wind differences (>2 m/s) as opposed to ERA5*. By eye there seems to be a strong correlation between wind differences in the Southern mid-latitudes and the time difference between IFREMER and the local equator crossing time of the ascending and descending nodes (18:00 and 06:00) of HY-2B. These differences in time can possibly be cause by the time interpolation in the IFREMER product. Because IFREMER is a 6-hourly product it collocates less well with HY-2B winds.

The tropics (between 20°S - 20°N) are a region where IFREMER correlates better with HY-2B than ERA5*. This is shown by a lower RMSD for IFREMER than ERA5*, 0.81 and 0.94 m/s respectively. Both ERA5* and IFREMER generate similar $\overline{\Delta ws}_{x,y,T}$ of 1 m/s, but ERA5* has a higher $\sigma \Delta ws_{x,y,T}$ than IFREMER. Specific areas of interest are the Indian Pacific Warm Pool and the ITCZ because the $\sigma \Delta ws_{x,y,T}$ stands out compared to the rest of the tropics. Reasons for IFREMER having a closer correspondence to HY-2B could be a consequence of the spatial filtering in HY-2B. As a result, HY-2B winds are smoother which overlap better with less-detailed IFREMER wind fields than ERA5*. Another reason could be that quality control of HY-2B winds leads to conditional sampling in the collocated wind fields. HY-2B observations <3 m/s are not reliable and removed from the sample by quality control. This means that errors are introduced when comparing HY-2B winds only larger than 3 m/s to IFREMER/ERA5* winds <3 m/s. The tropics are particularly prone to these errors because of their low average wind speeds (< 5m/s).

6.2. Recommendations

Based on results and conclusions in this study, this section describes the recommendations for future research.

The results in this research are based on a yearly data set (2019). A global analysis should also be tested for a longer period of time to validate if the same differences occur and to check the influence of weather events such as El Nino.

The results suggest that ERA5* is a better wind product than IFREMER, except for in the tropics. It is recommended to further investigate the behaviour, of especially ERA5*, in the tropics by comparison with independent in situ measurements. For example, an analysis with triple collocation with one of the wind products, scatterometer and buoy data could be carried out to validate tropical ERA5* winds. This is a reliable method that allows to better comprehend the differences observed in dual collocation (Vogelzang and Stoffelen, 2012). The goal of this recommendation is to help to inform users on the be-

haviour of ERA5* in the tropics and perhaps give advice on ERA5* product development for improved performance in the tropics.

Furthermore, it is recommended to repeat the collocations for different samples based on different quality control flags. For example, this analysis is based on dry conditions only, ie. all HY-2B wind observations taken during rain conditions were removed after applying the KNMI flag. Thus to check if similar observations are observed, data samples representative for other weather conditions should be tested.

An extra analysis of the positioning of the wind vector cell (WVC) in the swath would be beneficial to verify the results of this study would change. As it is known that the quality of the observations varies along the scatterometer swath, especially for a rotating pencil-beam spectrometer such as HY-2B, the correlation with the L4 products may change accordingly. This would lead to improved understanding of the L4 surface wind fields.

This study applied several statistical parameters to help quantify the differences observed between the various data sets. These parameters can be a source of uncertainty in the results.

It would be interesting to also look at other statistical measures to gain more insights about the IFREMER and ERA5* wind products. In this study, the standard deviation measure is computed using an annual average wind. By using this method to calculate the standard deviation, seasonal effects are also taken into account. This means that this standard deviation is a rougher measure of the spread of the differences across a year. In order to look at the standard deviation that only considers the differences between the scatterometer and the L4 product, the daily standard deviation can be computed because it excludes seasonal effects.

A

Level-4 wind product methods

A.1. Flowchart for IFREMER wind product

Figure A.1 shows the steps that are involved to create the L4 IFREMER blended wind product.

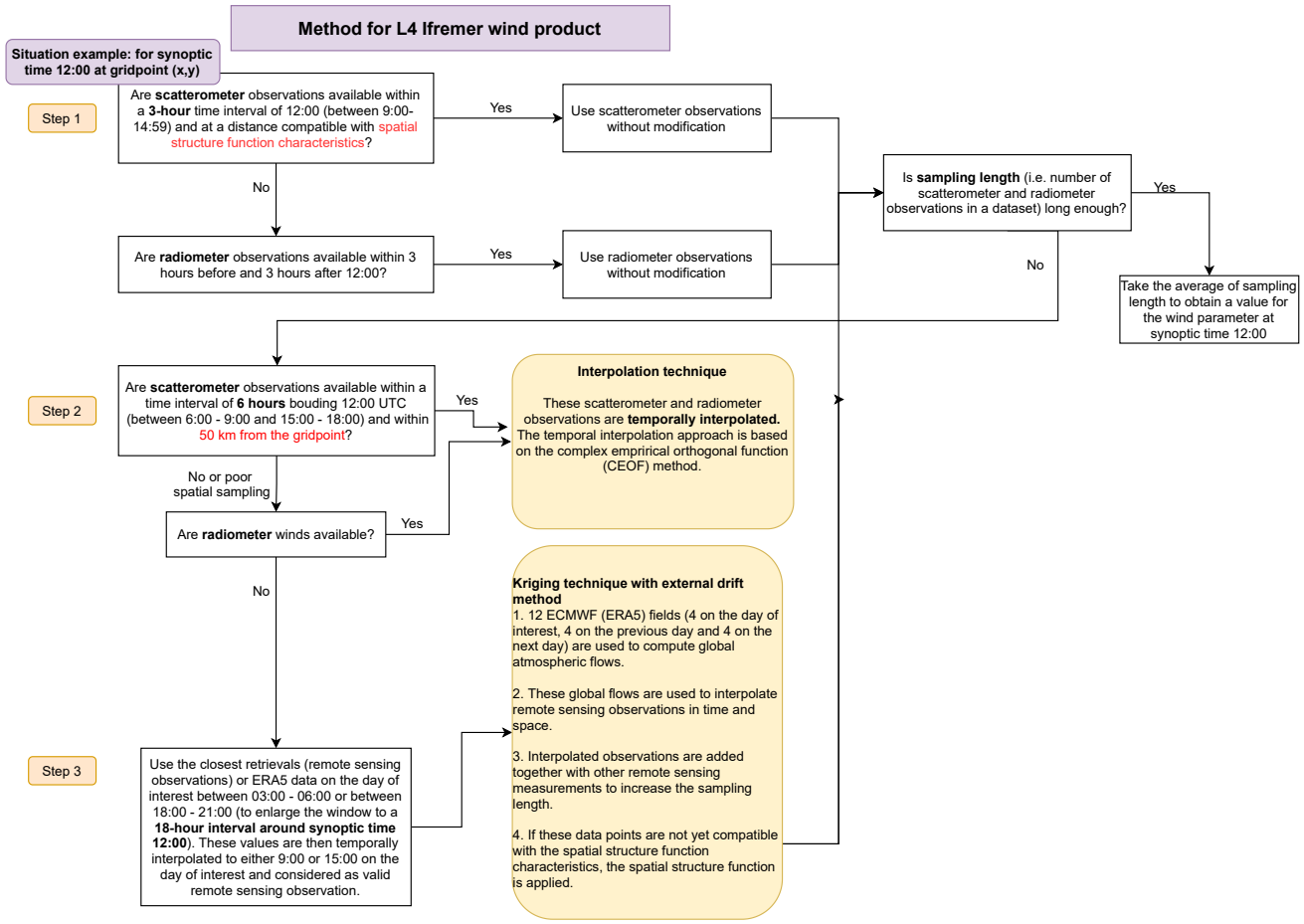

Figure A.1: Flowchart representing all the steps taken in the method to create the l4 blended wind product by IFREMER.

A.2. ASCAT observations in IFREMER product

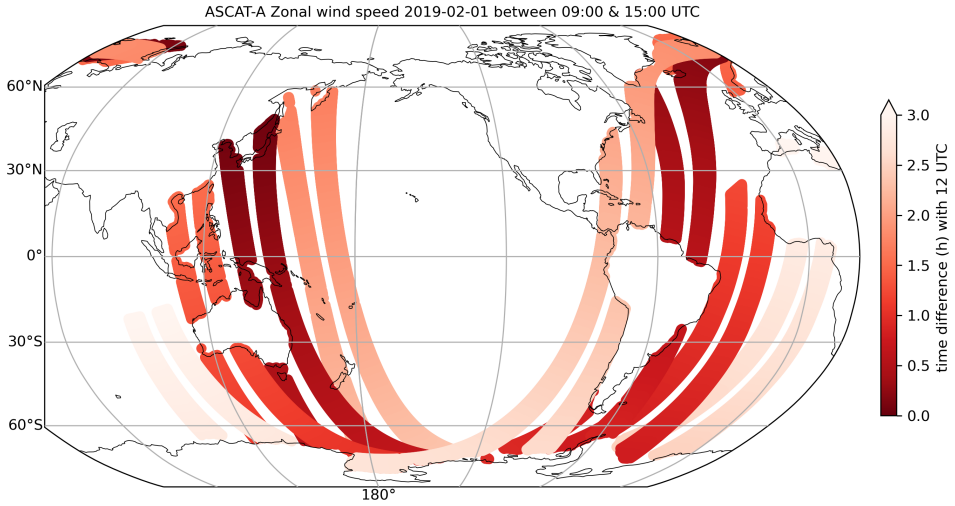

Figure A.2: The time of ASCAT-A observations occuring in a 6-hour window used in the IFREMER wind product at 12:00 UTC. The colour graduation indicates the time difference with 12:00 UTC, whereby darker red are observations close to 12:00 UTC.

A.3. Flowchart for ERA5* wind product

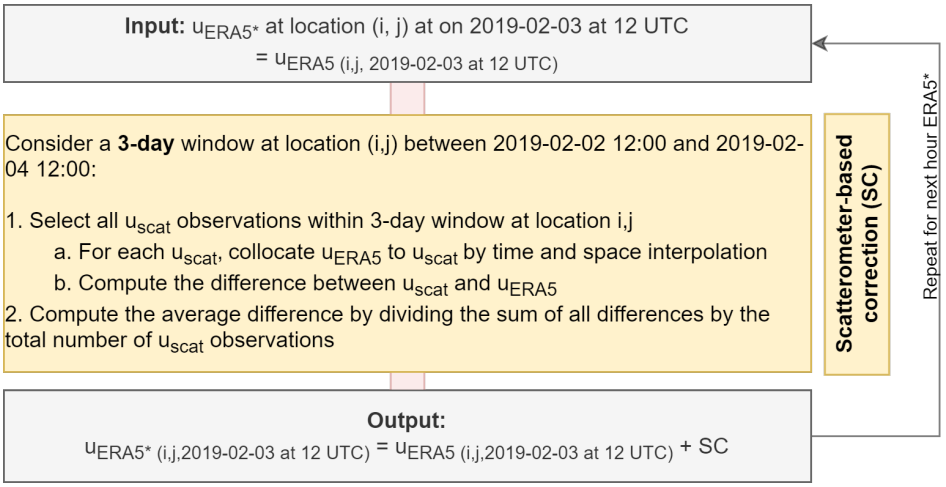

Figure A.5: Example of a scatterometer-based correction (SC) calculation at gridpoint (i,j) on 2 February 2019 at 12 UTC. u_scat refers to the collocated scatterometer measurements from ASCAT-A, B and C and OSCAT.

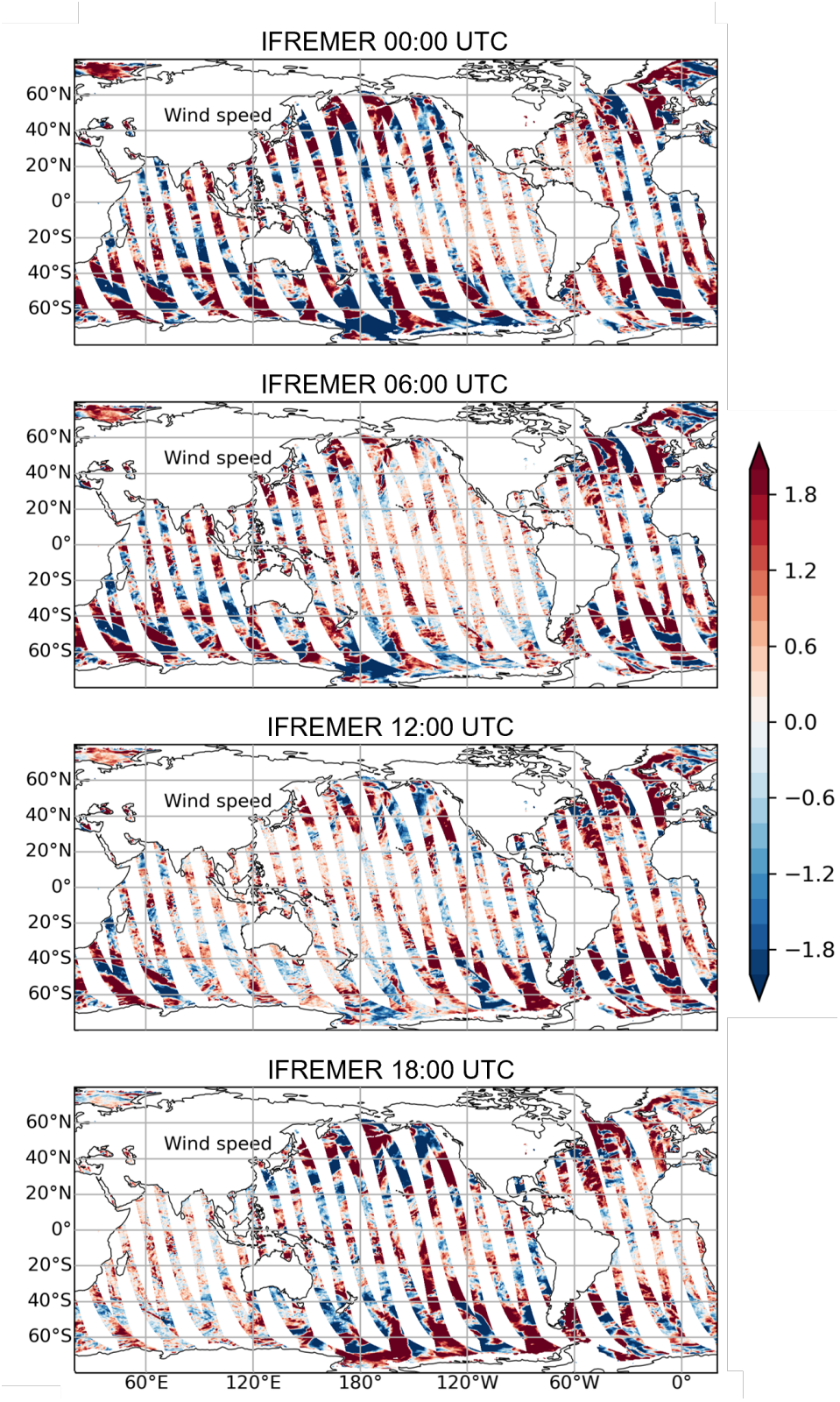

Figure A.3: ASCAT-A ascending daily data subtracted from IFREMER wind at 00:00, 06:00, 12:00 and 18:00 UTC on February 1st, 2019.

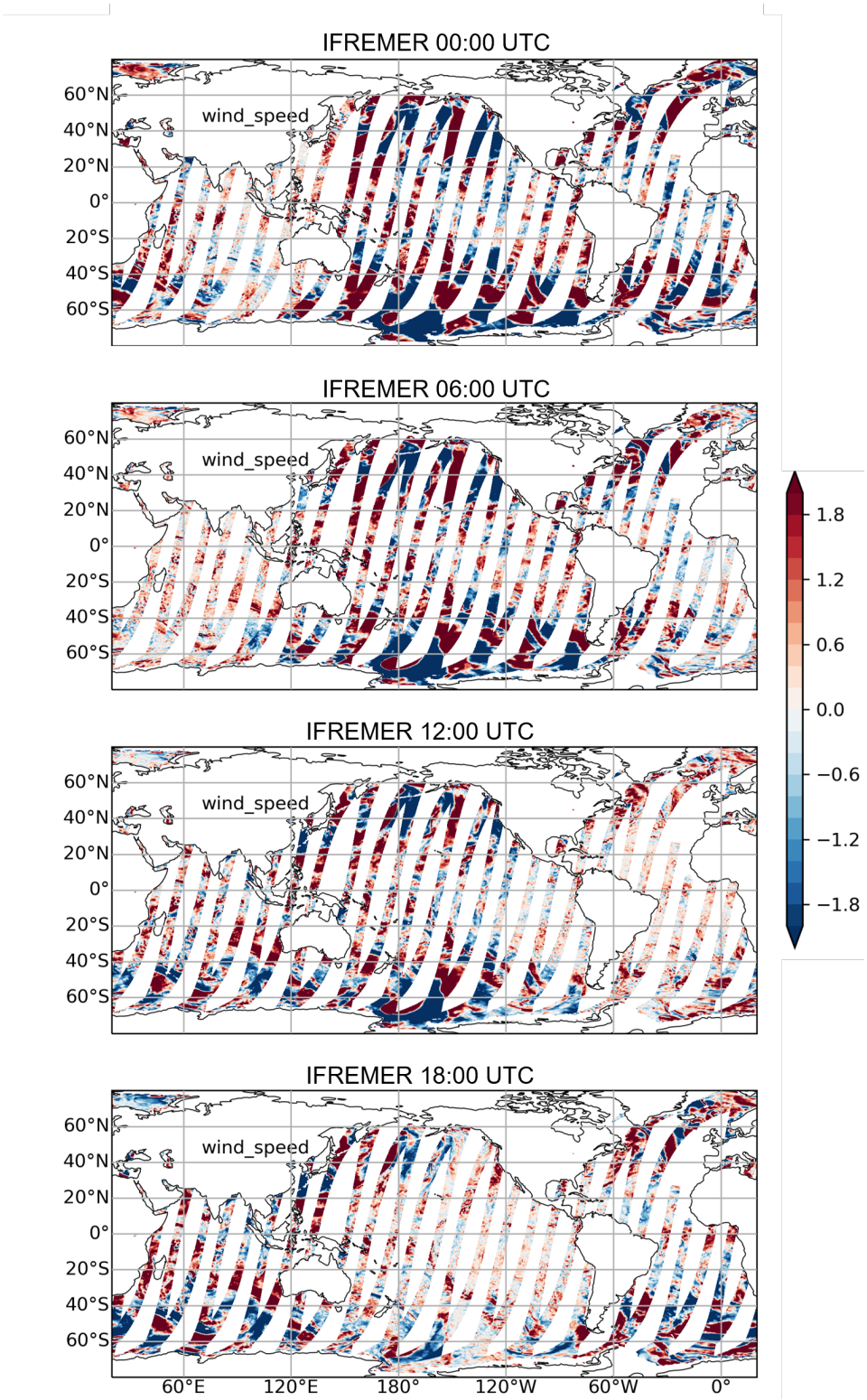

Figure A.4: ASCAT-A descending daily data subtracted from IFREMER wind at 00:00, 06:00, 12:00 and 18:00 UTC on February 1st, 2019.

B

Data Processing

B.1. Grid & resolution

A data point with coordinates (x, y) is located at the center of a grid cell and is representative for the entire square of 0.25°by 0.25° or 0.125° by 0.125° for ERA5* at its original resolution. This means that by averaging 4 neighbouring data points at 0.125°resolution (see B.1a), a new corresponding value at 0.25°is obtained (see Figure B.1b). This averaging is a two-step process; first 2 data points are averaged in the longitude direction, then 2 data points are averaged in the latitude direction. This method is repeated for all data points to obtain a new data set for ERA5* values at a reduced 0.25°grid.

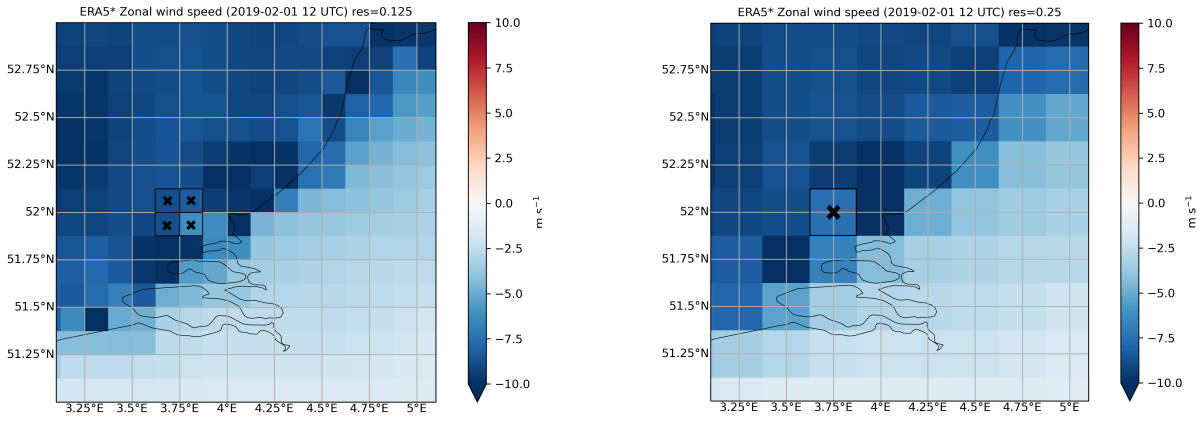

(a) ERA5* (0.125°)

(b) ERA5* (0.25°)

Figure B.1: Averaging with equal weight to reduce ERA5* resolution from a 0.125°grid to a 0.25°grid.

B.2. Land-sea ice mask

The IFREMER L4 product contains a land-sea mask that filters out most grid cells that are contaminated with land, but not all (Figure B.2a). Many data points still exist on land along the coastlines of the UK as well as of the Netherlands, Belgium and North of France.

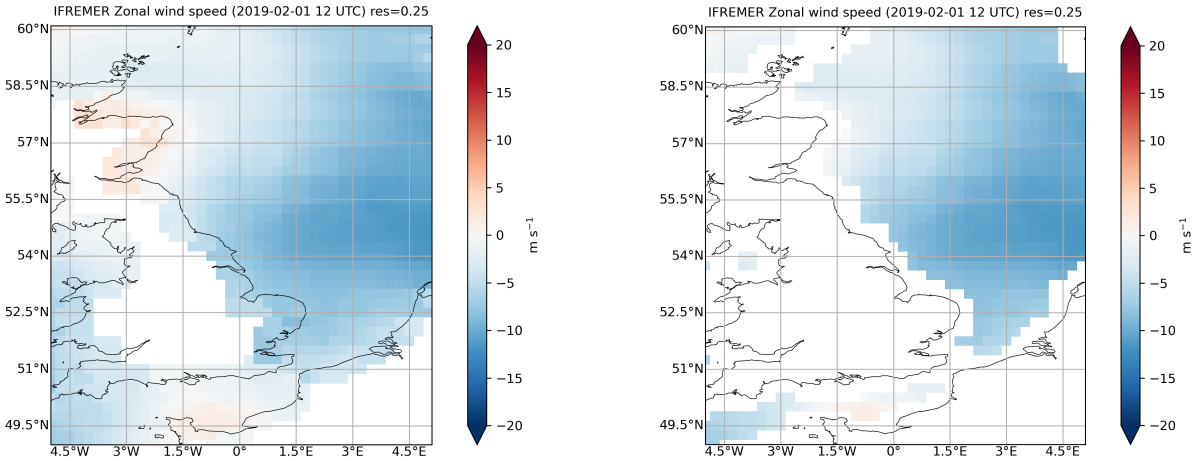

(a) IFREMER without ERA5 land-sea mask

(b) IFREMER after ERA5 land-sea mask

Figure B.2: Application of land-sea mask, retrieved from ERA5 from CDS.

To make sure that grid points with pure and only ocean water are considered, the land-sea mask from the ERA5 product obtained from the Climate Data Store (CDS) is applied to IFREMER, shown in Figure B.2b. This means that only data points for which the land-sea mask parameter in the ERA5 data equals to 0 (i.e. the entire grid cell exists of only ocean) are considered. The same procedure was applied to ERA5*. Other alternative land-sea masks such as an internal KNMI database could have also been chosen. However, for the purpose of this research the land-sea mask from the ERA5 (Climate Date Store) file was the simplest option to achieve the desired outcome. This ensures that for all products only the same ocean grid points are considered and compared.

B.2.1. Neutral vs stress-equivalent ERA5 winds

To investigate the effect of using neutral-equivalent winds in IFREMER vs stress-equivalent winds in ERA5*, the root mean square difference (RMSD) between ERA5 stress-equivalent and neutral-equivalent wind was computed Figure B.3 as function of latitude. The RMSD is smaller than 0.2 m/s South of 40°N. The RMSD increases to up to 0.4 m/s North of 40°N. These values are representative for a day in February and are likely to change per season when the temperature and hence air mass density also changes.

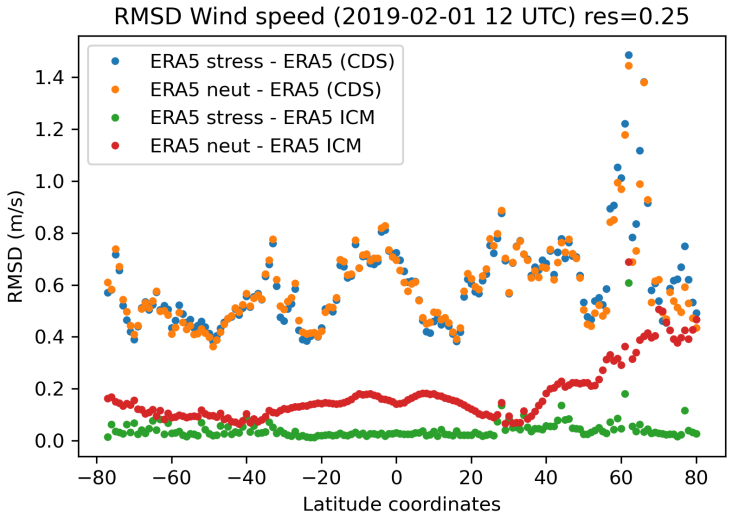

Figure B.3: RMSD of ERA5 stress-equivalent winds and neutral-equivalent winds with ERA5 retrieved from the CDS and produced by the ICM as function of latitude.

C

Short time-scale characteristics for ws and u

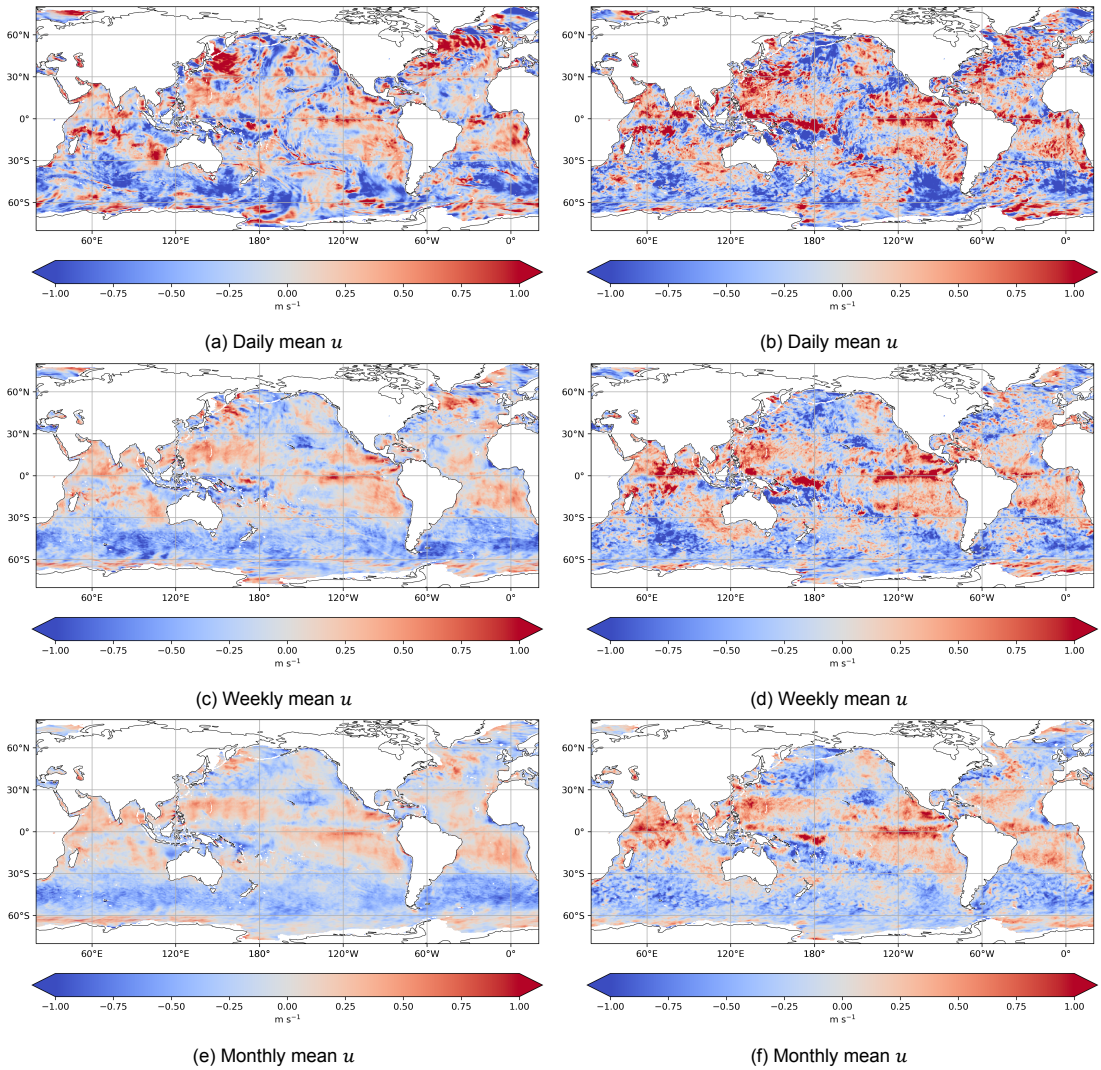

(a) Daily mean u

(b) Daily mean u

(c) Weekly mean u

(d) Weekly mean u

(e) Monthly mean u

(f) Monthly mean u

Figure C.1: Mean zonal wind (u) differences between IFREMER and ERA5 (a, c, e) and ERA5* and ERA5 (b, d, f) averaged over a day (2 February 2019), a week (2-9 February 2019), and a month (February 2019) plotted on a 0.25°grid. Positive differences in red indicate that ERA5 is larger than either IFREMER or ERA5*.

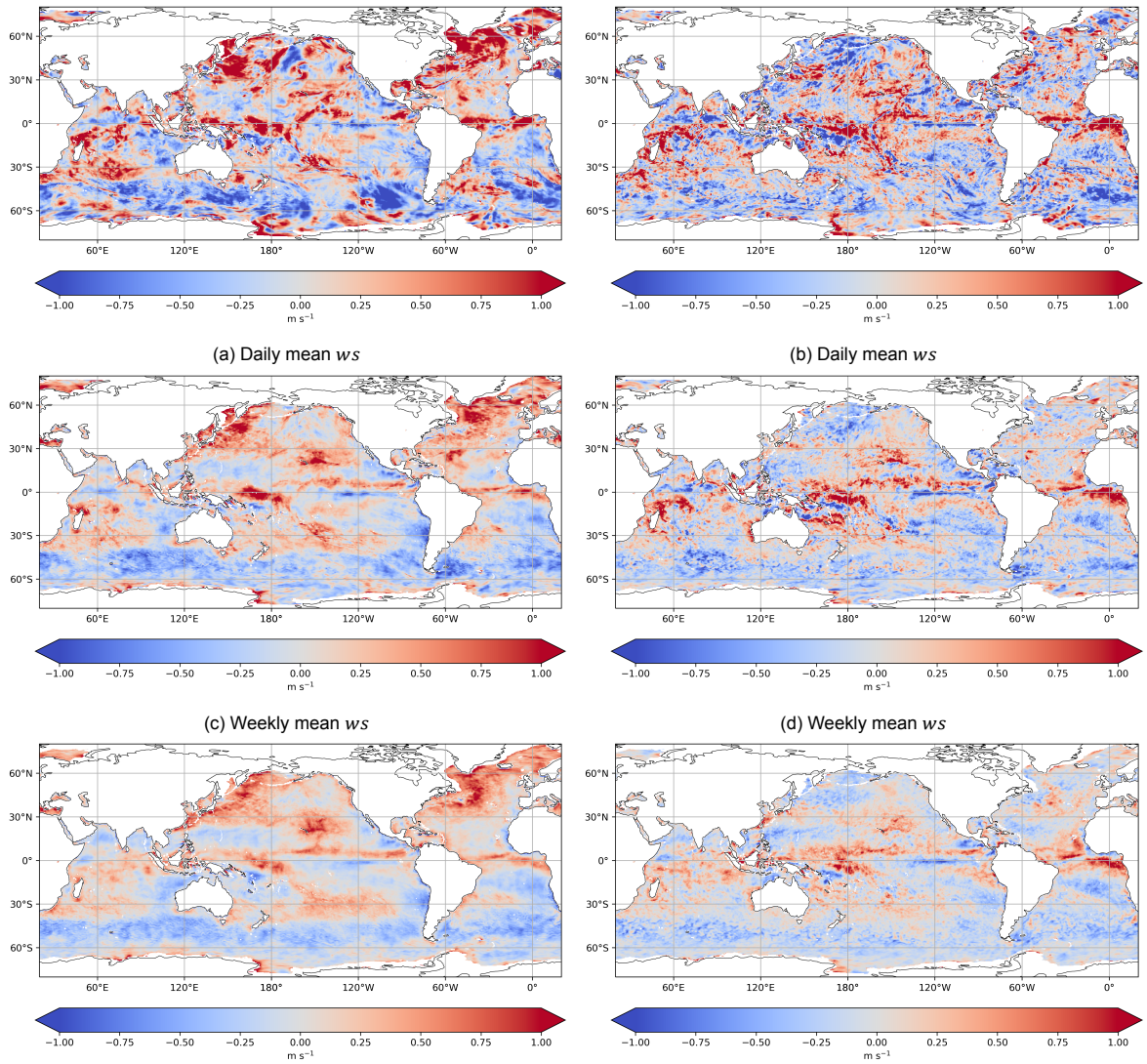

(a) Daily mean ws

(b) Daily mean ws

(c) Weekly mean ws

(d) Weekly mean ws

(e) Monthly mean ws

(f) Monthly mean ws

Figure C.2: Mean wind speed (ws) differences between IFREMER and ERA5 (a, c, e) and ERA5* and ERA5 (b, d, f) averaged over a day (2 February 2019), a week (2-9 February 2019), and a month (February 2019) plotted on a 0.25°grid. Positive differences in red indicate that ERA5 is larger than either IFREMER or ERA5*.

D

Product characteristics of descending data

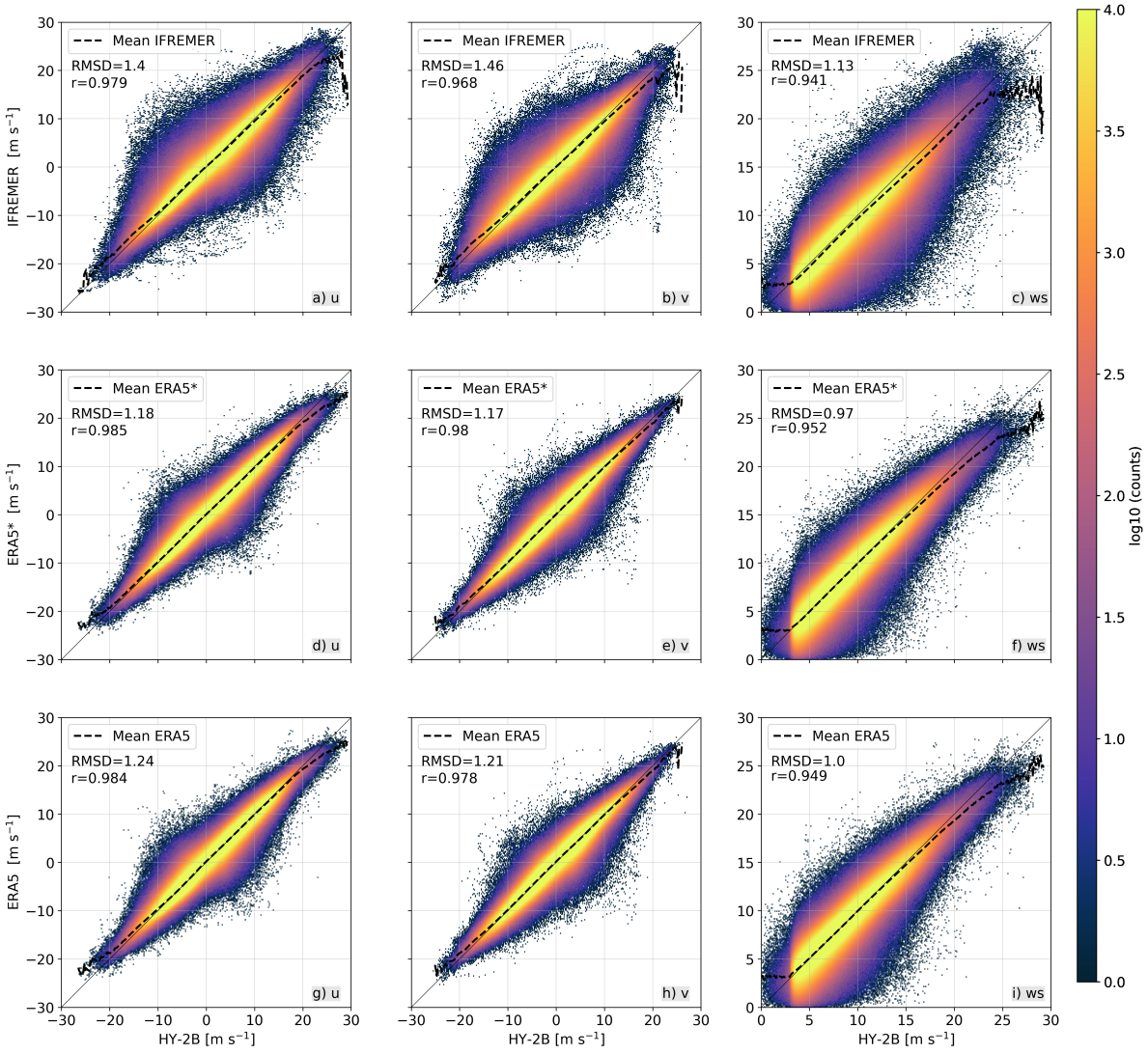

Figure D.1: HY-2B global descending quality-controlled winds for 2019 plotted against collocated IFREMER winds (a,b,c), ERA5* winds (d,e,f) and ERA5 winds (g,h,i) for variables u, v and ws.

E

Effect of diurnal cycle on tropical coasts

In a study by Turk et al. (2021), daily cycle winds in the tropics were examined using scatterometer observations (screened on quality control including rain) from RapidSat. The maximum daily zonal wind component (u) from Rapidscat (Figure E.1a) is highest in specific coastal regions such as West of Madagascar, N. Australia and W. Central America. In these 3 specific regions, there is also a large standard deviation (σ) of the differences of u between HY-2B and IFREMER. The meridional wind component (v) seems to show a similar pattern in Central America and E. of South America. The relation in u seems to be more apparent than for v. This suggests that diurnal wind variations that are especially strong in coastal regions cause larger differences in IFREMER with HY-2B winds.

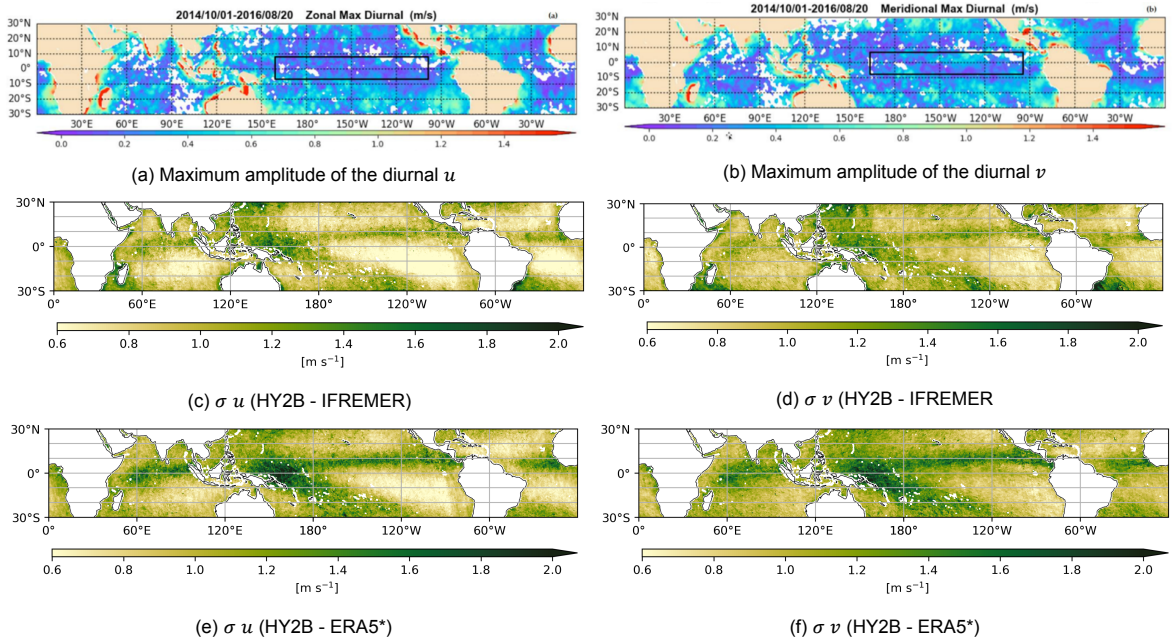

(a) Maximum amplitude of the diurnal u

(b) Maximum amplitude of the diurnal v

(c) σ u (HY2B - IFREMER)

(d) σ v (HY2B - IFREMER

(e) σ u (HY2B - ERA5*)

(f) σ v (HY2B - ERA5*)

Figure E.1: Comparing the maximum amplitude of diurnal wind components for RapidScat observations between October 2014 to September 2016 shown in the top row (a,b) (Turk et al., 2021) to standard deviation of 2019 (σ) of HY2B-IFREMER (c,d) and HY2B-ERA5* wind components.

However, there are also regions of large σ between HY2B and IFREMER winds that do not correspond to an extreme diurnal wind in the Rapidscat observations. The study by Turk et al. (2021) is based on wind data from a different period in time than used in this study, 2014-2016 versus 2019. One significant difference between these years is the effect of El Nino. In 2015 and 2016 there was a strong El Nino, whereas 2019 was only a weak to neutral El Nino year (Lindsey, 2021). This will have

affected the weather and winds between these years and could be a reasons why not all areas of large σ correspond to an extreme in diurnal wind components measured by Rapidscat.

F

ScatSat-1 satellite orbits

ScatSat-1 is a sun-synchronous satellite launched by the Indian Space Research Organization (ISRO) in 2016. It carries the OSCAT scatterometer which is a rotating pencil-beam scatterometer operating at Ku-band frequency. As a result of the rotating pencil-beam antenna, the quality of the wind retrieval depends on the position of the swath. The backscatters from the nadir and outer part of the swath tend to have lower quality wind retrievals. Because ScatSat-1 has a short repeat cycle of only 2 days, the satellite will observe the same location from the same angles once every two days. This means that some regions are only observed from the nadir part of the swath and have the largest differences (bias) with NWP model winds (Figure F.1).

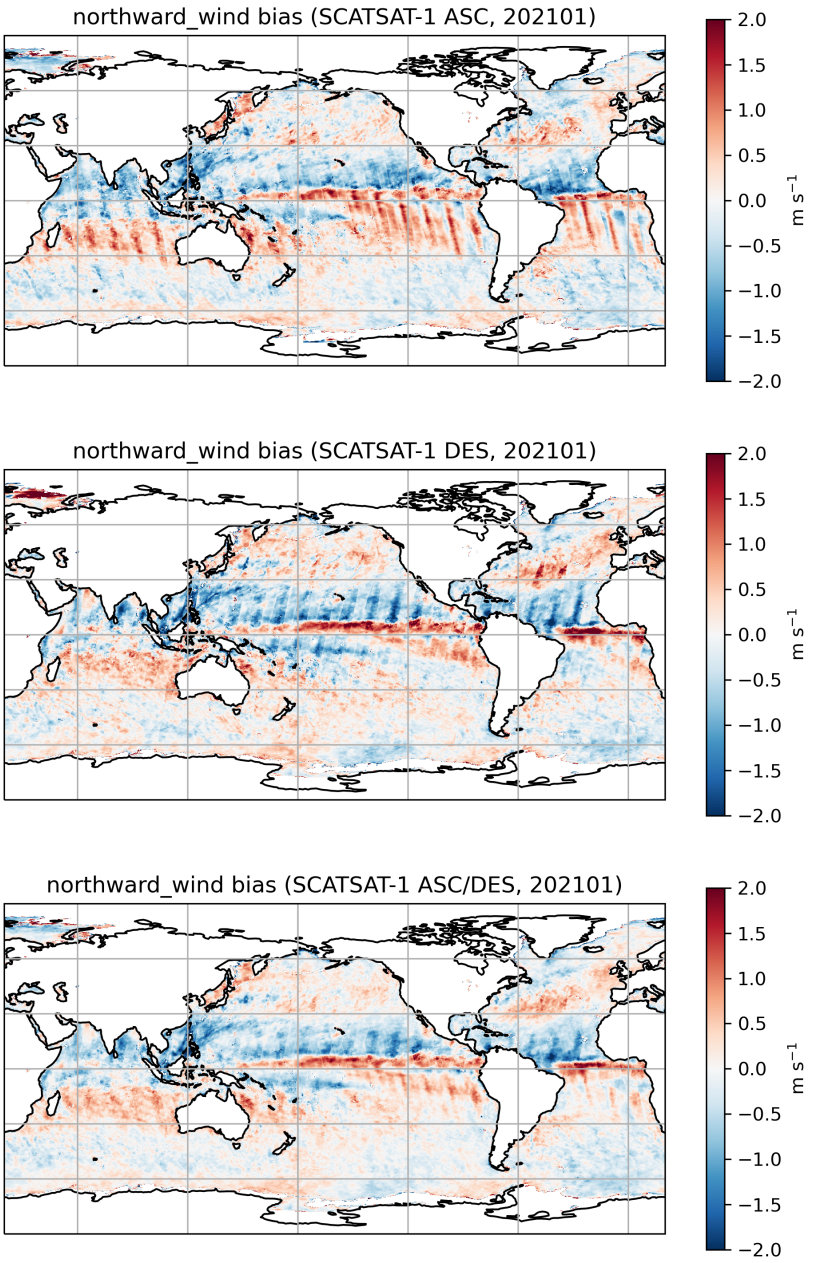

Figure F.1: Meridional wind differences between ScatSat-1 and ECWMF for January 2021 (produced by R. Giesen)

G

Effect of quality control on data sample

Figure G.1 shows the number of collocated HY-2B winds on which the results and statistical parameters of the results are based.

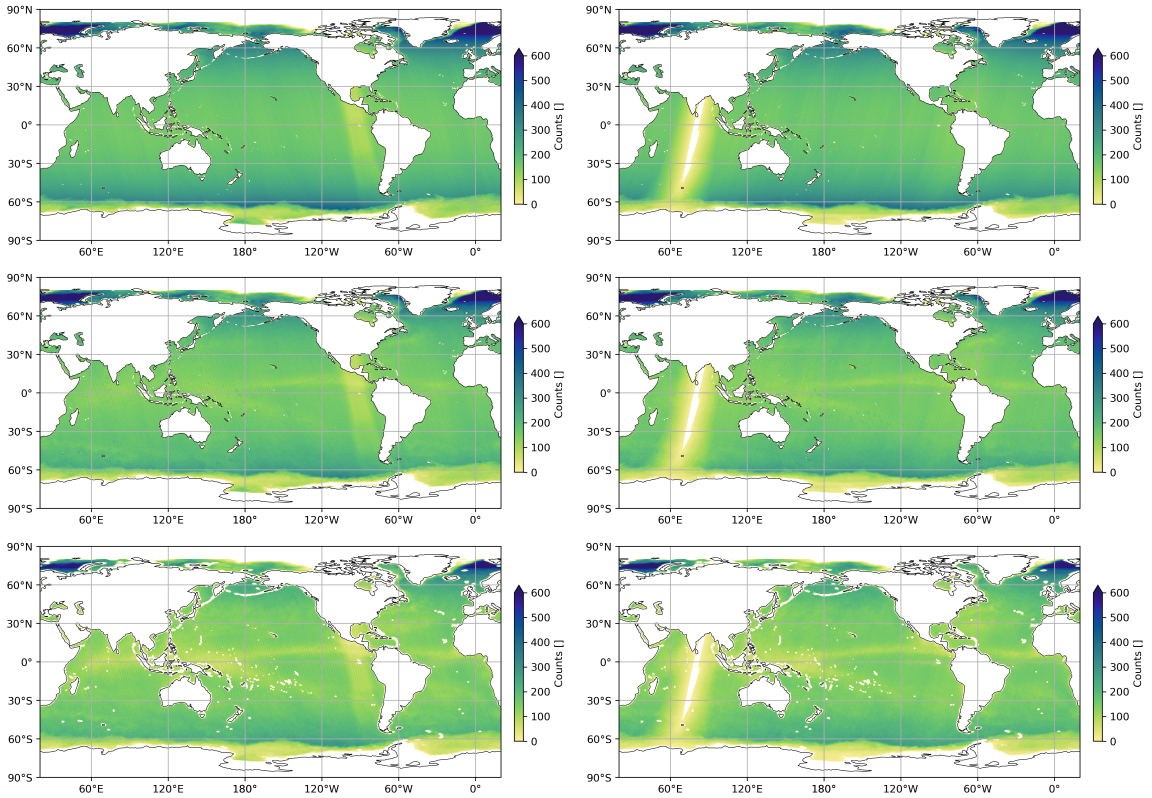

Figure G.1: Number of collocated ascending (left) and descending (right) HY-2B winds for 2019, without quality control (top), after the rain flag (middle) and after all quality control flags (bottom).

Bibliography

Belmonte Rivas, M. and Stoffelen, A. (2019). Characterizing ERA-Interim and ERA5 surface wind biases using ASCAT. *Ocean Science*, 15(3):831–852.

Bentamy, A. and Fillon, D. C. (2012). Gridded surface wind fields from Metop/ASCAT measurements. *International Journal of Remote Sensing*, 33(6):1729–1754.

Bentamy, A., Grodsky, S. A., Cambon, G., Tandeo, P., Capet, X., Roy, C., Herbette, S., and Grouazel, A. (2021). Twenty-Seven Years of Scatterometer Surface Wind Analysis over Eastern Boundary Upwelling Systems. *Remote Sensing*, 13.

Bentamy, A., Piollé, J. F., and Prevost, C. (2020). For Wind product WIND_GLO_WIND_L4_REP_OBSERVATIONS_012_006.

Bôas, A. B., Ardhuin, F., Ayet, A., Bourassa, M. A., Brandt, P., Chapron, B., Cornuelle, B. D., Farrar, J. T., Fewings, M. R., Fox-Kemper, B., Gille, S. T., Gommenginger, C., Heimbach, P., Hell, M. C., Li, Q., Mazloff, M. R., Merrifield, S. T., Mouche, A., Rio, M. H., Rodriguez, E., Shutler, J. D., Subramanian, A. C., Terrill, E. J., Tsamados, M., Ubelmann, C., and Sebille, E. v. (2019). Integrated observations of global surface winds, currents, and waves: Requirements and challenges for the next decade. *Frontiers in Marine Science*, 6(JUL):1–34.

Chelton, D. B., Schlax, M. G., Freilich, M. H., and Milliff, R. F. (2004). Satellite Measurements Reveal Persistent Small-Scale Features in Ocean Winds. *Science*, 303(February):978–983.

Chelton, D. B. and Xie, S. P. (2010). Coupled ocean-atmosphere interaction at oceanic mesoscales. *Oceanography*, 23(4):54–69.

Coleman, J. S. M. (2015). Atmospheric Science: Meteorology and Climatology. 1450(1687):1–7.

COMET (2015). Using Scatterometer Wind and Altimeter Wave Estimates in Marine Forecasting.

Dawei, L. and Hui, S. (2015). EVALUATING THE EFFECT OF RAIN ON HY-2A SCATTEROMETER MEASUREMENTS. *IEEE International Geoscience and Remote Sensing Symposium (IGARSS)*, pages 4913–4915.

De Kloe, J., Stoffelen, A., and Verhoef, A. (2017). Improved Use of Scatterometer Measurements by Using Stress-Equivalent Reference Winds. *IEEE Journal of Selected Topics in Applied Earth Observations and Remote Sensing*, 10(5):2340–2347.

Dee, D. (2022). The Climate Data Guide: ERA5 atmospheric reanalysis.

Desbiolles, F., Bentamy, A., Blanke, B., Roy, C., Mestas-Nuñez, A. M., Grodsky, S. A., Herbette, S., Cambon, G., and Maes, C. (2017). Two decades [1992–2012] of surface wind analyses based on satellite scatterometer observations. *Journal of Marine Systems*, 168(January):38–56.

Dias, J., Gehne, M., Kiladis, G. N., Sakaeda, N., Bechtold, P., and Haiden, T. (2018). Equatorial waves and the skill of NCEP and ECMWF numerical weather prediction systems. *Monthly Weather Review*, 146(6):1763–1784.

ECMWF (2020). Reanalysis Fact Sheet.

ESA (2020). Polar and Sun-synchronous orbit.

EUMeTrain (2017). Tutorial on Satellite Derived Wind Products.

Figa-Saldaña, J., Wilson, J. J., Attema, E., Gelsthorpe, R., Drinkwater, M. R., and Stoffelen, A. (2002). The advanced scatterometer (ascat) on the meteorological operational (MetOp) platform: A follow on for european wind scatterometers. *Canadian Journal of Remote Sensing*, 28(3):404–412.

Giesen, R., Clementi, E., Bajo, M., Federico, I., Stoffelen, A., and Santoleri, R. (2021). The November 2019 record high water levels in Venice, Italy. In *Copernicus Marine Service Ocean State Report, Issue 5*, chapter 4.3, pages 156–162. Journal of Operational Oceanography.

Haupt, S. E., Jiménez, P. A., Lee, J. A., and Kosović, B. (2017). Principles of meteorology and numerical weather prediction. *Renewable Energy Forecasting: From Models to Applications*, pages 3–28.

Hersbach, H., Bell, B., Berrisford, P., Hirahara, S., Horányi, A., Muñoz-Sabater, J., Nicolas, J., Peubey, C., Radu, R., Schepers, D., Simmons, A., Soci, C., Abdalla, S., Abellan, X., Balsamo, G., Bechtold, P., Biavati, G., Bidlot, J., Bonavita, M., De Chiara, G., Dahlgren, P., Dee, D., Diamantakis, M., Dragani, R., Flemming, J., Forbes, R., Fuentes, M., Geer, A., Haimberger, L., Healy, S., Hogan, R. J., Hólm, E., Janisková, M., Keeley, S., Laloyaux, P., Lopez, P., Lupu, C., Radnoti, G., de Rosnay, P., Rozum, I., Vamborg, F., Villaume, S., and Thépaut, J. N. (2020). The ERA5 global reanalysis. *Quarterly Journal of the Royal Meteorological Society*, 146(730):1999–2049.

Jing, Y., Li, Y., and Xu, Y. (2022). An assessment of the North Atlantic (25–75°N) air-sea CO2 flux in 12 CMIP6 models. *Deep Sea Research Part I: Oceanographic Research Papers*, 180(December 2021):103682.

Klinker, E., Rabier, F., Kelly, G., and Mahfouf, J.-F. (1999). The ECMWF operational implementation of four-dimensional variational assimilation. *Quarterly Journal of the Royal Meteorological Society*, pages 1191–1215.

Landberg, L. (2015). *Meteorology for Wind Energy: An Introduction*. Number 1. John Wiley & Sons, Incorporated.

Li, H. and Bao, J.-W. (2021). *Uncertainties in the surface layer physics parameterizations*. Elsevier Inc.

Lindsey, R. (2021). Climate Variability: Oceanic Niño Index.

Marshall, J. and Alan Plumb, R. (2008). *Atmosphere, Ocean, and Climate Dynamics*. Elsevier Academic Press, Cambridge, Massachusetts, 93 edition.

Morey, S. L., Bourassa, M. A., Davis, X. J., O'Brien, J. J., and Zavala-Hidalgo, J. (2005). Remotely sensed winds for episodic forcing of ocean models. *Journal of Geophysical Research C: Oceans*, 110(10):1–15.

NOAA (2020). The Jet Stream.

Osi, G. (2019). EUMETSAT Advanced Retransmission Service ASCAT Wind Product User Manual. (March):1–23.

Portabella, M., Stoffelen, A., Lin, W., Turiel, A., Verhoef, A., Verspeek, J., and Ballabrera-Poy, J. (2012). Rain effects on ASCAT-retrieved winds: Toward an improved quality control. *IEEE Transactions on Geoscience and Remote Sensing*, 50(7 PART1):2495–2506.

Portabella, M., Trindade, A., Grieco, G., and Makarova, E. (2021). W ORLD O CEAN C IRCULATION A LGORITHM T HEORETICAL B ASIS D OCUMENT FOR. (4000130730):0–28.

SAF, O. (2021). Product User Manual (PUM) for the HY-2 winds. Technical report.

Sobel, A. H. (2012). Tropical Weather. *Nature Education Knowledge*.

Stoffelen, A. (1998a). *Scatterometry*. PhD thesis, Universiteit Utrecht.

Stoffelen, A. (1998b). Toward the true near-surface wind speed: Error modeling and calibration using triple collocation. *Journal of Geophysical Research: Oceans*, 103(3334):7755–7766.

Stoffelen, A. (2019). Sea Surface Vector Winds.

Talagrand, O. (1997). Assimilation of Observations, an Introduction. *Journal of the Meteorological Society of Japan*, 75(43):191–209.

Trindade, A., Portabella, M., Stoffelen, A., Lin, W., and Verhoef, A. (2014). ERAstar : a High Resolution Ocean Forcing Product. *IEEE Transactions on Geoscience and Remote Sensing*, 13(9):1337–1347.

Turk, F. J., Hristova-Veleva, S., and Giglio, D. (2021). Examination of the daily cycle wind vector modes of variability from the constellation of microwave scatterometers and radiometers. *Remote Sensing*, 13(1):1–19.

Verhoef, A., Vogelzang, J., Verspeek, J., and Stoffelen, A. (2017). Long-Term Scatterometer Wind Climate Data Records. *IEEE Journal of Selected Topics in Applied Earth Observations and Remote Sensing*, 10(5):2186–2194.

Vogelzang, J. and Stoffelen, A. (2012). Triple collocation, EUTMETSAT report. Technical report.

Vogelzang, J. and Stoffelen, A. (2018). Improvements in Ku-band scatterometer wind ambiguity removal using ASCAT-based empirical background error correlations. *Quarterly Journal of the Royal Meteorological Society*, 144(716):2245–2259.

Vogelzang, J., Stoffelen, A., Verhoef, A., and Figa-Saldaña, J. (2011). On the quality of high-resolution scatterometer winds. *J. Geophys. Res*, 116:10033.

von Schuckmann, K., P.-Y. Le Traon, N., Smith, N., Pascual, A., Djavidnia, S., Gattuso, J.-P., Grégoire, M., and Nolan, G. (2021). Copernicus Marine Service Ocean State Report. *Journal of Operational Oceanography*, (5):4–7.

Wang, Z., Stoffelen, A., Fois, F., Verhoef, A., Zhao, C., Lin, M., and Chen, G. (2017). SST Dependence of Ku-and C-Band Backscatter Measurements. *IEEE Journal of Selected Topics in Applied Earth Observations and Remote Sensing*, 10(5):2135–2146.

Wang, Z., Stoffelen, A., and Verhoef, A. (2016). Ku-band scatterometer SST sensitivity and geophysical model function. *International Geoscience and Remote Sensing Symposium (IGARSS)*, 2016-Novem:4629–4632.

Wanninkhof, R. (2014). Relationship between wind speed and gas exchange over the ocean revisited. *Limnology and Oceanography: Methods*, 12(JUN):351–362.

Wikipedia (2022). Pearson correlation coefficient.

Xie, X., Wang, J., and Lin, M. (2020). A neural network-based rain effect correction method for HY-2A scatterometer backscatter measurements. *Remote Sensing*, 12(10).

Yang, J. and Zhang, J. (2018). Evaluation of ISS-RapidScat wind vectors using buoys and ASCAT data. *Remote Sensing*, 10(4).

Zhao, K., Zhao, C., and Chen, G. (2021). Evaluation of Chinese Scatterometer Ocean Surface Wind Data: Preliminary Analysis. *Earth and Space Science*, 8(7):1–14.